Turbulence and airflow variations in complex terrain: A modelling and field measurement approach for wind turbine siting

---

A thesis

submitted in partial fulfillment

of the requirements of the

Degree of

Doctoral of Philosophy in Environmental Science

in the

University of Canterbury

Marwan Katurji

University of Canterbury

2011

Abstract

As the demand for global renewable energy grows, so does the demand for more efficient energy conversion machines and better wind resource assessment. The need to convert as much energy as possible with little cost remains the biggest challenge. In the wind energy sector, the quantity of the resource "wind" is not hard to locate, as with current ground and space based remote sensing technologies, and climate reanalysis techniques, the mapping of average wind speeds across the globe is achievable. The difficulty lies in identifying the "quality" of the wind resource. "Quality" is the measure of the time variant properties of the wind, and time scale here does not represent seasonal, monthly, or the daily variability, but rather the changes within hours, minutes, seconds, and sub-second periods. Wind possesses a highly unpredictable, and non-universal character, which is referred to as turbulence. These intermittencies in the wind speed create variable mechanical loads on the structure of wind turbines leading to fatigue, and ultimately failure. Identifying site specific qualities of the wind resource is very crucial in the design and selection process of the wind turbine.

Physical theories explaining wind turbulence phenomena over flat terrain have been critiqued and tested by observations, and in general, have achieved reasonable success in explaining surface layer wind dynamics that can be applied universally. This universality, and the extrapolation of flat terrain theories to complex terrain applications, breaks down most of the time due to the newly recognized spatial and temporal spectrum of interaction modes, mechanically and thermodynamically, with the surrounding complex terrain.

In terrain as found in New Zealand, most of the wind farm development is carried out over complex terrain, with ridge top and mountainous installations. In this study, an experimental campaign was carried out over a coastal ridge top, proposed for wind farming, to investigate mean and turbulent wind flow features significant for wind turbine selection and placement across the ridge. The steep sloped faces of the ridge, high wind speeds and its proximity to the sea made this location ideal for a benchmark investigation site. Ultra-sonic

anemometers, a sodar (sound detection and ranging) wind profiler, and high resolution LES (large eddy simulation) numerical modelling were all utilized separately and in an interconnected way to provide a comprehensive analysis of the wind dynamics over the ridge top. The three principal components of the investigation were: the effect of the upstream topography and the thermal circulation associated with the proximity to the sea on the observed and modelled wind shear vertical profile; the role that the near upwind terrain plays in shaping the turbulence energy spectrum and influencing the predicted spectrum, ultimately affecting isotropy in the flow field and turbulence length scales; turbulence advection from far topography, and the role that far upwind terrain plays in altering the wind turbulence in a measurement area or at a single point.

Results showed that the thermal wind circulations and upstream steep topography could dictate the wind shear profile, and consequently have a large impact on wind turbine height selection and placement. The sodar proved to be a very useful tool in identifying vertical shear zones associated with effects of steep upstream terrain, vertical mixing of horizontal momentum, and thermal circulation from the local sea breeze.

In complex terrain, the added multi-directional perturbations from the underlying roughness redistribute the statistical variations (measured by variances) in the three spatial dimensions. Isotropy, based on measured variances, was attained for both sites on the ridge. Isotropy also held true for the energy spectrum via Fourier analysis of the high temporal resolution data, but not for both sites. In general, local isotropy can be attained in cases of higher wind speeds and increased terrain relief. Measured spectral ratios did not converge to the limit suggested by the local isotropy hypothesis. These results identify contradictions in assessing the turbulence isotropy in both real space (statistically through variances) and Fourier space (through power spectrum analysis), which suggests caution in deriving or interpreting turbulence information for wind turbine design and selection.

2D-LES experiments showed that turbulent kinetic energy (TKE) can attain long range memory of underlying terrain, which can then react accordingly with upcoming terrain. Under the high wind speed scenarios, which are suitable for wind farming, and over relatively complex terrain, the flow retained some aspects of terrain information at least 30H (H is the terrain height) upstream and downstream of the terrain. In general, as the turbulence field travels over new terrain it tends to increase in intensity downstream of that feature. The newly modified TKE field acquires geometric features from the underlying terrain; mainly these features register as amplifications in the wave structure of the field at wavelengths comparable to the height of the underlying terrain. The 2D-LES sensitivity experiments identified key areas of high mean wind speed and turbulence in relation to terrain effects, all of which should be taken into consideration when thinking of locating a wind farm in such areas.

Acknowledgements

This accomplishment would have not been realized if I did not exist, so thank you **Najat** and **Hisham** for playing the most essential role in my creation and all the hard work you put into me. Now I know what these words exactly mean as I raise up **Meer** who is 9 months old, thankfully with my considerate and loving wife **Houda**.

I want to thank **Peyman Zawar-Reza** and **Andrew Sturman** for being outstanding supervisors. They have provided a professional, constructive, friendly and supportive environment that aided in the successful completion of my degree. I have been tremendously educated on science in both the political and technical arena by working with each one of them in a different beneficial way. They have provided excellent opportunities for widening my research application and methods, which I hope I can make use of all of them in the future.

Thank you for the **Department of Geography** and all colleagues and staff within it for hosting me, and providing a warm and relaxed atmosphere to carry out research in. Many thanks to all the people I shared interesting talks with, either professional or casual ones. In a way or another, every single thought in a conversation had its share in the outcome of this dissertation. Thank you **Justin Harrison** and **Nick Key** for the fieldwork setup**. Mainpower's** sponsorship and permission to conduct the fieldwork on their site is highly appreciated. Acknowledged also is **Tony Dale** from the High-Performance Computing Centre at the University of Canterbury (BlueFern), and **Colin McMurtie** for their efforts in keeping the super computer up and ready at all times, and help in computer code installation.

Part of this research was supported by a grant from the U.S. National Science Foundation through grant CDI-0941373 and ATM-0646299 in accordance with Michigan State University (MSU) and the U.S. Forest Service Northern Research Station (USDA). So I want to thank all the research staff in MSU and USDA, especially **Dr. Sharon Zhong**, for the special time I spent in Michigan.

Contents

Part I: Research Outline

1. Introduction

1.1. An initial statement

"Of each particular thing, ask: What is it in (and by) itself? What is its nature?"

Marcus Aurelius (121 to 180 AD)

The subject of this PhD thesis (Turbulence) has a high degree of uncertainty, no known universality and has been under intense research for more than 150 years, and remains a prominent unsolved problem in classical physics!! If that isn't difficult enough, turbulence is bounded by a solid undulating hard surface from underneath (the Earth) in a medium that allows an unwieldy spectrum of eddy sizes (the atmosphere).

The reader is encouraged not to run away from reading this dissertation, so please don't, but rather appreciate the complexity of the topic covered in it. The above mentioned "de-merits" are certainly not valid for the research presented here, but are almost certainly valid for the subject covered, which is turbulence, or to be more precise and to reduce the degrees of freedom, atmospheric turbulence.

The author will not attempt to define turbulence at this very early stage – if there is an appropriate definition, but will leave the reader to discover its properties as measured and modelled in a particular location in due course. The following sections in this chapter should provide a comprehensive introduction to turbulence, especially its theoretical development from the 15th to the 21st century. What should be mentioned is that turbulence is a subject that is viewed differently by different disciplines, and this is totally justified based on these disciplines' objectives, and the simplifications they apply to the subject. Engineers are forced to simplify it, and contaminate their solution with many semi-empirical formulations that are usually derived from physically bounded

lab experiments, while other numerical modellers tend to abuse computer machines to endlessly attempt to cast some light on the spatial and temporal scale invariance of the solution. Mathematicians are still competing to win the Clay Mathematics Institute 1 million-dollar prize for finding an analytic solution for the full Navier Stokes Equations. Other species, like salmon fish, don't try to explain it, but use turbulent eddy cycles, produced in the wake of rocks, to passively propel themselves forward to their spawning areas (Beal et al. 2006). The author of this thesis could be likened to a very well engineered salmon swimming with a bible of mathematics and physics, trying to escape the grizzly bear's bite, to reach the spawning grounds of new knowledge. Yet, by relying on vast contemporary computing power, he is still humbled by the subject's complexity.

While the attempts are ongoing, a universal theory that unifies turbulent flow solutions across various disciplines currently does not exist, and some mathematicians, like Phillip Saffman, have already expressed an opinion on the subject as follows:

"…Perhaps there is no 'real turbulence problem', but a large number of turbulent flows and our problem is the self-imposed and possibly impossible task of fitting many phenomena into the Procrustean bed of a universal turbulence theory. Individual flows should then be treated on their merits and it should not necessarily be assumed that ideas valid for one flow situation will transfer to others. The turbulence problem may then be no more than one of cataloguing. The evidence is against such an extreme point of view as many universal features seem to exist, but nevertheless cataloguing and classifying may be a more useful approach than we care to admit." *P.G. Saffman (1977)*

The present author cannot yet express an opinion on the subject with only 3 years of humbling experience, but can, on the other hand, probe the subject's hidden consequences in a real experimental and numerical domain for practical purposes. As a result, the title of this thesis indicates, the application of this experimental research campaign is towards understanding turbulent flow features over complex terrain to assist in proper siting of wind turbines in such

settings. Spatial and temporal scales of the phenomena are addressed by relevant instrumentation and methods. For this reason, a field measurement exercise was carried out sampling instantaneous wind velocities at 60 Hz temporal resolution, and collecting average vertical wind velocity profiles. In addition to the field measurement exercise, computational fluid dynamic simulations were utilized to supplement the analysis, focusing on some specific research themes.

Wind turbines are energy conversion machines. They harness the available kinetic energy of the wind and convert it to mechanical and then electrical energy via the generators inside the nacelle. Fortunately enough, nature has put limitations on human kind's greedy appetite for energy. According to the first law of thermodynamics and Newton's second law of motion, a wind turbine's maximum theoretical energy conversion efficiency (from kinetic to mechanical energy) is 60 %, this is also known as Betz's law. To convert 100 % of the wind kinetic energy leaves no air coming out the turbine swept area, and this would stop the airflow and the blades would stop rotating. Unfortunately, the 40 % lost energy is not the only price to pay, as turbulence is always present at high levels within the atmospheric surface layer, and should be avoided. The main sources of turbulence can come from a mechanical one (wind shear due to surface roughness), a thermal one (buoyant eddies accelerating upwards), or even an advected upstream source. All these sources will perturb the main streamlined flow and ultimately dissipate the mean energy into unusable heat, leaving behind it an intermittent flow causing vibration loads on any structure in its way. From whatever source it comes, the resulting cyclic and intermittent mechanical force from a multitude of spatial and temporal scales impinge endlessly on the wind turbine blades and structure, and can consequently reduce the expected life time (~20 years) of a wind turbine and its performance level. Therefore, turbulence also imparts economic cost. Identifying a site's turbulence intensity (in accordance with the International Energy Commission, IEC, standards) will dictate a suitable type of wind turbine installation. The IEC standards rely solely on statistics from 10 minute averages, and the turbulence spectrum information is derived from flat terrain experimental results. It is easily arguable that

turbulence over complex terrain varies significantly, in its length and time scales, from site to site. And standards, like the IEC ones, rely on this data for developing better regulations for building and installing wind turbines.

In this research, the sources of wind turbulence and its evolution are numerically assessed and put into context with available industry standards, as part of site suitability assessment for wind farming. The presented results are not by any means suitable for a decision on a wind turbine type for the proposed site, and this is because of the limited resources used and time constraint of the field work campaign. This work presents a scientific endeavour into identifying patterns, behaviours, and methods in turbulence analysis and research. The aspects of this work that make it attractive for turbulence research are two fold:

- The first is the proposed wind farm site itself and the design of the measurement campaign. The wind farm is located over a steep faced coastal ridge top with the coast downstream of the prevailing winds, which adds more complexity and difficulty in assessing the wind resource. Providing both a coastal and complex upstream terrain configurations, allows the investigation of the effects of different upstream topographic complexity on measured turbulence over the ridge line for two distinctive locations, and also the opportunity to look into the interference of the sea breeze thermal circulation winds with winds from the prevailing direction.

- The second attractive aspect about this work is the utilization of high resolution large eddy simulations (LES) in 2D and 3D idealized scenarios for assessing the interaction of the sea breeze with the prevailing winds, and the study of long range transport of turbulent kinetic energy. An LES formulation is designed to resolve explicitly the turbulent structures at the large eddy length scales in the domain and restrict parameterizations to the smaller eddy length scales. This increases confidence in the large scale (greater than the cutoff filter length) turbulent solution. The cutoff spatial filter is usually a function of the computational grid size. For the purpose of the introductory nature of this section, the author will reserve

providing details of the LES model used at this stage, and encourages the reader to follow up on this in Sections 4.2 and 4.3.

The research method incorporated in this work was inspired by the notion of analyzing the turbulence energy spectrum, in which energy cascades from large turbulent structures down to molecular dissipation going through the successively decreasing spatial scales (Frisch 1995). For this reason, the approach taken to this research involves use of the best available tools and analogous to the preceding sentence, a three step cascading strategy. The research cascade starts with an overall assessment of the wind resource in the proposed wind farm site, then goes into studying the effects of proximal upwind terrain features on various turbulent flow properties, and finally into studying effects of transported or advected turbulence from terrain features from a long range perspective. More details on each of these themes are provided in Chapter 3.

1.2. Background

1.2.1. Atmospheric turbulence, a brief history

Turbulence is a universal topic in atmospheric sciences because of its significant role in a range of practical problems, such as air pollution, aviation safety, and wind energy. Atmospheric flows can be confidently classified as fully developed turbulent flows due to the low viscosity of air (less than the viscosity of water by a factor of 10^3) and the large length scales associated with boundary layer flows ($\sim$1-2 km), which produce a Reynolds number (Re) in the order of 10^9. Probably the first scientist to provide a visual depiction of turbulence was Leonardo da Vinci (1452-1519), as some of his sketches of water flow in open canals and ducts showed streamlined water pouring out of a pipe and mixing into chaotic eddies or vortices. He also detailed flow around an obstacle with “horseshoe” vortex tubes forming around the sides with upstream blocking and lee side wake formation (Costantino and Sandro 1956). Da Vinci’s sketches recognize the importance of organized coherent structures in the flow and the significant variability of length scales that many basic theories of turbulence revolve around. The earliest descriptive studies of turbulence and transition from

laminar to turbulent flow resulted from experiments of Taylor and Bénard in 1923, and Reynolds in 1883, as outlined in Davidson (2006). The concept of laminar-turbulent transition was first proposed by Reynolds in 1883 – hence the famous Re –, while Taylor and Bénard's experiments revealed interesting flow structures relating to the instability of vortices and critical fluid velocities. Attempting to order the hierarchy of turbulence, Lewis Fry Richardson (1881-1953) suggested a cascading behaviour in which large vortices transport energy into smaller and smaller ones through a continuous one-way energy flux route, with energy consequently dissipating at the micro scale as heat. This theoretical idea is popular and robust, but the possibility that the cascade could work in the other direction (i.e. vortices of the same direction and frequency resonating to add more energy, lifting the system to a higher energy level, and consequently forming a bigger vortex) is still plausible (Hrebtov et al 2010; Scott and Wang 2005). The idea of the break up of large eddies into smaller ones and the existence of a spectrum of scales in the flow led Andre Kolmogorov (1903-1987) to define turbulent length/time/velocity micro scales that became universal in their application and are dimensionally related to the viscosity of the fluid and the energy dissipation scale. Kolmogorov's (1941a, b) theories have come to represent contemporary understanding of isotropic homogenous turbulence (same statistical quantities of turbulent flow along the three dimensions), and are valid under an extensive range of conditions. Statistical and semi-empirical theories of turbulence are numerous and problem specific, relying heavily on experiments to prove or disprove them.

1.2.2. Turbulence over flat terrain

In atmospheric turbulence, Geoffrey Ingram Taylor (1886-1975) pointed out the importance of eddy motion in the atmosphere and described mathematically the mechanism of vertical transport of momentum and heat by eddy motion, trying to explain the associated velocity profiles (Taylor 1915). One of the most relevant turbulence theories relating to atmospheric flows is the theory of boundary layer flows that was pioneered by Ludwig Prandtl (1875-1953), Theodore von Kármán (1881-1963), and Joseph Valentin Boussinesq (1842-1929), in which the concept of eddy viscosity originated for modelling the

transfer of momentum via turbulent eddies. This is described in the published work of Prandtl (1925, 1932, 1945) and von Kármán (1930, 1935). After that, it was well known and experimentally proven that the near-surface velocity profile, under neutral well-mixed conditions, can be modelled by a logarithmic profile with two universal constants. Similarity laws, relating complex turbulent processes with simple dimensionless surface variables, were then derived for more complicated parameters like wind/energy spectra and density fluctuations (Townsend 1956), and the Monin-Obukhov surface layer similarity theory was derived for modelling the mixed turbulent shear layer using the Obukhov length scale, which is a function of surface friction velocity and virtual potential temperature heat flux (Obukhov 1941, 1971). Since the development of Monin-Obukhov similarity theory many experimental studies were carried out to investigate its applicability, the most famous being the experiments held at the field station Tsimlyansk in Russia, where sonic anemometers from different countries (United States, Canada, Australia, and the former USSR) were used to undertake measurements (Tsvang 1985; Tsvang et al. 1973). In general, the Tsimlyansk experiments over flat terrain revealed similar energy spectra plots that followed the $5/3^{rd}$ law derived from similarity theory. Kolmogorovs's $5/3^{rd}$ law describes the universal relation of the energy spectrum of turbulence as a function of wave number at the high frequency end of the spectrum, otherwise called the inertial subrange (Uriel 1995). The only noticeable inconsistencies were the turbulent scalar fluxes and the measured variances. The variance inconsistencies were then justified by instrument calibration, while the turbulent scalar flux inconsistency was later explained by Tsvang et al. (1998), who showed that the inhomogeneous temperature field distribution over flat terrain had a direct effect on the turbulence characteristics, and this was not accounted for in the similarity theory. Moreover, the importance of variations in the flux footprint of the sensor was highlighted, which led to scatter in the results obtained.

The Kansas experiments (also over flat homogeneous terrain) followed those in Tsimlyansk under the leadership of Kaimal et al. (1972) who showed that the spectral plots of the neutral atmosphere at low frequency scaled according to the

Monin-Obukhov similarity theory surface parameters, while the high sampling frequency data showed inertial sub-range slopes of -5/3, and assessment of the isotropic nature of turbulence differed with stability conditions. In later work by Kaimal et al. (1976), measurements were taken throughout the well mixed convective boundary layer and showed that velocity spectra were similar throughout, showing a peak at the wavelength corresponding to the inversion height, and following the -5/3 inertial sub-range slope down to levels close to the ground with no discontinuity in the spectra. Based on the elaborate Tsimlyansk and Kansas experiments, more trust was put in similarity theory and despite attempts to disprove the theory in non-neutral conditions, it became well understood that in neutral well-mixed boundary layers large scale motions have no effect on the flow near the ground, and that relationships between variables in the surface layer are a function of the length scale z/L where z is the height above the surface and L the height where above which buoyant production of TKE begins to dominate over shear production.

Many experiments have been carried out over flat terrain under various stability conditions and the Monin-Obukhov theory has continued to be put to the test. Yaglom (1994) argued that the Kansas experiments were filtered at the high frequency range and by analyzing the variances of the horizontal velocities in a convective situation one can postulate new models that take into account large scale coherent structures that interact with surface layer turbulence. Hunt and Morrison (2000) and Hogstrom et al. (2002) have also suggested that the interaction between large scale and surface layer turbulence does exist. They derived a conceptual dynamic model explaining this interaction that can be stated as follows: during the turnover cycle of medium to large eddies, they hit the ground surface causing deceleration all through the eddy vertical length scale. The tops of those eddies are being continuously sheared by the mean flow driven by even larger scale eddies (for further details see Figure 1 in Hunt and Carlotti (2001)). According to the recent conceptual model, also referred to as a top-down approach, the process of eddy shedding in the shear zone of interaction between the mean flow and the top of the eddy, which has its lower part dragged by the surface, happens slower than that associated with internal

smaller eddy turn-over cycles, and thus energy is transported between the two scales of turbulent motion. Moreover, the total vertical velocity variance in the surface layer was shown to be a function of both surface turbulence that scales to the friction velocity and turbulence due to the blockage of upper layer eddies.

The idea of having two scales of turbulence is not new, but was pointed out by Bradshaw (1976) and Townsend (1961). Neglecting buoyancy effects, they proposed that large scale or "inactive turbulence" did not interact with the surface layer or "active turbulence". Instead, the existence of "inactive turbulence" resulted from a combination of a source of external vorticity and the zero vorticity field caused by pressure perturbations that oscillate from the surface layer and cause boundary layer waves. On the same line of thought, another mechanism was proposed by McNaughton and Brunet (2002), but for unstable atmospheres. They proved the existence of two interacting scales of turbulence, but in this case the interaction is initiated from the surface upward by unstable thermal eddies that rise and fill up the surface layer until they interact with the mean flow. The resulting body of warm air can be visualized as surface roughness, but on an elevated surface of air rather than the ground. As the mean flow hits the air bumps (rising from the surface), it folds upon itself forming cross-wise rolls of vortices that transform due to instability and flow perturbations into a horse-shoe or hair-pin-like vortex structure, referred to as the TEAL structure or (Theodorson ejection amplifier-like). Those TEAL structures continue to develop and break up into smaller ones going down the cascade to dissipation, while continuously new structures are formed and each goes through its own cascade of energy transfer towards dissipation. In McNaughton and Brunet's (2002) work, the experiments were carried out again over flat terrain with unstable upwind conditions generated over a dry area, ensuring the generation of large eddies prior to their advection across the sensors that were situated over a damp moist flat area. Evidence of outer layer and inner layer interaction was presented by spectral plots of horizontal velocities, revealing a gap in the spectrum and the occurrence of a double peak in the plots. Proof of interaction of the two layers was presented by an enhancement in the temperature flux spectrum in the frequency range of the

spectral gap in the velocity spectrum. McNaughton and Brunet (2002) suggested that the nature of interaction is through the coherent TEAL structures that are involved in turbulent heat exchange.

1.2.3. Turbulence over complex terrain

Flat terrain turbulence was and is still being extensively researched and generalized velocity, temperature and spectral characteristics have been well established by elaborative benchmark experiments (Kaimal et al. (1972); Tsvang 1985; Tsvang et al. 1973, with the occasional re-examination of the theory from time to time. This implies that there is always a necessity for more evidence that proves or disproves existing theory, or suggests a new turbulence theory.

The situation gets even more complex when inhomogeneous surface properties are examined, such as topographic complexity and moisture and temperature distributions that alter the near-surface turbulent fluxes and structures. General average behaviour of meteorological parameters in complex mountainous terrain is well described in many textbooks, such as Whiteman (2000), but the literature lacks any benchmark experiments describing the turbulence dynamics and structures that can help in model derivation and newer parameterization techniques. Until recently, whenever complex terrain turbulence was investigated the flat terrain assumptions and similarity rules were applied.

Early turbulence studies over slightly rough terrain, like sinusoidal hills, were conducted by Jackson and Hunt (1975) and a 2-D analytical solution of wind flow was presented, revealing flow modifications as a function of steepness. This was followed by a 3-D topographical component of the solution by Mason and Sykes (1979). Attempts to describe surface layer turbulence in accordance with Monin-Obukhov similarity theory were also conducted by Jackson and Hunt (1975). They suggested a two layer turbulence structure (upper and lower) with the lower near-surface layer in equilibrium with the terrain and surface layer similarity laws considered applicable. In the upper level, large scale eddies having length scales larger than hill length scale are transported across the terrain within a time period less than their own turnover time, following the rapid distortion theory discussed in Townsend (1972). Britter et al. (1981)

provided evidence supporting the rapid distortion theory by showing that the longitudinal variances decreased in relation to the vertical and transverse variances, as eddies rolled over the hill, suggesting a transfer of energy from the longitudinal component to the other two dimensions. Zeman and Jensen (1987) also supported this theory and showed that this transfer of energy happens in the near-surface layer.

The rapid distortion theory was not always reflected in observations when analyzing the variances and relating them to the eddy length scales as they pass over a hill top. Several studies showed small or no changes in streamwise variances (Bradley 1980 and Mickle et al. 1988). Panofsky et al. (1982) also showed, through observations of spectra over different fetch distances in complex terrain and surface types, that the response rate differs for small and large eddies. While the small high frequency turbulent eddies adjust to the new terrain quickly, the large low frequency ones still hold memory of the terrain upstream of the flow. They also provided evidence supporting the rapid distortion theory.

Experiments like this are very helpful in evaluating and developing theory, but prior knowledge of the turbulent boundary layer properties such as turbulent momentum and heat fluxes, and a general description of the boundary layer height and interaction with the underlying complex terrain, were lacking until the experiments of the Mesoscale Alpine Program (MAP) were carried out in the Riviera Valley, Switzerland (Bougeault et al. 2001, Volkert and Gutermann 2007). The key findings are summarized in Rotach and Zardi (2007). Based on MAP results, spatial variability of turbulent variables was not unexpected, and results suggested the use of spatially averaged turbulent flux rather than a single point value to represent the flux. This basically highlighted the importance of scintillometers for surface heat flux measurements rather than point measurements, essentially questioning the reliability of point measurements in complex terrain. Some surface layer scaling parameters adopted from flat terrain measurements were often used in the complex terrain situation and found to be valid (de Franceschi 2004). Also, the free convective velocity scale (w*) was suggested for use in non-dimensional turbulent kinetic energy (TKE) profiles

from the centre of a valley, although the surface heat flux from sloping terrain was used in the derivation of w*. The difficulty in selecting the sloping surface for this calculation was identified, since the up-slope and down-slope winds in complex topography strongly influenced the measurements (Weigel and Rotach 2004). Also, the dominant turbulent production component in the TKE budget was found to be shear production, although the measurements were taken on a sunny day with convective conditions (Weigel et al. 2005; Weigel at al. 2007). This is a direct effect of topographically induced flow modifications. Another result that highlights boundary layer evolution and thus governs the turbulence regime during both daytime and night time is the existence of a stable layer on top of a convective one during daytime and even in summer, which was explained for a straight valley by Rampanelli et al. (2004) to be the result of subsidence of stable air aloft to compensate for the thermally driven up-slope air, which damps the turbulence to some extent. As for more realistic curved valleys and mountain ridges, a secondary force due to curvature enhances the mechanism. Weigel and Rotach (2004) pointed out that the effect of the centrifugal force on the air following a curved path produced density differences in the cross-wise valley direction, and sometimes observations of upslope flows on shaded relatively cold slopes were observed. Although the MAP experiments did not concentrate on the details of turbulence mechanisms and airflow structures, it is obvious that in complex topography the sources of turbulence can be non-conventional, and large-scale circulations that develop in the Alps can definitely provide an insight into the dynamics of complex terrain turbulence and the mechanism of its formation.

Turbulence in all its scales of application — from molecular dynamics, to micro-fluids, to larger bounded engineering applications —, and in the highest Re cases in the atmospheric boundary layer (ABL), remains a grey area with many unanswered questions. Even after 100 years of research there are few hypotheses resulting in all-inclusive theory (Lumley and Yaglom 2001). As already discussed, most of the published work is descriptive and experimental, and aimed at proving or disproving a hypothesis. As for the complex terrain situation, it is clear that turbulence mechanism theories are still in their infancy

and their development can be either an extension from the flat terrain situation with modifications, or a newly proposed theory that will require further experimental evidence. Experimentally, we are always restricted by instrument capability and unfortunately there is no “super instrument” for turbulence visualization. Yet, as in assessing individual turbulent structures (coherent or non-coherent) this thesis is like all others, highlighting the aggregate behaviour of turbulent structures and relying on scientific imagination to explain them. This work provides an insight into air flow turbulence over complex terrain, under the framework of wind turbine siting, through in-situ measurements and high resolution modelling, in an attempt to provide further evidence in support of previous theories or to help in the development of new ones.

2. Wind Farm Siting techniques

2.1 Current micro-siting techniques

The energy harnessed from the wind is found to vary with the cube of the wind speed, so that an error in wind speed readings is raised to the power 3 when converting to the potential power production of a given site. It is this relationship that dictates the need to obtain accurate wind speed measurements for a particular site before the wind farm construction phase. A good wind resource is an essential criterion for the initial selection of a site, and understanding how wind speed varies over a period of time, usually a year or more, for a particular site should provide a reasonable estimate of its power production capability and allow a parameter called the availability factor to be obtained. The availability factor, which is the percentage time a site is able to produce power, can be deduced from wind speed and energy histograms. An ideal location for a good wind resource would be on high altitude flat terrain located inland or near the coast. Some wind farms are located in slightly hilly terrain to take advantage of the speed-up of wind near the tops of hills. Also, a wind farm site should be located in close proximity to an electrical distribution point easily accessible by personnel and vehicles, and away from populated urban environments.

After recording variations of wind speed and direction, a full resource assessment can be derived showing histograms and distribution plots of wind speed, direction, gusts, vertical wind shear, and turbulence intensity variations derived from descriptive statistics. Power curves showing the power changes with respect to wind speed, power density curves, and annual energy output can also be obtained. The above information should be derived for any kind of wind farm situation from the simplest terrain to the most complex (Burton et al. 2001, Sathyajith 2006). Basically, as the terrain gets more complex one cannot simply extrapolate or translate the measurements from one point to the entire field in vertical and horizontal directions. Ridges and steep slopes, trees and canopies, static structures, and soil property variability are all factors influencing the accuracy of assumptions made in dealing with wind resource assessment in both simple and complex terrain. Simple terrain can be characterized by a flat surface with very low surface roughness and consistent soil properties, and most importantly it has very little influence on the larger scale wind flow pattern. On the other hand, complex terrain causes significant perturbation of the incoming large-scale flow, producing turbulence and local fluctuations that are often very random in behaviour and hard to predict. Figure 1 shows some examples of wind farms in simple and complex terrain.

(a)

From: www.rpmaccess.com

(b)

From: www.treehugger.com

(c)
From: www.robertdawson.com

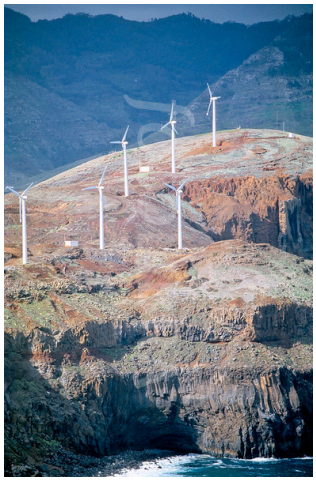

(d)
From: www.fotolibra.com

Figure 1. Four examples of wind farms in different terrain types: (a) is a simple flat terrain, (b) is a simple flat coastal terrain, (c) is a wind farm over rolling hills, and (d) exemplifies a coastal complex terrain site with steep terrain slopes.

Complex terrain can alter the wind speed distribution and consequently the power output of turbines. The topography can change the three-dimensional flow structure of the wind and cause speed-up regions with wind shear in regions of steep slopes, in addition to vertical motion. The vertical profile of wind speed often deviates from the well known logarithmic or power law profile derived for homogeneous simple terrain. The topographic features may cause aerodynamic imbalances and higher mechanical stress factors, which alter the design coefficients of turbine blades, leading to issues of design and selection. A comparative study of the behaviour of 24 experimental turbines was carried out by Migoyaa et al. (2007), illustrating the significant effect of topography in complex terrain on the performance of individual turbines.

Micro-siting is a step that proceeds after the general wind resource assessment of a potential site. It deals specifically with optimally locating wind turbines in the wind farm to increase overall power production from the whole wind farm. Turbulence is the major enemy for micro-siting wind turbines and its production can be mechanical (dynamic effects of terrain), thermal (due to surface heating and cooling), and from neighboring turbines whose wake or downstream turbulent air can affect the aerodynamics of the incoming flow of other turbines placed downstream. Thus, understanding as much detail as possible about the

airflow structure and the sources and dynamics of the turbulent flow over a wind farm will assist in proper wind farm layout.

There are two main methods for micro-siting a wind farm. The first standard strategy is a full-scale measurement plan in which extensive wind measuring equipment (sonic and cup anemometers, wind vanes, remote sensors such as sodars and lidars) are deployed over the site and spatially distributed (horizontally and vertically by erecting tower masts) to capture the wind flow patterns in numerous parts of the site. Data will then be collected over a suitable period of time, usually a year and sometimes more depending on the availability and the quality of the data, so that a detailed wind resource map can be derived depicting the wind patterns detected by the sensors and deduced from extrapolating and interpolating data (both horizontally and vertically). Long-term trends, more than a year can sometimes be obtained by correlating with measurements from a nearby site. This method is rather expensive and time consuming, requires continuous monitoring of equipment, and is often limited to application in homogeneous simple terrain in which wind movement is dictated by the large-scale motions during day and night, rather than from the effect of complex terrain. Moreover, the layout of turbines in a wind farm over simple flat terrain can be selected relatively easily since the only limiting factor is the wake effects of one turbine on another.

A more demanding strategy is required for more complex terrain. In this kind of environment it is hard to simply rely on measurements from anemometers and relate them to turbine locations, since these measurements can be greatly affected by topography and any extrapolation or interpolation can be misleading. A second strategy can therefore be used to deal with micro-siting issues. This requires a computational tool called a computational fluid dynamics (CFD) model, a strategy adopted in computational wind engineering (CWE) and gaining acceptance. However, the accuracy of the results can vary depending on the data used, model complexity and also the user. Mathematicians and physicists of the 18th and 19th century were responsible for the use and development of CFD models. Simply put, CFD is a technique used to solve the fundamental fluid flow conservation equations called the Navier-Stokes equations, which govern all

physical flow phenomena. With the aid of high speed numerical computing we can solve these complex equations that until now have no complete analytical solution. CFD solvers are numerous and each has an improvement or different technique for solving the conservation equations over the domain of interest. They are applied for viscous and non-viscous fluids, multiphase flows and aerodynamics, and from flows in nanometer tubes to large geophysical flows. Navier-Stokes equations coupled with heat transport equations can characterize the physical behaviour of the atmosphere in the boundary layer to a good level of accuracy. For the application of micro-siting of wind turbines there are a number of CFD packages available in the commercial market that are used extensively in the industry to model and simulate a wind farm under various wind flow patterns to derive the turbine design layout optimized for maximum energy output from individual turbines, and consequently the entire wind farm. Simply put, these computer codes divide the terrain into elements of a known size or volume, discretise the conservation equations and solve the resulting algebraic equations over every grid volume, sequentially in space and time. These solvers can be steady (time independent), unsteady (time dependent), compressible or uncompressible, viscous or non-viscous and the list of assumptions can be long, depending on the application and degrees of freedom the user is satisfied with.

One of the earliest models applied to wind farm micro-siting is the WAsP (Wind Atlas analysis and application Program) developed by the Wind Energy Department at Risø National Laboratory, Denmark (www.wasp.dk). The European Wind Atlas system (Troen and Petersen, 1989) relied on linearized models from Jackson and Hunt (1975) and Mason and Sykes (1979). It has been used for 20 years and is considered a reliable model for wind farm micro-siting, but with limitations. This model is not considered a full CFD model since it linearizes the Navier-Stokes equations before attempting to solve them, thus solving a very simplified version of them. WAsP is therefore based on linear equations than on the complete differential form of the conservation equations. These simplified equations are a result of removing terms describing viscosity to obtain the Euler equations, and then removing terms describing vorticity (or rotational motion) to obtain the full potential equations, and finally these

equations can be linearized to yield the linearized potential equations. An example of a CFD model that solves the non-linear Navier-Stokes equations is WindSim (www.windsim.com). It is a wind flow solver based on the 3D Reynolds Averaged Navier-Stokes equations. The model solves the atmospheric flow for a "steady-state" case for a chosen wind direction. By "steady-state" it is meant that the model is run until the solution converges to one wind and turbulence distribution for the entire domain that does not vary outside a pre-set convergence limit. By simulating for several different wind directions an annual average wind speed can be generated. This solver along with most CFD solvers requires at least one wind measurement from the site. The wind climatology can be derived from a weather station in the field and then be divided accorded to wind direction sectors of the model and translated to the entire grid, weighting it with the ratio of the computed wind speed between the climatology's location and the new location. A more detailed description of the wind direction sectoring method will be addressed in the following section.

Resolving the smallest-scale atmospheric boundary layer flow poses a huge computational challenge, and to overcome this scientists develop simplifications of the physical system and try to reduce the solution so as not to cover the full turbulence scale. An example of this is the ongoing development of large eddy simulations (LES). LES was first pioneered by Smagorinsky (1963), in which large-scale turbulence is fully resolved and the sub-grid scale effect is parameterized, based on the energy cascading principle. Details of the numerical process can be found in Mason (1994) and Sagaut (2001). Turbulence information is crucial for characterizing the cyclic structural loads that ultimately lead to fatigue and failure of the turbine structure. LES provides more accurate dynamic turbulence information as opposed to the traditional methods used in the European Wind Atlas system (Troen and Petersen, 1989) that were ultimately designed for flat terrain, attached flows, and relied on linear models from Jackson and Hunt (1975) and Mason and Sykes (1979).

2.2. Limitations of current techniques

Due to the linearizations mentioned in the previous section, linear models are suitable for simple terrain and their accuracy is rather questionable when applied to complex terrain. Many studies reported the underestimation of flow separation, turbulence intensities and gust measurements in the linear model solver, thus stressing the importance of using non-linear models in wind resource prediction (Palma et al 2008; Maurizi et al. 1998; Castro et al. 2003). Fully featured CFD models have an advantage over linear models in the way that they solve explicitly for average properties, and model or estimate the high frequency fluctuating components of these properties. Time averaging the original equations after introducing average and fluctuating components produces the Reynolds Average Navier-Stokes (RANS) equations. This technique of solving the RANS equations has been the basis of all CFD models and the accuracy of turbulence results relies significantly on the accuracy of the model being used to describe the turbulence closure equations. The implicit solution for turbulence is an advantage of most fully featured CFD simulations over linear model simulations. Nonetheless, sometimes a linear model can perform better for certain wind direction sectors for a given area of complex terrain when compared to observational data, as revealed in a recent comparison of WAsP and two CFD models (WindSim and 3DWind) Berge et al. (2006). However, as far as separation and turbulence is concerned, the two CFD models captured the phenomena while WAsP missed it.

Current CFD applications to micro-siting of wind farms have some drawbacks in reflecting the true nature of wind behaviour in complex terrain. A major assumption in most CFD models is the assumption of a neutral atmosphere throughout the domain under study, so that the modelled atmosphere can be considered thermally well mixed, justifying the assumption of neglecting the heat transport equation. In reality, however, a combination of thermal and mechanical turbulence production can occur due to the range of vertical temperature profiles normally observed. This limitation means that stratified flow (e.g. at night) cannot be realistically handled, and any thermally produced winds from local circulations such as sea breezes and up-slope flows are not considered in

the model simulation. This assumption of a neutral atmosphere simplifies the models being used and requires less computational effort, since the coupling between the energy equation and momentum equations is not required. Differential heating of complex terrain due to different slope orientations can cause local instabilities and may produce vertical shear and thermal turbulence that are not taken into account when dealing only with a neutral atmosphere. Another limiting factor is the steady state approach adopted by some CFD tools, as described in the previous section, which requires a finite number of wind directions to be applied in the derivation of the annual average wind speed. This is referred to as sectoring the wind flow domain with respect to direction. In this case, the long-term wind speed is composed of wind flows from all different directions. For example, 12 sectors may be selected and solved individually using a steady state approach and then integrated over the entire domain. Turbulence is a time varying phenomenon and might be under-estimated through the process of direction sectoring. A third drawback in using the CFD approach to micro-siting is in not including variations associated with meso-scale flow (few to several hundred kilometres spatial resolution), which links vertical stability and the effect of the large scale wind flow.

3. Research themes and objectives

3.1. Thesis structure

The reader is encouraged to read this section that provides a description of the logical structure of the thesis. By the time this thesis was written, three manuscripts had been produced based on its material (M1, M2 and M3 introduced in chapters 4, 5 and 6). Manuscript M1 is in preparation for sending to the peer revision process, M2 is already peer reviewed and published in the Journal of Boundary-layer Meteorology, and M3 is also peer reviewed and published in the Journal of Atmospheric Chemistry and Physics Discussions. Chapters 1 and 2 introduced the research background and its relevance to the scientific community. Chapters 4, 5 and 6 include an insert of the actual manuscripts and published papers as they appear in their relevant journals that cover the carried out work in accordance with the main research themes

included in the prefaces in sections 3.2, 3.3 and 3.4. Finally, chapter 7 concludes with a summary and future perspectives of this research.

The main objective underlying this thesis is to understand, quantify, and analyze the difficulties that arise from wind turbine siting in complex terrain. Effects of localized flow features related to upwind topography and coastal proximity of the proposed wind farm site would be put in context with the overall quality of the wind resource, where, 'quality', means the turbulent or intermittent component of the wind. This research utilizes state of the science atmospheric numerical models and in-situ field measurement techniques to explore wind turbulence and flow variations over a proposed wind farm site. The proposed wind turbines will be sited over an isolated ridge located in a coastal setting, thus creating an ideal environment to examine the interaction of different flow regimes resulting from synoptic and meso-scale atmospheric forcing and their interactions with the proximal and distant complex topography.

A breakdown of the main objective reveals three more focused research themes, which will be outlined in the following sections that include prefaces to the more in depth focus in each of the presented manuscripts.

3.2. Preface to manuscript M1

This manuscript is entitled: Ridge-top surface layer wind dynamics as seen by a SODAR and a large eddy simulation experiment. The manuscript attempts to quantify the wind resource over the proposed wind farm site and assess its suitability for wind turbine placement. Vertical profiles of wind speed and direction were measured between January and April 2009 by utilizing a sound detection and ranging instrument (SODAR) placed on the highest point of the ridge-line. The sampling period represents the time of the year when the wind resource is at its strongest, and mainly blowing for the north-west direction.

The investigation is mainly focused on the effects of upstream topography and the site's vicinity to a water body (Pacific Ocean) on the measured wind speed and direction vertical profile. Wind shear models used in the industry were also tested against measured data. This method is used to outline the difficulties in using flat terrain techniques as the basis for siting wind turbines over coastal

ridge tops, and to understand the flow dynamics responsible for these effects. To complement the understanding of features revealed by the sodar measurements, 3-dimensional idealized atmospheric model simulations were carried out over the same area. These simulations were intended to reproduce the thermal circulation of the land and sea breeze over the ridge top to aid in the analysis of the sodar data.

As a result, this manuscript sets the large scale flow picture into perspective with the ridge top wind farm site and investigates the effects that might alter the wind shear profile from the well-used neutral wind profile in the industry. The manuscript covers the first step of three research themes that define the main focus of this thesis.

3.3. Preface to manuscript M2

This manuscript is entitled: An investigation into ridge-top turbulence characteristics during neutral and weakly stable conditions: velocity spectra and isotropy. The manuscript attempts to present a closer (spatial and temporal) insight on the effects of proximal upwind topography on measured turbulence during a high wind speed event scenario, and examine the fine details of turbulent length scales, velocity spectra and isotropy, comparing the results to standards used in the industry. It presents a natural transition from the research focus of manuscript M1 by focusing on smaller scale phenomena related to turbulence that would be very useful in the decision making of wind turbine selection and siting and in addition to the current knowledge of ridge-top wind turbulence.

The motivation for this research theme can be summarized as follows:

1) To understand surface layer turbulent flow characteristics in very complex terrain situations, which will highlight causes of the variable and unpredictable nature of turbulence over steep ridges as a function of near upwind terrain complexity and thermal forcing.

2) To reassess the application of current spectral theories of turbulence to more complex terrain configurations for the selection of wind turbines, highlighting new situations where these theories can be further critically examined.

Two ultra-sonic anemometers collected data from two sites along the ridge top comprising different upwind terrain characteristics, after which turbulence properties (velocity spectra, turbulent length scales, and isotropic turbulence evaluation) were deduced via the Fourier-spectrum analysis. The experimental setup is ideal in the sense that it permits examination of turbulent flow regimes along a ridgeline with different up-wind terrain characteristics, as well as providing an insight into the variability of these regimes under strong winds when a near neutral ABL is expected.

3.4. Preface to manuscript M3

This manuscript is entitled: Long-range transport of terrain-induced turbulence from high-resolution numerical simulations. The manuscript attempts to examine the long-range transport of turbulence kinetic energy (TKE) produced by terrain upwind of the ridge top and its significance for the optimal siting of wind farms. Being the third and last research theme its research focus is transferred from proximal alterations of the wind flow by terrain to the distant terrain effects and its implications.

Acquiring real measurements of turbulent eddies, or coherent turbulent structures in the ABL can be a very difficult task, especially if large area measurements for long periods of time are required. The limitation is the absence of an instrument that can take a long range snapshot of turbulence as the eddies travel over terrain, interact with each other, change in their productive and dissipative properties, and are then observed tens of kilometres downstream of their source. Through Large Eddy Simulation (LES), the long-range transport of turbulence generated by topographic features in the ABL is examined. The research approach in this theme is purely numerical, and this is due to the technical and economic difficulty in measuring TKE at such a large scale. The basic idea behind the current design of numerical simulations is to be able to simulate a high wind speed scenario that is capable of generating

consistent turbulent eddies or rotors in the wake of a terrain feature. The perturbations produced by the terrain feature travel downstream over a relatively long distance of approximately 20 km before they encounter an experimental series of terrain configurations with varying aspect ratios (AR). The turbulent intensity of the rotors as they travel downstream over terrain of varying steepness or AR is also examined.

This research theme, in addition to the previous two, complement each other by providing a detailed record and analysis of wind turbulence and its relevant phenomena occurring at a variety of length and time scales. The three research themes and their respective implications will help in the proper siting and selection of wind turbines and prospecting of future wind farms in New Zealand. In addition to that, this knowledge will provide a deeper insight into the underlying scientific phenomena that governs such processes.

With the above introduction to the three research manuscripts that will be covered in following three chapters, the main research aim is now broken down into three more focused research aims:

1) To investigate the overall wind dynamics measured between January and April 2009 and the effect of the thermal circulation of the sea breeze on wind energy production and the modelled velocity profile.

2) To identify the effects of proximal upwind topography on measured turbulence during a high wind speed event scenario, and examine the fine details of turbulent length scales, velocity spectra and isotropy, comparing the results to standards used in the industry.

3) To examine the long-range transport of TKE produced by terrain upwind of the ridge top and its significance for the optimal siting of wind farms.

Having a detailed record and analysis of such physical phenomena, occurring at a variety of length and time scales, will help in the proper siting and selection of wind turbines and prospecting of future wind farms in New Zealand. In addition to that, this knowledge will provide a deeper insight into the underlying scientific phenomena that governs such processes.

4. Research manuscript M1

RIDGE-TOP SURFACE LAYER WIND DYNAMICS AS SEEN BY A SODAR AND A LARGE EDDY SIMULATION EXPERIMENT

Marwan Katurji *, Peyman Zawar-Reza, and Andrew Sturman

Centre for Atmospheric Research, Department of Geography, University of Canterbury, Private Bag 4800, Christchurch 8140, New Zealand.

* Corresponding author: marwan.katurji@gmail.com

Abstract: Sodar measurements over a coastal ridge top, a potential site for a wind farm, were made over a period of 4 months during which vertical profiles of wind velocity were assessed up to a height of 300 m. Day and night average profiles revealed significant differences over the entire sampling period, these differences were related to the interaction of locally generated thermal winds, such as sea breezes, with synoptic weather patterns. The maximum difference between average day and night wind speed magnitudes reached 1 m s-1, which equates to a relative wind power density loss of 37%. The industry standard assumption of a neutral surface layer wind speed profile failed to fit the real data, but a power law profile with a shear exponent coefficient of 0.05 provided a better fit, resembling a convective surface layer shear profile. Evidence of an Ekman spiral was observed, and this should be taken into consideration if large wind turbines were to be selected for this site. Vertical profiles of averaged wind speed revealed three distinctive zones with different wind dynamics. High resolution three-dimensional large eddy simulation model results were very similar to observed wind measurements and captured the same dynamic character that was observed by the sodar.

Keywords: *Ridge top winds, sodar, wind shear models, large eddy simulations*

BACKGROUND AND INTRODUCTION

The terrain of New Zealand is known for its complexity and mountainous character, and its location across the prevailing synoptic westerly winds – the 'Roaring Forties' – provides it with an excellent wind resource, varying across the country with an annual average between 6.5-10.5 m s^{-1} (Sinclair Knight Merz 2006). The current installed wind energy capacity feeds 3% of the total electricity demand and is expected to grow to 15-20% by the year 2025 (NZWEA 2009). With the projected plan for investment in wind farming and the difficulty in wind resource assessment in complex terrain comes the necessity of accurately representing hub height (the height of the center of rotation of the turbine blades) wind speeds and wind shear across the diameter of the blades. Current methods for estimating the vertical profile of wind velocity for potential wind farm sites include very simple methods relying on surface wind measurement extrapolation using an empirical wind profile law for a specific atmospheric stability case; applying a correction to the estimated wind profile model equation using atmospheric stability parameters; using wind profilers to measure the wind shear; or applying a computational fluid dynamic numerical model to simulate the wind field over the desired domain. Although these techniques are standard in the wind energy industry, refinement of methods and testing their applicability over complex terrain are always required when increasingly sites selected for wind farm development experience various atmospheric stability constraints and complex localized meteorological conditions.

Ridge top wind speed distributions can vary considerably given the direction of the wind, atmospheric stability, and turbulence intensity. The vertical profile of horizontal wind speeds can significantly deviate from the logarithmic or power law empirical models, which are more suited to simple flat terrain cases. Coastal sites present other challenges, where winds have a local diurnal variation altering the profile and making the prediction of wind speeds from profile models very difficult (Perez et al. 2004). Even the power law speed profile based on a vertical extrapolation of surface wind speeds has shown many discrepancies in calculating its coefficients in relation to the time of the day and

also the season (Rehman and Al-Abbadi 2007; Farrugia 2003; Hussain 2001). Topographic features alone, without any variations in atmospheric conditions, can induce variable and unpredicted stresses on turbines located downwind of them. Migoyaa et al. (2007) investigated the effects of topography on individual turbine power output and related high uncertainty in the measurements to the position of the turbine in the topography.

Vertical wind profilers, especially sodars (sound detection and ranging – or acoustic wind profilers), have been used extensively in the wind energy industry, given the cost advantage over anemometer-equipped towers. Many studies have derived reliable wind speed and direction measurements from sodars with regression correlations reaching 0.95 against tower measurements (Vogt and Thomas 1994; Crescenti 1997; Dupon and Flori 2007). The performance of a wind turbine depends strongly on the vertical wind shear profile, which can show a high degree of variability both in time and space. Ideally, measurements from more than one level in the atmosphere for different sites are required in complex terrain. The mobility of a sodar therefore provides an economical and logistical advantage over traditional anemometer towers. Dupon and Flori (2007), when comparing the performance of three different sodars to the measurements made by sonic anemometers, provided evidence that the error in derivation of the vertical profile of wind speed can decrease by a factor of 3 when compared to a power law derived from a surface cup anemometer measurement. Although a sodar can be affected by fixed echoes from ground clutter, background noise and rain, and may need calibration as outlined in de Noord et al. (2001), Mellinghoff and Albers (2000) and Crescenti (1997), proper experimental design and sampling methodology can minimize measurement error.

In general, little is known about wind flow dynamics over ridge tops leeward of complex terrain, and although there are many scaling parameters and applied theories explaining surface layer dynamics, many do not apply to complex terrain and have been developed strictly for flat terrain or simple hilly landscapes. For that reason, and in an attempt to understand the wind flow dynamics over a complex coastal ridge top proposed for the development of a

wind farm, the results of a combined measurement and high resolution numerical modelling experiment are presented. The key objectives are to outline the difficulties in using empirically derived wind shear models for wind resource assessment in highly complex situations, and to understand the wind dynamics that can cause difficulties in siting wind turbines in similar complex sites. This research is the result of a 4 month experimental study carried out using sodar measurements averaged over 10 minutes, with their analysis coupled with large eddy simulation (LES) model results from a comprehensive atmospheric numerical model developed for storm and tornado scale studies called ARPS – Advanced Regional Prediction System (Xue 2000).

EXPERIMENTAL SITE DESCRIPTION

The potential wind farm site used for this investigation is located on Mt Cass, about 6 kilometres east of Waipara in North Canterbury, New Zealand, as shown in Figure 2a. The proposed wind farm project is expected to generate 41-69 MW of power that will supply between 11,000 to 24,000 homes (Mainpower 2009). The Mt Cass wind farm will be developed along a 6.5 km long ridge and between 26 and 83 turbines will be located along this ridge line (depending on the model selected). The ridge is oriented south-west to north-east, so that its northwest slopes are perpendicular to the 350 degrees azimuth direction, with the Pacific Ocean coast to the south south-east. The ridge line height above sea level varies from 450 m to 525 m at Mt. Cass, which is the highest peak on the ridge. The northwest face of the ridge is characterized by an average slope of 14 degrees, as shown in Figure 2b. The terrain is very complex in nature, characterizing the site as being an island of complex topography situated in relatively flat terrain on the lee side of the main South Island's mountain divide, with the sea on the eastern side. Both the western plains and the eastern coast on either side of the ridge top can be seen in Figures 12a and 12b.

ANALYSIS OF RESULTS

Data were collected using a Scintec Flat Array Sodar (SFAS) placed on the peak of the Mt. Cass ridge. The sodar was not repositioned during the collection period and its location coincided with two previous sodar measurement campaigns, one of which was carried out using an Aerovironment 4000 mini-Sodar and the other

by a Remtech PA2 sodar (Reid 2002). The sodar was setup to measure up to 350 m above ground at 5 m intervals and recorded 10 minute averages. The measurement period extended for the 4 months of January, February, March and April 2009. This period includes the peak summer months of January and February, and the early autumn period in April when the lower sun inclination leads to changes in the thermal structure of the atmosphere. There was some missing data associated with low signal to noise ratios, which was because of the high ground level noise resulting from the wind interacting with nearby guy wires from meteorological and communication towers, and with vegetation. The total amount of available and unavailable data is illustrated in Table 1 at three different height levels. Data was sorted into day and night categories, where day corresponds to 08:00 am (LST) to 08:00 pm and night is 08:00 pm (LST) to 08:00 am.

The frequency distribution for wind velocity and direction at 30 m, 60 m and 80 m for the entire period is presented in Figure 4. The diagrams reveal that the highest wind energy containing sector was the northwest, reaching about 10% of the time at 80 m height. The second highest energy containing sector was the southwest, occurring for almost 6% of the time at the same level. Another feature is the north-east wind sector which is a dominant wind direction on the Canterbury Plains. It results from the lee-side pressure drop as westerly winds traverse the main mountain ranges of the South Island, forcing winds from the north-east into this region of reduced pressure, which can also be amplified by the sea breeze component. A common phenomenon also depicted in the average wind-rose diagrams is the backing of wind with altitude, which is shown clearly by the wind-rose arms as they shift anti-clockwise with height. This phenomenon is the Ekman spiral and is the dynamic result of the interaction of the Coriolis force with surface friction as winds approach the ground surface. This is again shown in the vertical profile of wind direction in Figure 7.

The monthly mean surface pressure charts in Figure 5 were derived by averaging daily surface pressure values from the 2.5 degree (276 km) resolution NCEP reanalysis gridded data. The averaged mean sea level pressure charts indicate the position of the high pressure zones that dominated the average

synoptic flow field over the respective months. January and March were similar in regard to the location of a high pressure zone to the northwest of the country. The interaction of this pressure field with the mountains of the South Island resulted in strong winds from the northwest direction. However, March had the high pressure zone slightly more to the west resulting in more frequent and stronger southwest winds (Figure 5c). February, on the other hand had wider isobars located over the South Island, with a very weak south-westerly synoptic wind (Figure 5b). This weak synoptic influence resulted in more frequent thermally generated local winds from the northeast and southeast sectors, as shown in the wind rose in Figure 4b, which is also reflected in the weak average wind speed. The final month of April had its high pressure zone located to the northeast of the country (Figure 5d). This situation resulted in a weather pattern where northwest winds picked up in intensity, but not as frequently as the northwest winds in January and March. However, the northeast to southwest pressure gradient increased the intensity of the northwest winds, as shown in the wind rose of Figure 4d.

OBSERVED VERTICAL SHEAR PROFILES

Averaged vertical profiles of horizontal wind speed for the total period, day and night times for the 4 month period are presented in Figure 6, with the vertical profile of wind direction in Figure 7, averaged on the hour and representing the previous 2 hour averaging period. In general, the wind speed profile is relatively uniform in the vertical, varying less than 1 m s^{-1} from 60 to 300 m. The wind speed profile can be separated into 3 main vertical zones, the first being a low level zone (A) up to 60 m, the second being the middle zone (B) between 60 and 125 m, and the third a high level zone (C) from 125 to 300 m. Zone A is characterized by the strongest wind shear associated with the steep slope of the ridge upwind from the sodar, and is consistent for both day and night-time periods, as shown in Figure 6. Zone B represents the height range within which wind speed exhibits less shear compared to zone A, changing by around 0.5 m s^{-1} for the night-time average profile and less than that for the daytime and total average profiles. Zone B's upper limit, at 125 m, clearly marks the location of maximum wind speed associated with elevated night-time layers decoupling

from the surface. This is associated with decaying daytime turbulence, as the near-surface stable layers develop over the night, reducing the thermal component of the turbulence budget. The largest difference between night-time and daytime profiles is well represented in zone C. Within this zone and the upper half of zone B, the daytime wind speeds decrease in magnitude compared to the night-time profiles, starting with a difference of 0.5 m s^{-1} at 125 m and reaching maximum of almost 1 m s^{-1} at 300 m. This difference is small, but it equates to a relative wind power density loss of 20% to 37%, given that the most frequent energy containing winds are from the west. This daytime reduction of wind speeds results from the development of winds from the easterly quarter due to the local sea breeze circulation system and the orographic trough on the lee side of the Southern Alps that is associated with the synoptic westerly winds. Evidence for this is provided in Figure 7, which shows the more variable daytime wind directions compared to the steady night-time wind direction, and clearly indicates the shift in wind direction from a north-westerly direction during the night to a more easterly one during the day. The directional shear presented in the vertical profile in Figure 7 is an indication of the Ekman spiral, with winds backing with altitude. There is also consistency between the shear zone A in the wind speed profile and that in the direction profile, so that zone A can be clearly seen as the surface shear layer up to around 60 m. The diurnal evolution of the 2 hour average wind speed profile is presented in Figure 8. The night-time hours are associated with the development of the elevated jet-like profile as discussed earlier, and the reduction of the daytime wind speeds from 100 m upwards is clearly shown as the thermally generated easterly winds develop.

ASSESSMENT OF VERTICAL WIND PROFILE MODELS

The shape of the vertical profile of wind speed can be directly linked to what is happening at the surface and to what level the thermal and mechanical friction exchanges are reaching. In general, and assuming that thermally-induced momentum transfer is limited to the surface and is less than the mechanically-induced momentum transfer, the wind speed profile takes the shape of the well known logarithmic neutral profile, and this is within the surface layer (up to 100-200 m). The profiles in strong convective situations can cause very vigorous

mixing in the surface layer (the first 20% of the convective boundary layer) resulting from thermally-induced turbulence carried by strong convective cells (Santoso and Stull 1998). This mixing can cause near-surface winds to increase more rapidly than is predicted by the logarithmic neutral profile and to become uniform with height closer to the surface. The empirical wind speed profile that describes this situation is the radix-layer profile model, which is an exponential function with coefficients relating the effects of the surface friction velocity scale (u_*) and the Deardorff convective velocity scale (w^*) to the momentum budget. During stable night-time conditions, thermal turbulence is damped as the surface cools and stratified layers are produced throughout the surface layer causing the wind speed profile to take a linear form increasing more rapidly with height than that of the logarithmic neutral profile (Stull 1988).

For wind energy applications the most likely operating atmospheric stability regime is the neutral one. In a neutral atmospheric condition, strong winds are responsible for mechanically mixing momentum through the surface layer (up to 100-200 m) so that it is evenly distributed, making the wind speed vertical profile uniform with height. This is true as long as there are overcast conditions limiting the strong surface heat fluxes that could make the atmosphere unstable. Although the logarithmic profile is mostly used in neutral stability conditions, there are correction factors that allow it to be used in stable surface layers, as outlined in Stull (1988) and Garrat (1992), and also presented in Equations 1 and 2. Because this profile applies under strong wind conditions it is therefore the preferred one for wind energy applications.

$$V_z = \frac{u_*}{k}\left(\ln\frac{z}{z_o} - \psi\right) \qquad (1)$$

where, V_z is the wind speed at height z

u_* is the friction velocity

k is the Von Karman constant (0.4)

ψ is the stability correction factor.

For a stable atmosphere: (L > 0) and $\psi = -5(z/L)$ or $-6(z/L)$

For an unstable atmosphere: (L < 0) and ψ = 2ln [(1 + A)/2] + ln[(1 + A)/2] - 2arctan(A) + π/2, where A=(1–16(z/L))$^{1/4}$

where L is the Monin–Obukhov length

For a neutral atmosphere: (L>>>) and ψ= 0, making the equation reduce to:

$$V_z = \frac{u_*}{k}\left(\ln\frac{z}{z_o}\right) \text{ or } V_{z2} = V_{z1}\left(\frac{\ln z_2/z_o}{\ln z_1/z_o}\right) \quad (2)$$

where, z_o is the Davenport-Wieringa roughness length scale.

Although the logarithmic profile is applied in numerous engineering applications and to flat terrain with simplified meteorological conditions, it is sometimes controversial when applied to complex terrain or even to sites close to the coast. A coastal site can have wind speed profile evolution from stratified night-time flows to convective daytime sea breezes making the prediction of wind speeds from profile models very difficult (Perez 2004). Even if the neutral atmospheric assumption was valid, a proper choice of the roughness length (z_o) for ridge top measurements is not defined in the literature. Normally, the Davenport-Wieringa roughness length classification (z_o) is based on a flat terrain 8 category landscape classification process from very smooth surfaces such as over sea or snow (z_o=0.0002) to chaotic centres of large cities or irregular forests (z_o >2) (Wieringa 1992,1993).

Another preferred wind speed profile model for wind energy applications is the power law speed profile based on a power law vertical extrapolation of surface wind speeds (Equation 3).

Power law wind shear model: $$\frac{V_{z2}}{V_{z1}} = \left(\frac{z_2}{z_1}\right)^e \quad (3)$$

where, z1 is the reference height at which the surface measurement is taken and e is the shear exponent.

The power law profile is very simple to use and represents all stability conditions with one power exponent variable (e). Empirically, it was found that

for neutral conditions that e has the value of 0.143, while for unstable convective conditions the shear exponent is lower and can reach as low as 0.05 (van den Berg 2007), and for stable conditions the profile has a shear exponent around 0.7. This law, although a good estimation for many engineering boundary layer applications, has generated many problems in calculating appropriate shear coefficients for different times of day and seasons (Rehman and Al-Abbadi 2007; Farrugia 2003; Hussain 2001).

Since the neutral logarithmic profile and the power law profile models are empirically evaluated for the surface layer, the analysis in this research paper to determine the best model fit for the observed sodar measurements was applied up to 150 m, or up to the upper limit of zone B. According to the wind speed profile in Figure 6, and as discussed earlier in Section 4, the 150 m height level clearly marks the layer above the ridge top at which the night-time winds accelerate after being decoupled from the decaying daytime thermal turbulence beneath. For assessing the validity of the neutral logarithmic profile assumption of Equation 2, and the power law profile of Equation 3, vertical profiles were extrapolated according to the model equations from 30 m reference values (as would apply if a 30 m high anemometer tower was to be used) and presented in comparison with the real sodar measurements. As shown in Figure 9, the daytime periods are separated from the night-time periods to isolate the effects of atmospheric stability, and three different values where selected for the roughness length scale used in Equation 2 and the shear exponent value (e) used in Equation 3. The roughness length scales used for the logarithmic profiles in Figures 8 (a, b, c) correspond to the following classifications, respectively, as they appear in the legend of Figure 9b: z_o=0.0002 (for a sea/snow covered/paved area classification), z_o=0.03 (for an open grass prairie/tundra classification), and z_o=2 (for a chaotic/centre of large cities/irregular forests classification). As for the shear exponent (e) used for the power law model profiles, they correspond to the following definitions as they appear in the legend of Figure 1e: e=0.143 (for a neutral atmosphere assumption or what is know as the $1/7^{th}$ power law), while e=0.08 and e=0.05 were selected to produce a better fit. The results in Figures 8a, b, c clearly show that the neutral

logarithmic profile fails to fit the sodar measurements for the various roughness length scales based on the defined classifications. The selection of the roughness length scale of 0.0002 (for the sea classification surface) was of course unrealistic, since the terrain over the ridge top is not remotely similar to the sea surface. Again, for the results in Figures 8d, e, f the closest power law model fit was for the shear exponent value of e=0.05, especially for the night-time and total average plots. This value of shear exponent surprisingly is not representative of the neutral profile assumption, but of strongly convective conditions. There seems to be a clear distinction between the daytime and night-time fits, and for both the logarithmic and power law model the night-time fits are better. Daytime thermal activity and the shift in wind direction towards an easterly flow can easily modify the profile, resulting in a greater difference.

LARGE EDDY SIMULATION EXPERIMENTS AND ANALYSIS

The Advanced Regional Prediction System model (ARPS) was used to run three-dimensional simulation experiments in an attempt to shed light on the surface layer meteorology of the ridge top, and to complement our understanding of features revealed by the sodar data. ARPS was developed by the Centre for Analysis and Prediction of Storms (CAPS) at the University of Oklahoma (Xue et al. 1995, 2000, 2001), and was specifically designed to simulate tornados. The model is capable of resolving atmospheric phenomena to a high degree of accuracy using large eddy simulation (LES) techniques. LES solves explicitly for the large energy-containing eddies, but it parameterizes the smaller universal eddy scales using sub-grid scale models. ARPS was used in several successful studies simulating steep valley flows down to a horizontal resolution of 150 m and vertical resolution of 20 m close to the ground (Chow et al., 2006; Weigel et al., 2006). Dupont et al. (2007) used ARPS in a 2-dimensional mode to investigate turbulent flow over a forested hill to compare with wind tunnel experiments.

Since the sodar measurements were taken over the 4 months of summer, ARPS was used to simulate the complex behaviour of winds over the experimental site during similar conditions in January. The reasoning behind this experiment is that ARPS should clearly resolve flow features that the sodar measured over the

ridge and give a clear indication of typical timing and magnitude of the wind system that dominates at this location. A 5-level nested grid setup was used starting at a horizontal resolution of 9 km, with the highest-resolution grid having a grid spacing of 250 m with 20 m vertical resolution close to the surface (Table 2). Grid nesting to higher resolutions forces the model to resolve flow at smaller spatial scales. Terrain information was specified to the model from an external surface elevation dataset. Information about the treatment of the lateral boundary conditions for each grid is provided in Table 2, alongside model grid setup and initial conditions. A dry, statically stable north-westerly flow, which is typical over Canterbury, was imposed on the modelled domain for the duration of the simulation.

Results from the highest grid resolution were extracted and saved every 5 minutes of integration time so as not to lose any details of the flow dynamics with long term averaging. For comparison, the U-velocity (east-west component) was extracted from the location in the grid corresponding to the sodar location on the ridge top. Time-height cross-sections were plotted for the entire model height, as presented in Figure 10a, and also up to 312 m, as presented in Figure 10b. In addition, 2 distinct individual time-height cross-sections of filled contour plots were extracted for 2 specific days in January from the sodar measurements (Figures 9c and 9d). Key features of the model simulation results in Figure 10a are the flow acceleration zones, marked by the (B) black arrows, and which develop during early night-time periods between 110 and 300 m and late night to early morning at higher altitude between 150 and 300 m. There is also a clear intrusion of the easterly sea breeze winds, characterized by the negative velocity values, as they undercut the drainage and synoptic westerly winds along the interface C1 (Figure 10a). This interface started developing from the morning, and then a more fluctuating pattern marked the evolution of a turbulent shear zone between westerly winds aloft and easterly winds below. This layer is referred to as interface C2 in Figure 10a. The shear interaction along the interface C2 causes downward momentum transfer from this layer to heights of around 150 m. The high speed downward intrusions are clearly marked with the arrows labelled A. This interaction, according to the simulation, adds more

evidence to the analysis as to why the sodar daytime wind speed profiles, in zones B and C, defined earlier in Figure 6, are less than the night-time wind speed profiles in magnitude. It is now evident that the interaction of the easterly winds undercutting the westerly winds causes the reduction in wind speed in zone B and above (Figure 6). Selected samples of the time-height cross-sections of U-velocity from sodar measurements, shown in Figures 9c and 9d, illustrate the same sort of behaviour as depicted in the simulation. There is the same evidence of downward momentum mixing of stronger winds aloft that penetrate down to around 100 m, as indicated by the black arrows labelled A in Figure9a. The development of an elevated night-time wind speed acceleration zone is also evident in both the simulation results in Figure 10b and the sodar measurements in Figures 9c and 9d. This is marked by the B arrows and this zone forms at around 150 m in both simulation and real measurements. There is also evidence of the evolution with height of the elevated night-time wind speed acceleration zone, as shown at points B1, B2, B3 and B4 in Figure 10c.

CONCLUSION

Vertical profiles of wind speed were measured by a sodar over a coastal ridge top located in complex terrain. Surface layer (up to 300 m) wind speeds were recorded every 10 minutes for a 4 month period and wind shear models were assessed based on observed data up to heights of 150 m. A three-dimensional atmospheric large eddy simulation model experiment was set up to reproduce the airflow regime specific to the ridge top, and time-height cross-sections were compared to the observed sodar measurements. Results can be summarized by the following points:

- Ridge top measurements of horizontal and vertical wind speeds revealed strong topographic flow features that are directly linked to the terrain upwind of the measurement point.
- Vertical profiles of wind direction showed evidence of an Ekman spiral that should be taken into consideration if large wind turbines were to be selected for this site.

- Three distinctive zones within the surface layer measurements were clearly defined. Zone A (the lowest up to 60 m) is the maximum shear layer in the wind speed vertical profile, which is associated with the effect of the steep face upwind of the measurement site on the prevailing westerly winds. Zone B (60 to 125 m above ground) is the most homogenous layer within the wind speed profile, showing minimum shear at the recommended height range for the turbine blades. Zone C (125 to 300 m) is the layer within which the night-time wind speed acceleration occurs, and which is highly affected by the boundary layer shear zone above 300 m, producing slower wind speeds during daytime periods.
- Existing logarithmic and power law wind shear models failed to fit surface measurements based on the neutral atmospheric assumption, and data showed that on the basis of the observed vertical profiles of wind speed the atmosphere over the ridge top resembled an unstable convective situation due to strong orographic lifting.
- The three-dimensional large eddy simulation model results produced similar results to observed measurements and captured similar wind dynamics to those observed by the sodar.

In general, this 4-month summertime experimental and modelling investigation has revealed characteristics of airflow over a ridge top resulting from effects of complex wind dynamics due to proximity to the sea and complex topographic features. It is evident that sodar measurements, although sometimes thought to be unreliable due to the lack of tower measurements to validate the results, can often provide knowledge of distinctive flow features that can be of importance to wind energy resource assessment. This research has also demonstrated the capability of high resolution atmospheric modelling for simulating atmospheric surface layer phenomena, and its complementary use with real data for validating the analysis.

LIST OF FIGURES

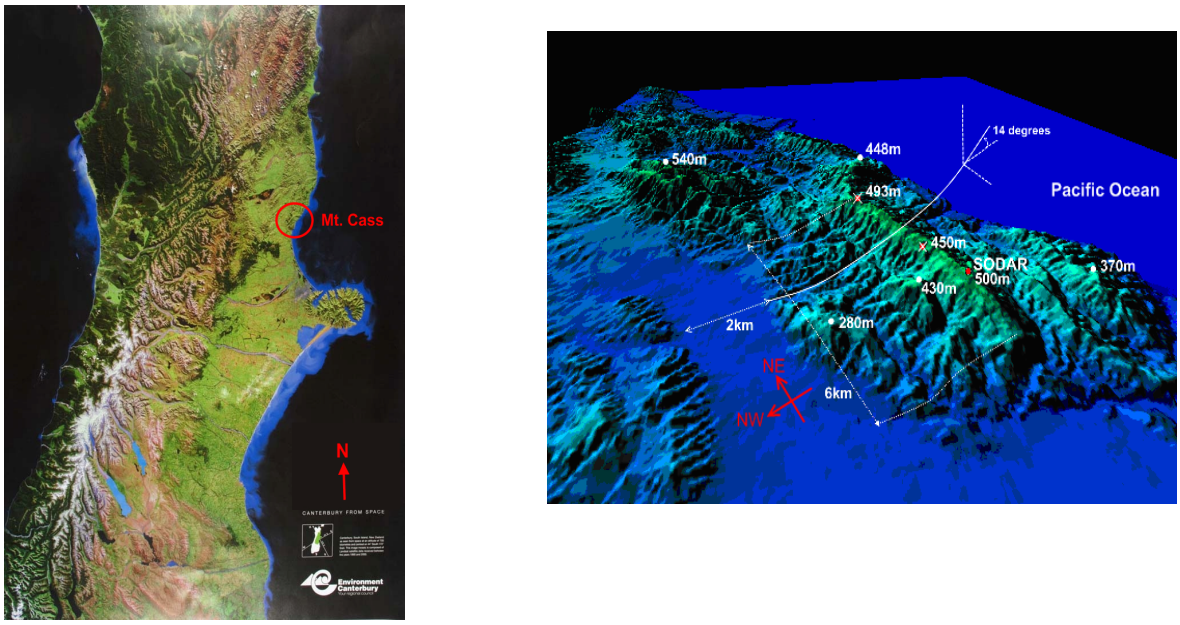

(a) **(b)**

Figure 2. (a) A satellite image showing the location of the Mt. Cass ridge wind farm site, and (b) a digital elevation three-dimensional perspective showing the complexity and steepness of the terrain.

(a) **(b)**

Figure 3. (a) A photo of the ridge looking northeast and showing the western face of the ridge, and (b) looking southward showing the east coast that runs to the south of the ridge.

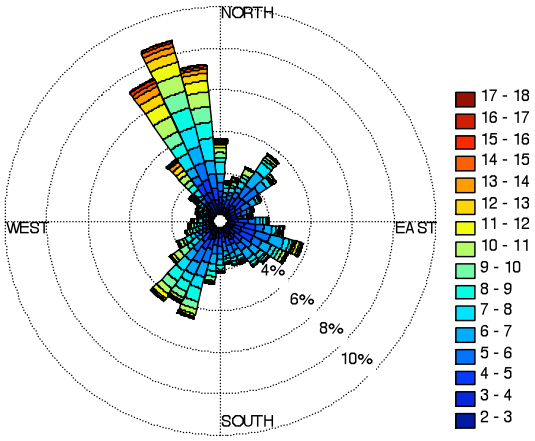

(a)

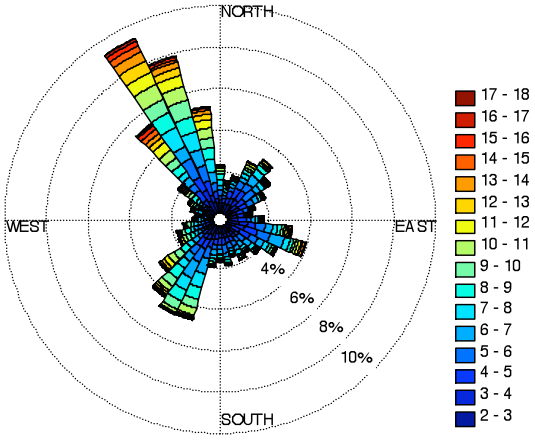

(b)

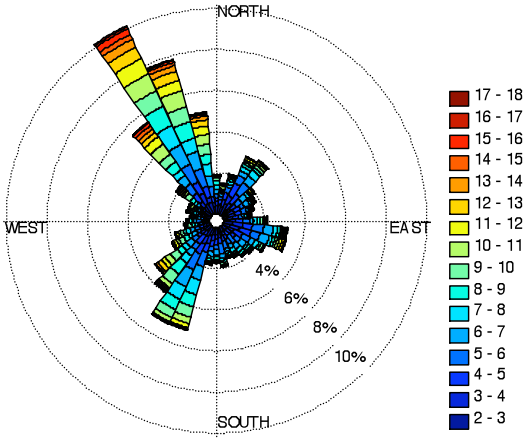

(c)

Figure 4. Wind roses showing the frequency distribution of wind speed (m s^{-1}) and direction for the total period at (a) 30 m, (b) 60 m, and (c) 80 m.

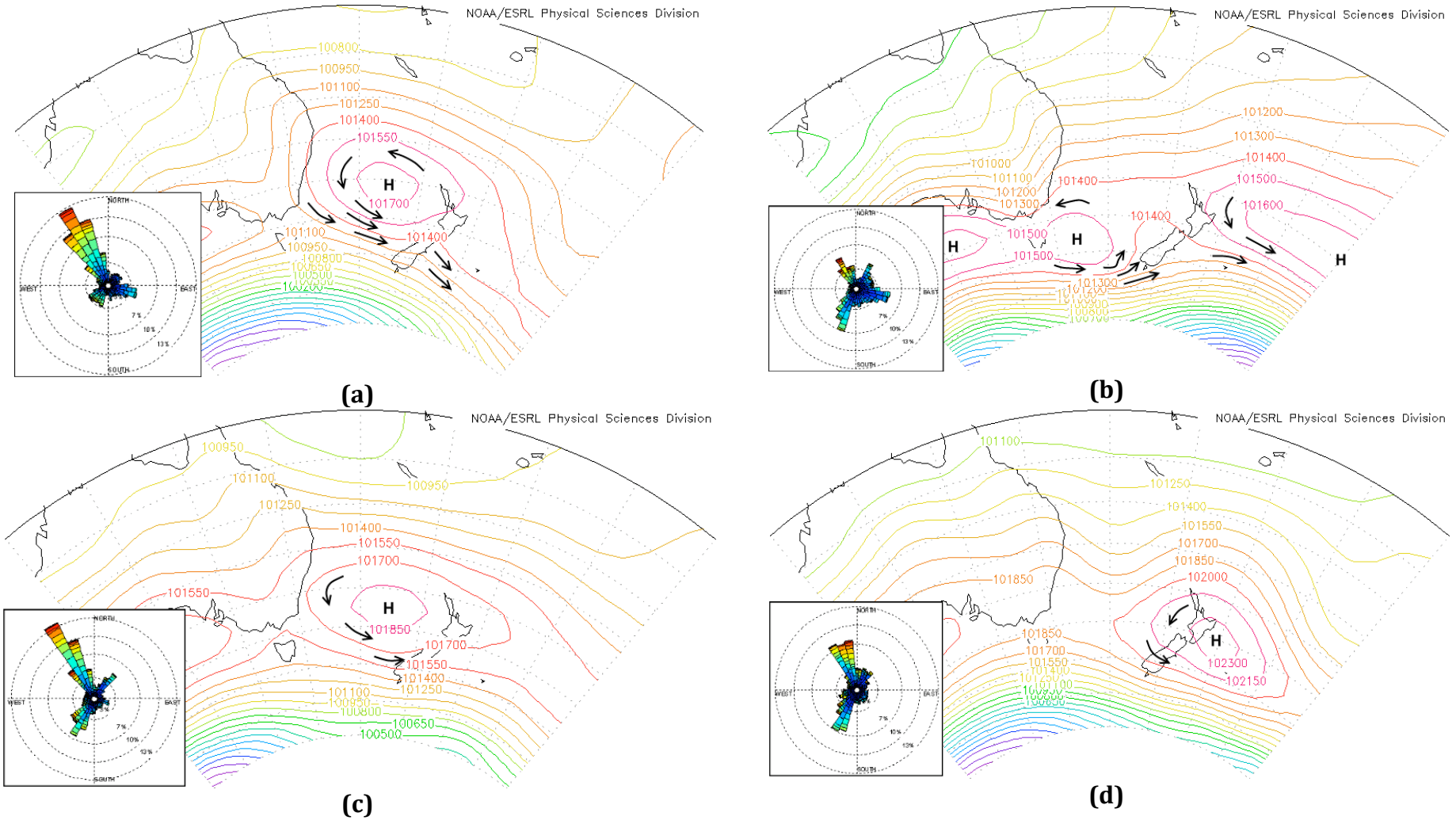

Figure 5. Monthly average mean sea level pressure for (a) January 2009, (b) February 2009, (c) March 2009, and (d) April 2009. Arrows indicate synoptic flow direction and the 80 m wind roses are inserted for reference.

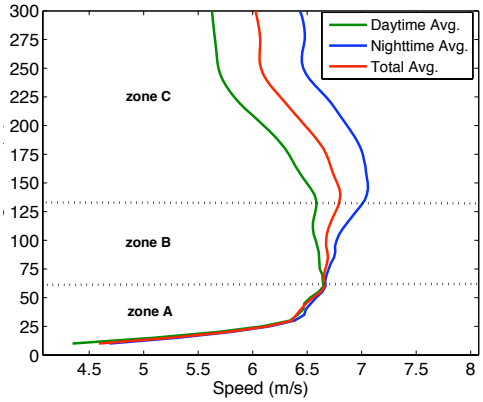

Figure 6. Vertical profile of average horizontal wind speed for the entire 4 month period.

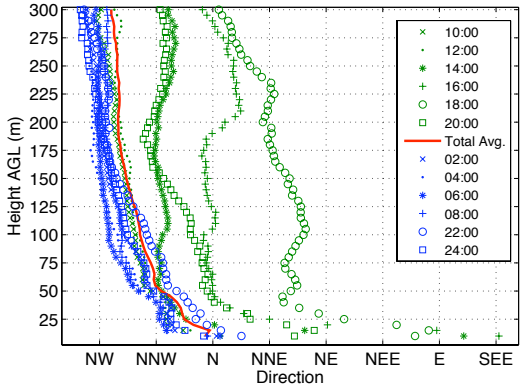

Figure 7. Vertical profile of 2-hour average wind direction for day and night-time for the entire 4 month period.

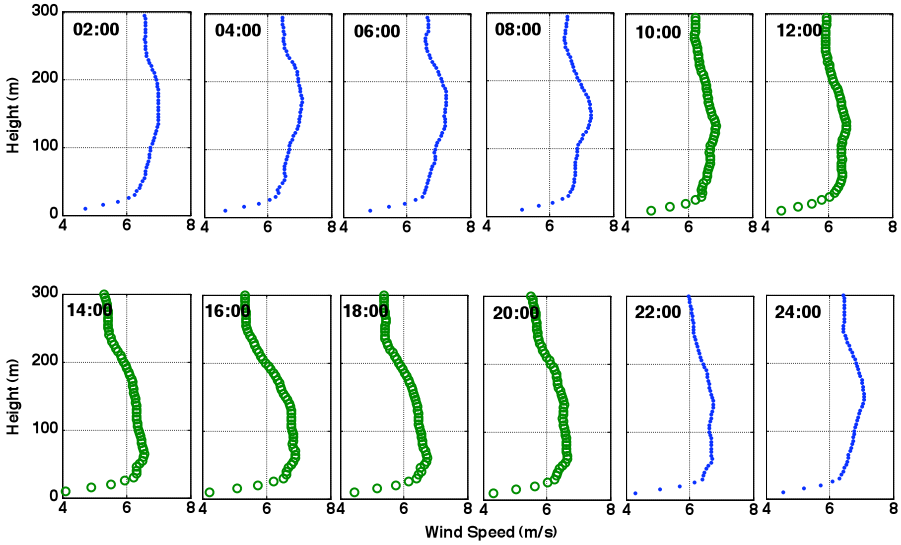

Figure 8. Wind profile evolution throughout the day. Each plot is on the hour of a previous 2-hour averaging period, and different symbols are used to separate day- from night-time profiles.

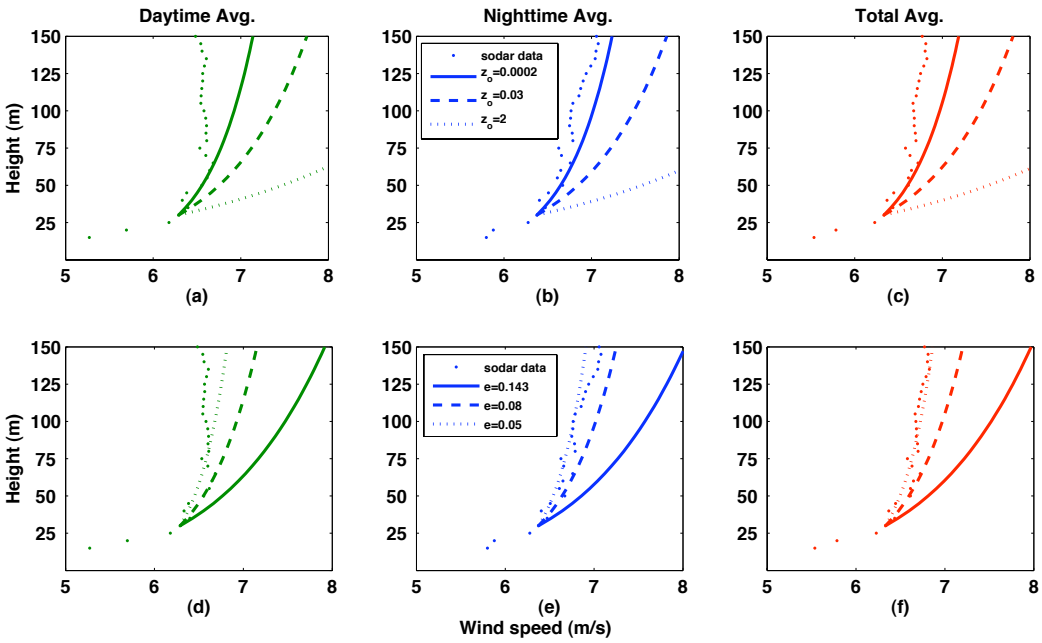

Figure 9. Logarithmic neutral and power law model profiles fit to the 30 m sodar wind speed measurements and compared to observed wind speed up to 150 m above ground. (a), (b) and (c) show the logarithmic neutral profile fit based on 3 selected roughness length scales (z_o). (d), (e) and (f) represent the power law profile fit based on 3 selected shear exponent values (e).

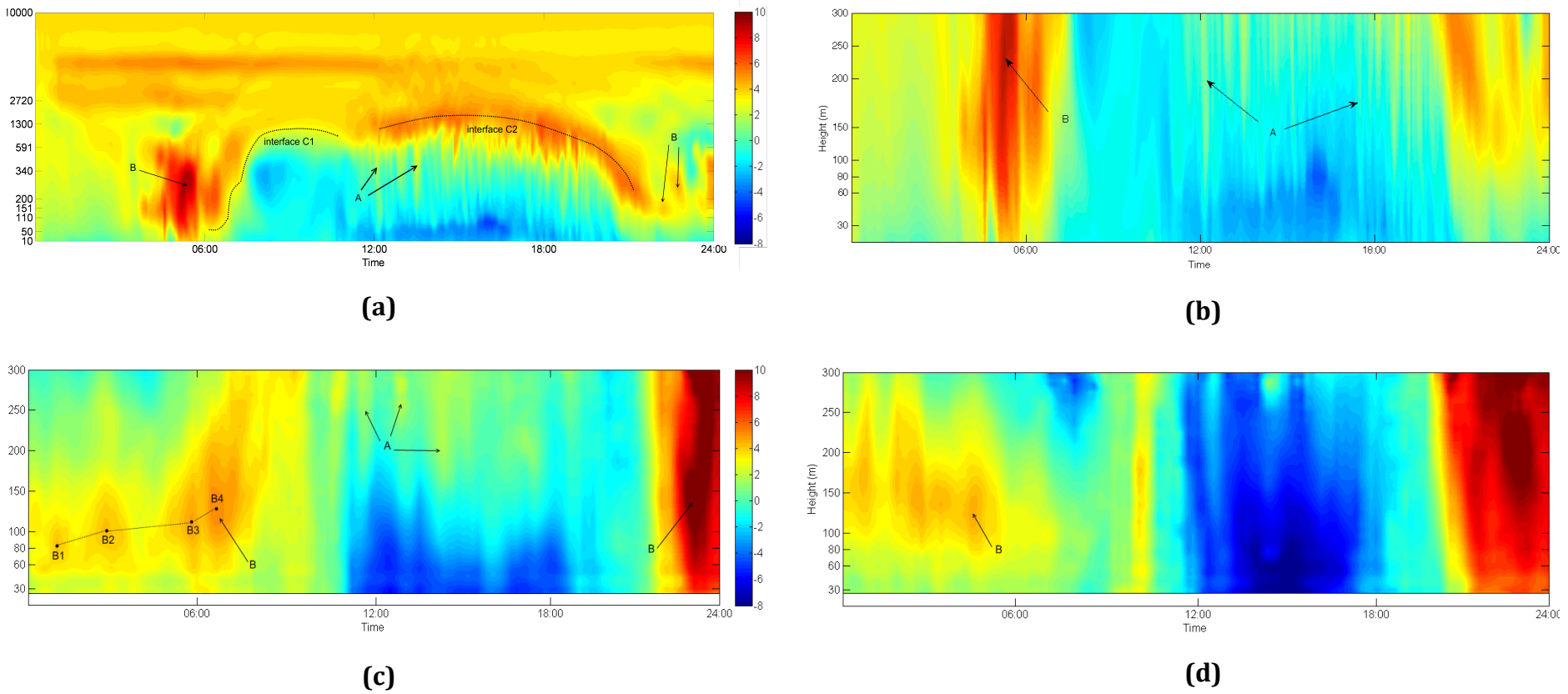

Figure 10. Time-height cross-sections of U-velocity (m s^{-1}) derived from 5 minute output data for model run (a) for 0-10000 m above ground, and (b) the first 312 m above ground, while (c) and (d) are time-height cross-sections of the U-velocity derived from sodar data for 5 January, 2009 and 24 January, 2009, respectively. Time axis is based on New Zealand standard time.

LIST OF TABLES

Table 1. Summary of the number of collected records. Missing data was a result of ground clutter noise and the removal of the top 50 m of sampling levels.

Total number of records collected	1,106,496		
Total number of records used for analysis	960,048		
	30 m **Day/Night**	**60 m** **Day/Night**	**80 m** **Day/Night**
January, 2009 (31 days)	3393/3482	3393/3616	3392/3571
February, 2009 (28 days)	3105/3024	3185/3226	3105/3024
March, 2009 (30 days)	3542/3542	3542/3586	3499/3542
April, 2009 (23 days)	2451/2616	2482/2650	2417/2550

Table 2. Model grid configuration and simulation initial setup conditions (N is the number of grid points, D is the grid resolution, Dt is the simulation time step, and x, y and z are the orthogonal cartesian coordinates..

Grid	**N_x, N_y, N_z**	**D_x, D_y, D_z, D_{zmin} (m)[1]**	**Dt (s)**	**LBC[2] update interval (s)**
1	103,103,53	9000,9000,500,50	5	Zero gradient
2	103,103,53	3000,3000,300,50	2	3600
3	103,103,53	1000,1000,300,50	1	1800
4	103,103,53	500,500,300,30	1	600
5	103,103,53	250,250,200,20	1	300

Atmosphere initial state	Standard temperature profile (-6.5 ^{o}C km^{-1}), 30 % RH logarithmic northwest wind speed profile ($WS_{surface}$=2.3 m s^{-1})
Model run start time	00:00 LST
3Soil-vegetation model	Noilhan/Planton scheme
Turbulence parameterization	Moeng and Wyngaard subgrid-scale parameterization
Initial soil temperature	15 ^{o}C (top level), 14 ^{o}C (bottom level)
Initial soil moisture	70 % saturation
Sea surface temperature	15 ^{o}C

[1] Vertical grid stretching was applied starting with first level D_{zmin}, then following a tangential function.

[2] Lateral boundary conditions used to drive the nested domains.

REFERENCES

Chow, F. K., Andreas, P. W., Robert, L. S., Mathias, W. R., and Ming, X., 2006. High-resolution large-eddy simulations of flow in a steep alpine valley. Part I: Methodology, verification, and sensitivity experiments. Journal of Applied Meteorology and Climatology. 45, 63-86.

Crescenti, G.H., 1997. A look back on two decades of Doppler Sodar comparison studies. Bulletin of the American Meteorological Society. 78, 651-673.

de Noord, M., Curvers, A., Eecen, P., Antoniou, I., Jorgensen, H.E., Pedersen, T.F., Bradley, S., Von Hünerbein, S., Kindler, D., Mellinghoff, H., Emeis, S., 2001. Report WISE (Wind Energy Sodar Evaluation), EC Contract n°NNES.

Dupont, E., Flori, J.P., 2007. Comparison of sodar measurements with ultra sonic and cup anemometers for wind energy applications. Report Electricité de France RandD/ENPC.

Farrugia, R.N., 2003. The wind shear exponent in a Mediterranean island climate. Renewable Energy. 28, 647–53.

Garratt, J.R., 1992. The Atmospheric Boundary Layer. Cambridge University Press, Cambridge.

Hussain, M., 2001. Dependence of power law index on surface wind speed. Energy Conversion and Management. 43, 467-472.

Mainpower 2009. Http://www.localgeneration.co.nz. Accessed on September 10, 2009.

Mellinghoff H., Albers A., 2000. Sodar measurements of the wind conditions in Oberzeiring, Austria. Report DEWI 4015O9903-35-01/2000-01.

Migoyaa, E.AC, Garcıa, J., Morenob, F., Manuela, F., Jimeneza, A., and Costac, A. 2007. Comparative study of the behavior of wind-turbines in a wind farm. Energy. 32, 1871-1885.

NZWEA 2009. New Zealand Wind Energy Association. Http://windenergy.org.nz. Accessed on September 19, 2009.

Perez, I.A., Garcia M.A., Sanchez M.L., de Torre B., 2004. Analysis of height variations of sodar-derived wind speeds in Northern Spain. Journal of Wind Engineering and Industrial Aerodynamics. 92, 875–894.

Reid, S., 2003. Hill top wind profiles using sodar. Boundary Layer Meteorology. 108, 305-314.

Rehman, S., Al-Abbadi, N.M., 2007.Wind shear coefficients and energy yield for Dhahran, Saudi Arabia. Renewable Energy. 5, 738-749.

Santoso, E. and Stull, R.B., 1998. Wind and temperature profiles in the radix layer: The bottom fifth of the convective boundary layer. Journal of Applied Meteorology. 37, 545-558.

Sinclair Knight Merz, 2006. Renewable energy assessment, Canterbury region. Report for the Energy Efficiency and Conservation Authority, Wellington, New Zealand.

Stull, R.B., 1988. An Introduction to Boundary Layer Meteorology. Kluwer Academic Publishers Group, Dordrecht.

Weigel, A., Chow, F. K., Mathias, W. R., Robert, L. S., and Ming, X., 2006. High-resolution large-eddy simulations of flow in a steep alpine valley. Part II: Flow structure and heat budgets. Journal of Applied Meteorology and Climatology. 45, 87-107.

Wieringa, J., 1992. Updating the Davenport roughness classification. Journal of Wind Engineering and Industrial Aerodynamics. 41, 357-368.

Wieringa, J., 1993. Representative roughness parameters for homogeneous terrain. Boundary Layer Meteorology. 63, 323-363.

Xue, M., Droegemeier, K.K., Wong, V., Shapiro, A., Brewster, K., 1995. ARPS Version 4.0 User's Guide, [Available from CAPS, University of Oklahoma, Norman OK 73072, USA].

Xue, M., Droegemeier, K.K. and Wong, V., 2000. The Advanced Regional Prediction System (ARPS) - A multiscale nonhydrostatic atmospheric simulation and prediction tool. Part I: Model dynamics and verification. Meteorology and Atmospheric Physics. 75, 161-193.

van den Berg, G.P., 2007. Wind turbine power and sound in relation to atmospheric stability. Wind Energy. 11, 151-169.

Vogt, S. and Thomas, P., 1994. Test of a phased array sodar by intercomparison with tower data. Journal of Atmospheric and Oceanic Technology. 11, 94–102.

5. Research manuscript M2

Katurji, M., Sturman, A., and Zawar-Reza, P. (2011). An Investigation into Ridge-Top Turbulence Characteristics During Neutral and Weakly Stable Conditions: Velocity Spectra and Isotropy. ***Boundary-Layer Meteorology***, 139(1), 143-160. doi: 10.1007/s10546-010-9576-y.

AN INVESTIGATION INTO RIDGE-TOP TURBULENCE CHARACTERISTICS DURING NEUTRAL AND WEAKLY STABLE CONDITIONS: VELOCITY SPECTRA AND ISOTROPY

Marwan Katurji[1], Andrew Sturman, Peyman Zawar-Reza

[1] *Centre for Atmospheric Research, University of Canterbury, Christchurch, New Zealand*

E-mail: marwan.katurji@gmail.com

Abstract An investigation into high Reynolds number turbulent flow over a ridge top in New Zealand is described based on high-resolution in-situ measurements, using ultrasonic anemometers for two separate locations on the same ridge with differing upwind terrain complexity. Twelve 5-hr periods during neutrally stratified and weakly stable atmospheric conditions with strong wind speeds were sampled at 20 Hz. Large (and small) turbulent length scales were recorded for both vertical and longitudinal velocity components in the range of 7-23 m (0.7-3.3 m) for the vertical direction and 628-1111 m (10.5-14.5 m) for the longitudinal direction. Large-scale eddy sizes scaled to the WRF (weather research and forecasting) model simulated boundary-layer thickness for both sites, while small-scale turbulent features were a function of the complexity of the upwind terrain. Evidence of a multi-scale turbulent structure was obtained at the more complex terrain site, while an assessment of the three-dimensional isotropy assumption in the inertial subrange of the spectrum showed anisotropic turbulence at the less complex site and evidence of isotropic turbulence at the more complex site, with a spectral ratio convergence deviating from the 4/3 or unity values suggested by previous theory and practice. Existing neutral spectral models can represent locations along the ridge top with simple upwind complexity, especially for the vertical wind spectra, but sites with more orographic complexity and strong vertical wind speeds are often poorly

represented using these models. Measured spectra for the two sites exhibited no significant diurnal variation and very similar large-scale and small-scale turbulent length scales for each site, but the turbulence energy measured by the variances revealed a strong diurnal difference.

Keywords: *Isotropy, Mountain ridge top, Turbulence, Velocity spectra*

BACKGROUND AND MOTIVATION

Due to the low viscosity of air (less than the viscosity of water by a factor of 103) and the large length scales associated with boundary-layer flows (~1-2 km), atmospheric flows can be confidently classified as fully developed turbulent flows with a Reynolds number (Re) in the order of 10^9. The idea of the break up of large eddies into smaller ones and the existence of a spectrum of scales in the flow led Kolmogorov to define turbulent length/time/velocity microscales that have become universal in their application and are dimensionally related to the viscosity of the fluid and the energy dissipation rate. Turbulence has been addressed in a more practical way in the models of fluid dynamicists, through either simplifying (parametrizing the physical behaviour) or avoiding (linearising the mathematical equations) it. In meteorology, the turbulence equation is particularly difficult to solve given the broad spatial and temporal spectrum involved, but the approach is still the same with simplification being an important response. Theories concerning dynamic interactions of atmospheric flow have developed over many years employing the same formulation of turbulence as for any other fluid flow, and evolving from simpler flat terrain turbulent theories to more complex modifications and hypotheses for complex terrain situations.

The very early research into atmospheric boundary-layer flows was conducted in the 1950s for flows over homogeneous and flat terrain. This simplistic approach was favoured by scientists since it allowed for direct comparison to wind-tunnel experiments (Kaimal and Finnigan 1994). The Monin-Obukhov similarity theory (MOST) was derived for modelling the mixed turbulent shear layer using the Obukhov length scale (L), which is a function of surface friction velocity (u_*) and heat flux ($\overline{w'\theta_v'}$) derived from the virtual potential temperature. Since the development of MOST, many experimental studies have been carried out to

investigate its applicability, the most famous being the flat terrain experiments held at Tsimlyansk in Russia (Tsvang et al. 1973; Tsvang 1985) and Kansas in the United States (Kaimal et al. 1972, 1976). Both provided good support of similarity theory as far as inertial subrange behaviour is concerned, but discrepancies in turbulent fluxes were identified that were related to the irregular temperature distribution over flat terrain that was not accounted for in the similarity theory (Tsvang et al. 1998), while assessment of the isotropic nature of turbulence showed that it differed with stability conditions (Kaimal et al. 1972, 1976). The generalisation of one similarity theory for applications under various stability and flow regimes, even for flat terrain, was never achieved, contributing to our limited knowledge of turbulence interaction theories. Nevertheless, new models were suggested outlining the large-scale turbulence interaction with the small-scale, and vice versa, thus proposing explanations behind the breakdown of similarity theories over flat terrain. Examples of the studies that propose large-scale or "inactive turbulence" that interacts with the surface-layer or "active turbulence" are Yaglom (1994), Hunt and Morrison (2000), Hogstrom et al. (2002) and McNaughton and Brunet (2002). Despite attempts to generalise the behaviour of turbulent mixing in the similarity theory, and given the highly non-linear mechanism of turbulence, there continues to be unexplained degrees of freedom and evidence of the breakdown of such theories, given the complexity of terrain-flow interactions in the surface-layer.

The situation is even more complex when inhomogeneous surface properties are examined, such as topographic complexity that alters the near-surface turbulent fluxes and structures. Average behaviour of meteorological parameters in complex mountainous terrain is well described in many textbooks, e.g. Whiteman (2000), but the literature lacks any benchmark experiments describing the turbulence dynamics and structures that can help in model derivation and the development of newer parametrization techniques. In many cases, whenever complex terrain turbulence was investigated, flat terrain assumptions and similarity rules were applied. Early turbulence studies over sinusoidal hills were conducted by Jackson and Hunt (1975). These experiments revealed flow modifications as a function of slope steepness and suggested a two-layer turbulence structure (upper and lower), with the lower near-surface-layer in

equilibrium with the terrain so that surface-layer similarity laws are considered applicable. At the upper level, the transport and modification of large eddies followed the rapid distortion theory discussed in Townsend (1972). Bradley (1980), Britter et al. (1981), Panofsky et al. (1982), Zeman and Jensen (1987) Mickle et al. (1988) provided evidence supporting this theory. More recently, the Mesoscale Alpine Program (MAP) carried out in the Riviera Valley, Switzerland (Bougeault et al. 2001; Volkert and Gutermann 2007) highlighted the importance of the spatial variability of turbulent variables in complex mountainous regions (Rotach and Zardi 2007). The validity, to a certain extent, of flat terrain similarity scaling parameters was pointed out by De Franceschi (2004), such as the use of the free convective velocity scale (w_*) in non-dimensional turbulent kinetic energy profiles. This can be derived from the surface heat flux for sloping terrain (Weigel and Rotach 2004), but even with that the generalisation did not hold for different stability and flow regimes. Moraes et al. (2005) showed that the validity of flat terrain similarity theories can extend to complex terrain situations only for certain wind speeds and direction, and they point out that this occurs only when the flow retains a memory of upstream flat terrain conditions before interacting with the complex topography. In a more recent study, Martin et al. (2009) demonstrated the limitation of certain stability parameters when surface-layer similarity theory is applied in complex terrain.

The above mentioned points clearly reveal that turbulence over complex terrain in the atmospheric boundary-layer remains problematic with many unanswered questions. Even now there are few hypotheses and no all-inclusive theory (Lumley and Yaglom 2001). Atmospheric surface-layer turbulence continues to be extensively researched, and generalised velocity, temperature and spectral characteristics have been established by elaborative benchmark experiments, with the occasional re-examination of the theory from time to time to remind us of the incomplete understanding of the subject. The motivation for our own research is threefold:

1) The need to understand surface-layer turbulent flow characteristics in very complex terrain situations, which will highlights causes of the variable and unpredictable nature of turbulence in such situations.

2) The need for the reassessment of the application of current theories to more complex terrain configurations, highlighting new situations where these theories can be further questioned.

3) The significant role that turbulence plays in practical problems, such as wind turbine siting in complex terrain and the need for its examination locally.

Given the above stated motivations, our study provides an insight into a unique flow regime generating turbulence over a steep ridge top in New Zealand, through in-situ measurements and derivation of velocity spectra, turbulent length scales, and isotropic turbulence evaluation in an attempt to understand the turbulent structure and mechanisms of flow over a mountain ridge top in the South Island of New Zealand. Three-dimensional wind components were collected at ultrasonic frequencies and the velocity spectra carefully examined for a neutral atmospheric boundary-layer case with mean wind speeds reaching 17 m s-1 at two locations on a ridge line facing the prevailing winds. The main difference between the sites is the complexity of the upwind fetch, with one of the sites having a more complex terrain configuration. Attempts were also made to present diurnal differences in turbulence characteristics at the two sites for three neutral atmospheric boundary-layer cases.

EXPERIMENTAL SITE

The experimental site is a ridge of 6 km length at North Canterbury, South Island, New Zealand. The ridge is oriented approximately south-west to north-east, with its north-west slopes facing a compass direction of 325 degrees with the Pacific Ocean coast to the south-south-east. The prevailing wind direction in this area is from the north-west, as indicated by the arrows shown in Figure 11a. The ridge line height above sea level varies from 450 to 525 m at Mt. Cass, which is the highest peak on the ridge. The north-west face of the ridge is characterised by an average slope of 14 degrees and by a secondary steep ridge of 25 degrees, shown in Figure 12b. Two ultrasonic CSAT3 anemometers were mounted on 20-m towers and placed at the Junior and Senior sites, shown in Figure 11b by the white vertical lines. The Junior tower was placed on the lower ridge around 40 m lower than the Senior tower, which is on the main ridge top 5 km to the north-east. The upwind terrain characteristics are different for the two sites, with relatively

smooth terrain immediately upwind of the Junior site compared with the Senior site, which has a prominent steep ridge face only 20 m from the tower on the upwind side, as shown in Figure 12b. Modelling the effects of terrain complexity are the areas of active research in digital terrain analysis, and different research disciplines in fact define their own tailored terrain complexity parameters and the definition varies from shape, ruggedness, curvature, fractals, etc. (Huaxing 2008). We have chosen to differentiate the two sites' upwind complexity by using the standard deviation of the terrain elevation, as presented in Figure 12a. This statistical approach provides a measure of the degree of steepness of the terrain. The Senior and Junior sites shown in Figure 12a each have distinctive upwind terrain complexity indicated by the standard deviation of terrain height derived from the digital elevation model results, as outlined in the figure caption. Standard deviation in the green and yellow colour ranges show a variation of 14 to 20 m in height over a 25 m horizontal distance, and these surface orographic features will have maximum effect on the incoming airflow when they are aligned perpendicular to the main flow direction. Of the two sites considered here, the Senior site is located downwind of two major crosswind terrain ridge features, as shown by the terrain complexity parameter in Figure 12a. This approach was used to differentiate the upwind terrain complexity between the two sites. The set-up is ideal in the sense that it permits examination of turbulent flow regimes along a ridge line with different upwind terrain characteristics, and as well as providing an insight into the variability of these regimes under strong winds when a near-neutral atmospheric boundary-layer is expected.

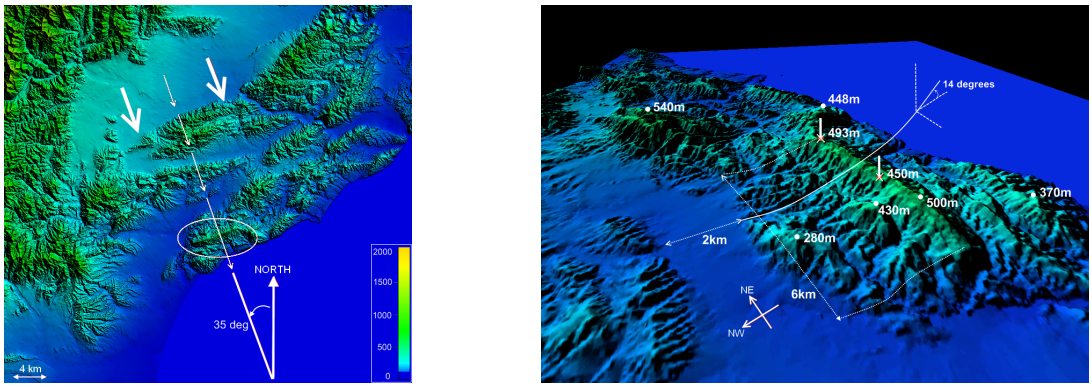

(a) **(b)**

Figure 11. (a) A digital elevation map showing the ridge line inside the ellipse and the direction of the prevailing wind perpendicular to the ridge line. (b) A three-dimensional digital elevation perspective showing the complexity and steepness of the terrain of the Mt Cass ridge. The Junior and Senior sonic anemometers are indicated by 450 m and 493 m white vertical lines, respectively.

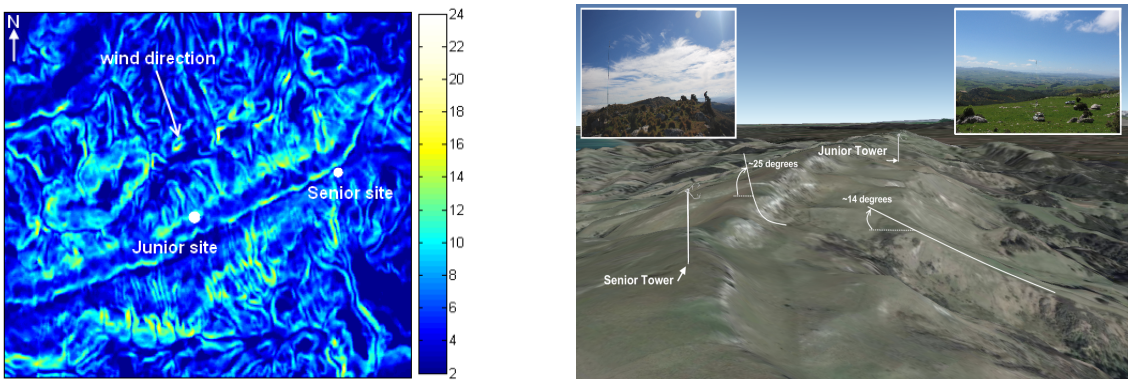

(a) **(b)**

Figure 12. (a) Terrain height standard deviation in (m) derived from a 50 m x 50 m window applied over a 25 m resolution digital elevation map. (b) A close up of the ridge top viewed from the north-east end, showing the Senior and Junior towers and the steep (25 degree) ridge face. Photos of the tower sites are inset in the upper left and right corners.

METHODOLOGY AND RESULTS

Data presented here are for the 6, 7 and 17 January 2009, when the prevailing flow over the ridge was from the north-west. This period also marks strong and gusty foehn wind conditions (Sturman and Tapper 2006) descending from the Southern Alps and passing over the area, and the sampling periods represent the strongest wind conditions that could be expected for the instrumented site. The atmospheric boundary-layer during this period is characterised by low relative humidity (32 % to 65 %), high wind speeds, a well-mixed deep neutral boundary-layer and mainly clear skies with short periods of cloud coverage. For these reasons, the data presented are for a unique atmospheric event characterised by a specific stability regime under high wind speeds over complex terrain. Atmospheric stability was not measured during the period of sampling due to the lack of vertical profilers, but an atmospheric model simulation was carried out to predict the boundary-layer thickness, as will be explained later. Average wind speed and direction for the three days were 13 m s-1 and 321 degrees relative to true north, while the sky was mostly clear, with only partly cloudy conditions on 17 January. The reason for selecting these particular days was to capture the upwind energy information in the spectral data associated with the prevailing wind direction, which is very close to the direction perpendicular to the ridge orientation (325 degrees from true north). The selected data allowed the analysis of turbulence spectrum characteristics of 12 sets of daytime and nighttime measurements, containing neutral daytime and weakly stable nighttime boundary-layer atmospheric stability conditions. The daytime (D) data extend for 5 hours (1200 to 1700 LST), and the nighttime (N) data also extend for 5 hours, but from 0000 to 0500 LST. The datasets are identified in the form R1JD, which corresponds to the first period (R1) for the Junior site (J) during daytime (D). The resulting names are provided in the first column of Table 3.

The sonic anemometer's raw sampling frequency was 60 Hz, which was block averaged to 20 Hz by the signal-processing unit and available at this frequency for the analysis. Wind speeds were transformed into longitudinal (streamwise) and transverse (crosswise) components, the former being along the prevailing wind direction and the latter in the perpendicular direction. The data were filtered for erroneous spikes, de-trended, and window tapered using the hamming window

before the power spectral density was calculated using a fast fourier transform (FFT) routine. Spectra were calculated for individual 30-min periods, examined carefully, and their inertial subrange slopes were compared to the (-2/3) similarity law slope to ensure that the time period represented the complete spectrum of energy production and dissipation (ensuring that data aliasing was not a problem). The overall power spectra for each day or night period (5 hours) were then produced from the average of 10 separate 30-min sets of spectral data. Additionally, the power spectral density was derived using the p-Welch method (Welch 1967), by which the data were divided into eight segments with 50 % overlapping, and the frequency response was calculated from the average of the power spectral density of the eight individual segments. The p-Welch overlapping and non-overlapping methods produced similar results, and both sets of spectral plots reflected the general shapes expected from measurements in the atmospheric surface-layer. Plots of power spectra normalised with the local variance are presented in Figure 13, and inter-compared between the two sites (J, S) for different daytime and nighttime (D, N) periods. The plots of ratios of crosswise and vertical power spectra to streamwise spectra are presented in Figure 14 to allow examination of the isotropic behaviour of turbulence at the two sites.

The turbulence spectrum provides information on the dominant frequencies within the wind speed fluctuations. Kolmogorov's law suggests that the velocity spectrum in the inertial subrange, if sampled adequately, on a log-log plot of spectral energy density versus frequency, will approach a straight line of slope -5/3. The common spectral models that represent this behaviour were derived from flat terrain and wind-tunnel experiments and are continuously tested for their validity under various topographical and atmospheric conditions. They are the Kaimal spectra (Kaimal et al. 1972) and von Karman spectra (Burton et al. 2001), respectively, and are compared to the experimental results contained here in.

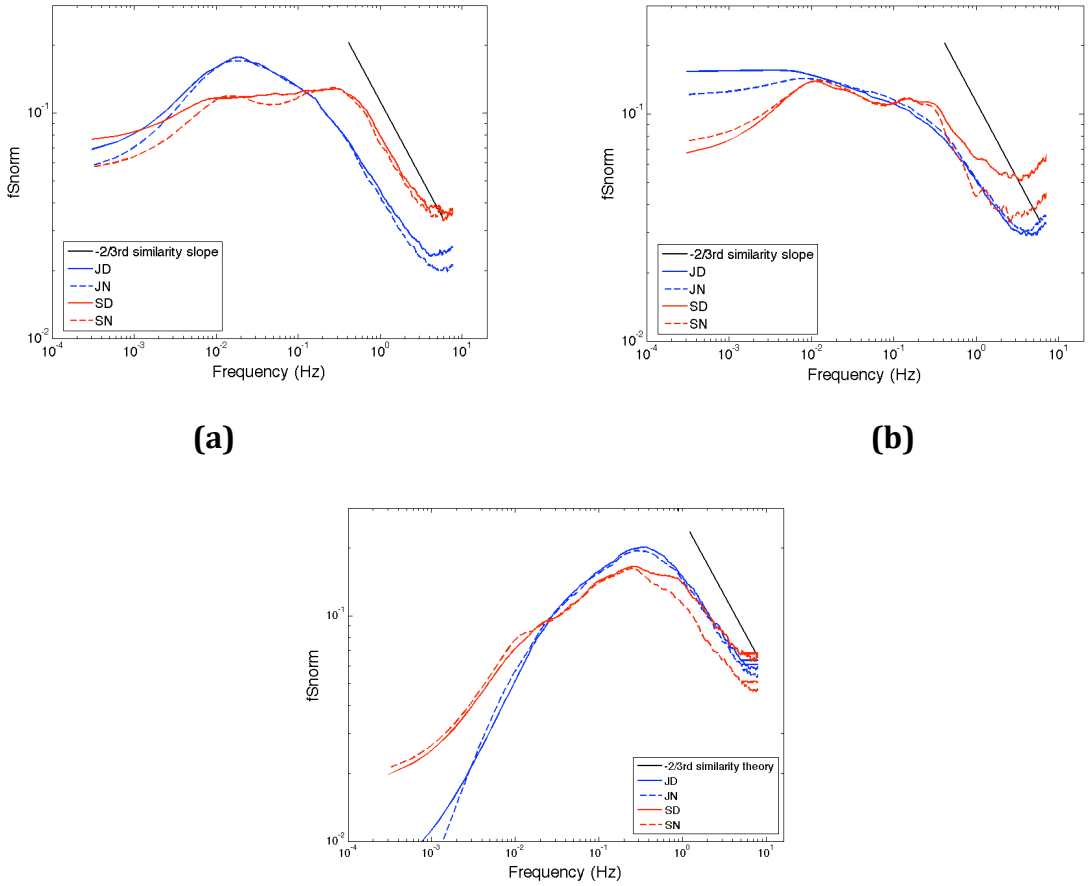

Figure 13. (a) Streamwise, (b) crosswise and (c) vertical power spectra normalised by local variances (the vertical axis label, fSnorm, is defined as the power spectra normalized by the variance) for the daytime (D) and nighttime (N) periods at the two sites Junior (J) and Senior (S). Day and night data are averages from the periods 1200-1700 LST and 0000-0500 LST of the three days used in this experiment. The solid black line represents the 2/3 slope suggested by similarity theory.

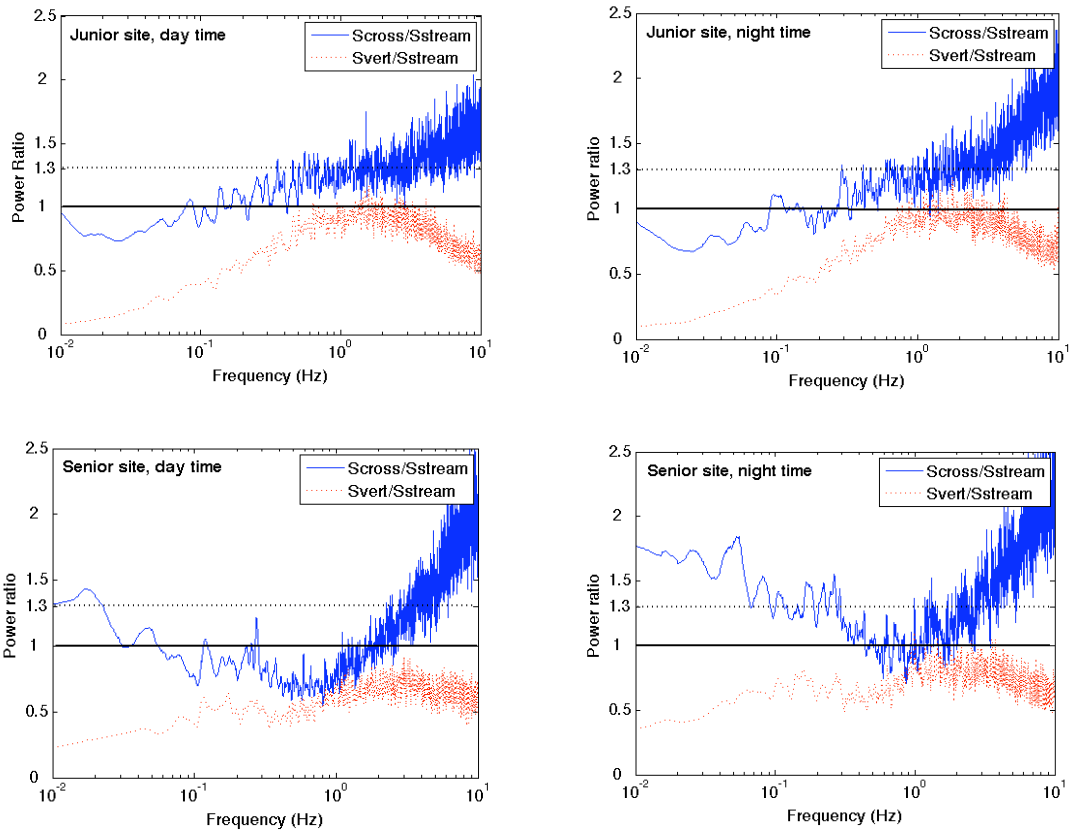

Figure 14. Ratios of cross-wise and vertical power spectra to streamwise spectra averaged from the 12 different datasets indicated in Table 3 and produced for the daytime (D) and nighttime (N) periods for the two site locations Junior (J) and Senior (S). Power ratios of 1 and 1.3 (4/3) are indicated by a full and dashed line to allow for assessment of isotropy.

The Kaimal spectral model is given by,

$$\frac{fS_i}{\sigma_i{}^2} = \frac{4 f_i L_i}{\left(1 + 6 f_i L_i / \overline{U}\right)^{5/3}} \tag{4}$$

where $i = u, v, w$ (three Cartesian components of velocity), L is the turbulent length scale, U is the mean horizontal wind speed, f is the frequency, S is the power spectral density, and σ^2 is the variance. The length scales are Lu = 170.1 m or $5.67z$ for z < 30 m, $Lv = 0.3333Lu$, $Lw = 0.08148Lu$.

The von Karman spectral model for the streamwise spectra is given by,

$$\frac{fS_u}{\sigma_u{}^2} = \frac{4 f_u L_u / \overline{U}}{\left(1 + 70.8 (f_u L_u / \overline{U})^2\right)^{5/3}} \tag{5}$$

where Lu = 73.5 m or $2.45z$ for z < 30 m. And for the crosswise and vertical spectra by,

$$\frac{fS_i}{\sigma_i{}^2} = \frac{4\left(f_i L_i / \overline{U}\right)\left(1 + 755.2 (f_i L_i / \overline{U})^2\right)}{\left(1 + 283.2 (f_i L_i / \overline{U})^2\right)^{11/6}} \tag{6}$$

where Lu = 73.5 m or $2.45z$ for z < 30 m and $i = v, w$ and $Lv = 0.5Lu$, $Lw = Lv$.

Comparison plots of measured and modelled spectra are presented in Figure 15.

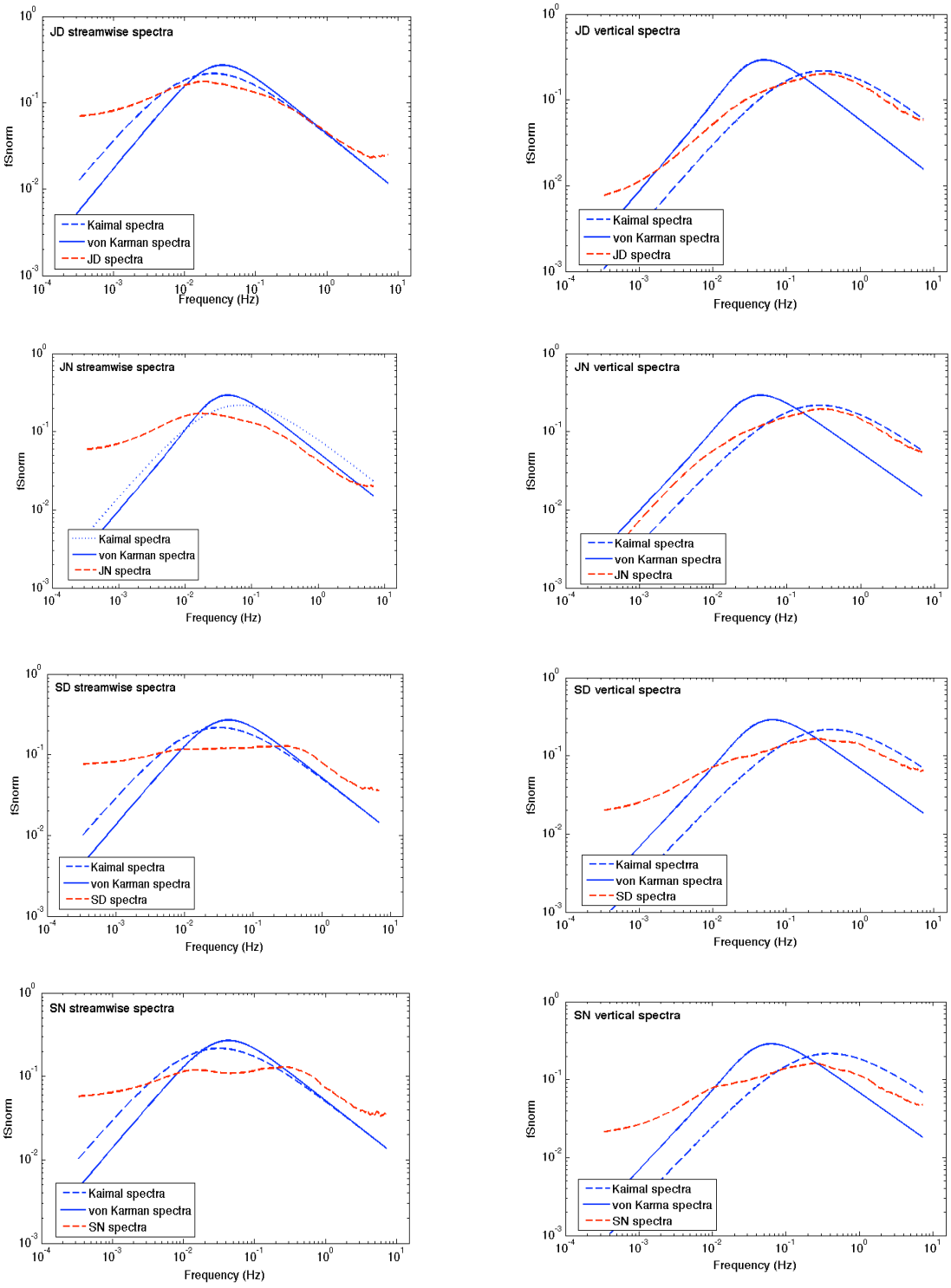

Figure 15. Normalised streamwise (left column) and vertical (right column) spectral intensities for the Junior (J) and Senior (S) sites for nighttime (N) and daytime (D), with the Kaimal flat terrain and the von Karman neutral spectral models reproduced from Equations 3, 4 and 5 for the measured wind velocities (the vertical axis label, fSnorm, is defined as the power spectra normalized by the variance).

The smallest turbulent length scales in the inertial subrange eddy sizes were derived from spectral plots of eddy dissipation rate using the spectral model equation in the inertial subrange after Kolmogorov (1941a) and Obukhov (1941). The dissipative frequency was selected corresponding to when the rate of change of the eddy dissipation rate approached zero within three decades of logarithmic units, thus showing evidence of the inertial subrange. This frequency was then used with the averaged horizontal wind speed to derive the length scale, after adherence to Taylor's theory of frozen turbulence, which was checked by ensuring that measured velocity standard deviations normalised by the mean velocity were less than one for each of the presented experimental cases. The largest longitudinal and vertical length scales were derived from the low frequency region at the maximum spectral power. A summary of those results is presented in Table 3 along with average values of day and night periods. To check for consistency in the measurement process, measured variances were compared to other published results for similar studies in complex and flat terrain experiments, and those are presented in Table 4.

The weather forecasting model WRF (weather research and forecasting) (Skamarock et al. 2008) was run in hindcasting mode for the entire period of sampling, to compensate for the lack of vertical measurements of temperature and winds to indicate upwind large-scale flow features. The model was initiated by NCEP re-analysis data with a horizontal resolution ~ 200 km and nested down to 27 km, 9 km and 3 km. The Mellor-Yamada-Janjic (MYJ) (Janjic 1990) boundary-layer parametrization scheme was used in the simulations. The model output was spatially and temporally averaged from three grid points (12.6 km) upwind of the experimental site for the respective daytime and nighttime periods, and the predicted wind speeds and directions for the 6 experimental cases are presented in the last two columns of Table 3. The planetary boundary-layer (PBL) thickness was derived using two different methodologies, the first from the prognostic formulation based on the Mellor and Yamada (1982) turbulence closure scheme. The second derivation of boundary-layer thickness and stability was obtained through examination of the west-east cross-sections of potential temperature perturbations that are presented in Figure 16, for a site over the ridge top that is marked by the black arrow (contour plotting interval is

1 K). For the MYJ method the PBL thickness produced an average daytime PBL thickness of 1260 m for the three days under study, and nighttime PBL thickness of 680 m for the MYJ method (based on the turbulent kinetic energy closure equation). While, upwind contours (~ 10 grid points or 30 km to the west of the site) of potential temperature perturbations shown in Figure 16 clearly indicate a well developed daytime neutral boundary-layer up to ~ 850 m above ground level, and a weakly stable atmosphere, up to ~ 580 m above ground level, during nighttime. The MYJ method clearly estimates deeper boundary-layers and this is because of the dependence on the turbulent kinetic energy in its formulation, so that higher wind speeds will produce a deeper boundary-layer. Since the model derived boundary-layer depths will be used as estimates of the real boundary-layer depth in order to scale the observed turbulent length scales, and to exclude any biases in the PBL thickness derivations, an average thickness of the model derived boundary-layer from the two methodologies will be used from here on in the analysis. The values are 1055 m daytime PBL thickness, and 630 m nighttime PBL thickness. In addition to atmospheric stability and boundary-layer depths, the balance between the inertial and buoyant forces over the ridge top was assessed by deriving the Froude number (Fr). The Froude number is a ratio that compares the inertial to the buoyant forces over hills (Kaimal and Finnigan 1994), and is derived by dividing the mean velocity by the product of the buoyancy frequency (or Brunt Vaisala frequency) and the ridge half-length at half-hill height. Values for Fr >>1, indicate a flow regime over the hill unaffected by thermal buoyancy and in which the flow downstream of the topography doesn't resonate with the topography dimensions. In the daytime neutral atmosphere over the ridge top, the Froude number doesn't appropriately define the flow dynamics and approaches infinity since the buoyancy frequency approached zero. As for the nighttime periods, the Froude number was 1.7, which still indicates the dominance of inertial forces over buoyancy effects.

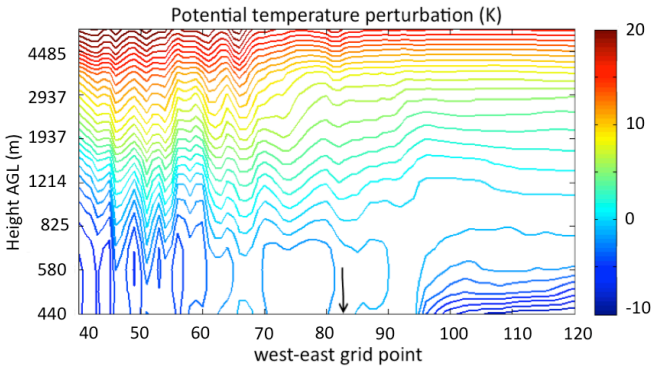

(a)

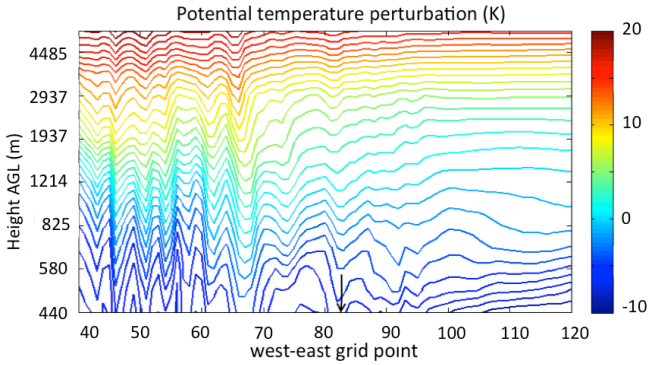

(b)

Figure 16. West-east vertical cross-section of potential temperature perturbation. The arrow indicates the experimental site. The data represent the average (a) daytime and (b) nighttime situation for the three days of 6, 7 and 17 January 2009. Each grid point is 3 km in length.

Table 3. Summary of data, turbulence statistics, and eddy sizes for the daytime (D) and nighttime (N) sampling periods from the sonic anemometers at the Junior (J) and Senior (S) sites. Last two columns correspond to the WRF simulation average data from three grid points (12.6 km) upwind of the experimental site.

		U [a] [m s^{-1}]	w [b] [m s^{-1}]	*Dir.* [deg]	σ_u^2 [c] [m^2 s^{-2}]	σ_v^2 [m^2 s^{-2}]	σ_w^2 [m^2 s^{-2}]	L_{u_s} [d] [m]	L_{w_s} [m]	L_{u_l} [m]	L_{w_l} [m]	$U_{(WRF)}$ [e] [m s^{-1}]	*Dir.* *(WRF)* [deg]
R1JD	7 Jan 2009	11.57	2.22	323	5.89	6.65	1.43	20.86	0.45	579	6	13.21	320
R1SD	7 Jan 2009	16.30	7.29	320	13.93	10.75	3.76	13.85	4.18	272	29		
R2JN	7 Jan 2009	10.05	1.89	327	4.19	3.54	0.95	18.19	0.84	670	8	14.83	325
R2SN	7 Jan 2009	17.58	6.82	319	7.04	5.30	2.56	11.49	4.37	1172	27		
R3JD	6 Jan 2009	10.92	2.07	324	4.43	4.45	1.09	6.00	0.60	546	7	12.73	317
R3SD	6 Jan 2009	17.70	7.12	316	4.32	6.86	2.14	8.25	1.75	1180	28		
R4JN	6 Jan 2009	10.24	1.84	317	4.10	4.56	1.04	7.26	0.75	682	6	8.39	299
R4SN	6 Jan 2009	11.59	3.80	321	1.11	1.79	0.63	10.76	0.97	1159	15		
R5JD	17 Jan 2009	12.11	2.33	334	5.23	6.65	1.62	11.23	1.10	712	8	9.15	315
R5SD	17 Jan 2009	12.42	5.42	272	7.75	6.14	2.40	12.06	2.70	621	10		
R6JN	17 Jan 2009	10.62	1.80	311	3.92	3.62	1.00	17.91	0.90	531	6	7.74	295
R6SN	17 Jan 2009	15.03	6.60	276	5.08	6.21	2.09	9.16	4.55	1002	26		
Average													
Junior Day (JD)		**11.53**	**2.21**		**5.18**	**5.92**	**1.38**	**12.70**	**0.72**	**612**	**7**		
Junior Night (JN)		**10.30**	**1.84**		**4.07**	**3.91**	**1.00**	**14.45**	**0.83**	**628**	**7**		
Senior Day (SD)		**15.47**	**6.61**		**8.67**	**7.92**	**2.77**	**11.39**	**2.88**	**691**	**22**		
Senior Night (SN)		**14.73**	**5.74**		**4.41**	**4.43**	**1.76**	**10.47**	**3.30**	**1111**	**23**		

[1] Mean horizontal wind speed computed from the five hour time section

[b] Vertical wind speed computed from the five hour time section

[c] Variances of streamwise (u), crosswise (v) and vertical (w) wind velocities

[d] Streamwise (L_u) and vertical (L_w) turbulent length scales derived from the inertial subrange frequency for the small (s) and the largest (l) eddy size

[e] WRF model predicted surface wind speed and direction for the ridge top site averaged from the corresponding experimental measurement period

Table 4. Summary of ratios of lateral to vertical variances from this and other relevant research. The variances were normalised using vertical variance for each set of data.

	U [m s^{-1}]	$\frac{\sigma_u^2}{\sigma_w^2}$	$\frac{\sigma_v^2}{\sigma_w^2}$	$\frac{\sigma_u^2/\sigma_w^2}{\sigma_v^2/\sigma_w^2}$
Ridge Top Junior	**10.91**	**3.88**	**4.13**	**0.94**
Ridge Top Senior	**15.10**	**2.89**	**2.73**	**1.06**
Bradley (1980) Complex terrain	8.30	2.14	2.56	0.84
Jiboori et al. (2001) Complex terrain	3.33	4.56	4.53	1.01
Teunissen (1980) Flat terrain	9.26	3.61	2.25	1.60
Counihan (1975) Flat terrain	5-7	4.00	2.25	1.78
Cao et al (2009) Flat terrain typhoon	20-30	3.24	2.25	1.45

ANALYSIS OF RESULTS

Variances, length scales and measured spectra

The average variances presented in Table 3 suggest that the Senior site was generally more turbulent, with higher horizontal and vertical wind speeds, which was expected since it was more exposed, 40 m higher in elevation than the Junior site, and has more complex topography in the near upwind vicinity of the measurement tower. There is also a diurnal variation in wind intermittency, as measured by the velocity variances. The diurnal change of the velocity variances is consistent between for sites; the nighttime variances for the (u, v, and w) wind components presented in the average section of Table 3 are smaller during the more stable nighttime period than the well mixed neutral daytime period, despite the high wind conditions during both daytime and nighttime. In some cases, such as for the Senior site, the nighttime streamwise variance was almost half the value of the daytime one. Statistical variances of wind velocity represent the physical fluctuation intensity of velocity perturbations about the mean, so it is a measure of the turbulent kinetic energy of the wind. Having higher velocity variances during the daytime as opposed to the nighttime indicates the contribution of an extra energy source, which comes from the thermally produced turbulence. It is intuitive to think that the vertical velocity variance should have the highest daytime increase due to vertical buoyancy of surface emerging eddies, but in this dataset the highest daytime increase for velocity variances was recorded for the lateral components for the Senior site, which has higher upwind terrain complexity. We believe that this additional upwind terrain complexity had an effect in transforming the energy associated with upwind vertical velocity fluctuations into the lateral direction, producing an increase in the horizontal velocity variances measured further downwind. As a result, the horizontal velocity variances for the Senior site had a maximum relative increase of between night and day of 96% when compared to the maximum of 51% for the Junior site. When analysing the ratios of the normalised streamwise to crosswise variances presented in the fourth column of Table 4 in comparison with other complex terrain findings they reveal a similarity, but with some differences that can be explained by the different averaging interval and

sampling frequency of the instruments used. The ridge top measured variance ratios in this column approach a value of 1, which is again depicted in the complex terrain measurements from Bradley (1980) and Jiboori et al. (2001), but not for the flat terrain data of Counihan (1975) and Teunissen (1980), thus suggesting near isotropic behaviour for complex terrain measurements as far as lateral variances are concerned. Another interesting result is that the variances over the ridge top are greater than the ones for a typhoon case over flat terrain with mean wind speeds of 20-30 m s-1, as described by Cao et al (2009), which suggests that locally produced fluctuations in winds due to terrain can be very significant.

The sampling methodology adopted in this study captured the entire range of the energy spectrum from the large and low frequency eddies to the small and high frequency eddies. Figure 13 shows that the streamwise, crosswise and vertical spectra followed the -2/3 slope suggested by similarity theory in the high frequency range, suggesting universality in the nature of small-scale turbulence. The Junior site daytime (JD) and nighttime (JN) spectra exhibit no diurnal variations and reveal very similar large (Lu_l, ,Lw_l) and small (Lu_s, Lw_s) turbulent length scales, as shown in the average results in Table 3. This result clearly suggests that the daytime and nighttime characteristic large and small-scale eddy sizes did not change diurnally, and there was no footprint of the diurnal signal in the turbulence spectrum energy. The Senior site spectral results also show similar day and nighttime spectral plots but with some differences. The streamwise spectrum of the nighttime case (SN) in Figure 13a show a spectral gap or depression at around 0.05 Hz that coincides with the dip in the crosswise spectrum in Figure 13b. The vertical nighttime spectrum of the senior site (SN) in Figure 13c reveals a decrease in eddy cycle intensity at the high frequency end of the spectrum and this behaviour also repeats itself in the respective crosswise spectrum in Figure 13b. The observed spectral gap and two peaked spectrum will be explained in the following sections when discussing multi-scale turbulent interactions, while a possible explanation for the decrease in eddy cycle intensity in the nighttime vertical spectrum for the Senior site (SN) in Figure 13c can be the lack of thermally produced turbulence that is reducing the energy of the high frequency (or smaller) nighttime eddies. As this occurred

in one isolated spectrum and did not repeat itself in the Junior site vertical spectra (JD and JN) of Figure 13c, it is believed that the upwind terrain complexity of the Senior site played a major role in the difference observed rather than the lack of thermally produced turbulence at night.

Two length scales were derived in Table 3, a large-scale length from the peak in the low frequency region (Lu_l, Lv_l, Lw_l), and a small-scale length corresponding to the frequency in the inertial subrange (Lu_s, Lv_s, Lw_s). The Senior site, in general, was characterised by larger turbulent length scales when compared to the Junior site. This result is due to the fact that lateral wind speeds were greater for the Senior site, producing on average large longitudinal turbulent length scales, while the vertical wind speed due to the steep ridge face upwind of the sensor produced higher vertical wind speeds and consequently large vertical length scales. The average large-scale streamwise turbulent length scales for the Junior and Senior site day and nighttime periods (JD, JN, SD, SN) all fall within, and scale to, the WRF model predicted day and night boundary-layer thickness (1055 m and 630 m respectively), and especially for the case of JN where the values almost match. The scaling of the measured eddy length scales to the upwind boundary-layer thickness suggests that there is minor or no effect of the ridge or near upwind topography on large-scale features, while this cannot be said for the small-scale features.

Double peaked spectra

An interesting feature in the spectral plots of the Senior site, as opposed to the more conventional Junior site results, is the double peaks depicted in both the streamwise and crosswise spectra. The difference in the lateral spectra of the two sites is strongly shown at around 0.4 Hz. At this frequency a secondary peak occurs for the Senior site and is consistent for both the streamwise and crosswise spectra, as shown in Figure 13a and Figure 13b. This phenomenon is not rare and was observed in several previous studies, such as in the near-neutral daytime surface-layer observations in a valley surrounded by complex terrain provided by Li et al (2007), and over flat terrain with convective unstable upstream conditions described by McNaughton and Brunet (2002). According to the conceptual model of Hunt and Morrison (2000), and later presented in

Hogstrom et al. (2002), the existence of the double peak spectrum in their results was caused by the process of eddy shedding in the shear zone of interaction between the mean flow and the top of the lower eddies that are decelerated by ground friction, causing turbulent momentum energy transport between the two scales of turbulence detected in the double peaks, and this is often referred to as the top-down interaction approach. This phenomenon, according to the literature, is restricted to near-neutral and unstable conditions where there might be coupling and turbulent momentum exchange between the outer layer scale and inner layer scale turbulence that correspond to the low and high frequency peaks, respectively. As far as the results from this study are concerned, this phenomenon only occurred for the Senior site lateral spectra, which is the site with the higher wind speeds, variances and higher upwind terrain complexity. Because the double peaked spectra did not occur for the Junior site, which is 5 km to the south-west of the Senior site and has the same large-scale eddy frequency, this rules out the fact that it might be a large-scale eddy interaction with surface sheared eddies. Moreover, another possible mechanism is based on the bottom up approach of McNaughton and Brunet (2002), but for unstable atmospheres, which can be explained by the existence of two interacting scales of turbulence. In this case, the interaction is initiated from the surface upward by unstable thermal eddies that rise and fill up the surface-layer until they interact with the mean flow. The resulting body of rotating eddies of warm air can be visualized as surface roughness, but on an elevated surface of air rather than the ground. This is not the case again for the observed spectra in this study for two reasons: the first being that the phenomena did not repeat itself for the Junior site, and the second was because the atmosphere was characterised by a neutral boundary-layer. The only possible explanation left is the existence of a small-scale turbulence scale produced from small eddies being shed by the steep terrain upwind of the sensor, which can be related directly to terrain induced turbulence. We believe that these small eddies (having a frequency of 0.4 Hz and characteristic turbulent length scale of $\sim$ 37 m), which are being mechanically shed from upstream terrain cause this modification in the spectrum. The intermediate length scale identified between the largest energetic and inertial subrange scales, and the consistent power signature

throughout the measurement period indicate the importance of close upstream terrain in modifying the cascading energy process by creating intermediate sized eddies. This process is similar to the bottom up approach presented by McNaughton and Brunet (2002), but with a fundamental difference, which is that the turbulent interaction is initiated by small surface-layer eddies that are mechanically sheared rather than thermally produced.

Isotropic turbulence assessment

According to Kolmogorov's theory, turbulent energy cascades to smaller and smaller scales, equally distributing energy amongst the three velocity dimensions and reaching an isotropic distribution as the scales approach similarity with viscosity. In high Reynolds number (Re) atmospheric flows, the cascade is well defined and the inertial subrange, if samples are taken at a high enough frequency, extends over 3 or more logarithmic decades. The significance of assessing the local isotropy comes from derivation of the eddy dissipation rate based on Kolmogorov's power laws (Kolmogorov 1941a, b), which are based on the isotropic assumption. Batchelor (1986) extended Kolmogorov's basic similarity laws into Fourier space, analysing streamwise and crosswise velocity structure functions, drawing the conclusion that the crosswise to streamwise spectrum ratios exhibit a 4/3 ratio, as also outlined in Frisch (1995) and Chamecki et al. (2004). Many authors agree with this hypothesis, but since the fundamental derivation is based on dimensional analysis and not physical principles, experimental results are necessary for its verification. Some studies suggest the convergence limit to be 1.0 rather than the theoretical value of 4/3 (Biltoft 2001), highlighting the importance of shear due to buoyancy in producing this convergence limit. Others, such as Chamecki et al. (2004), argue that at the current sampling frequency of sonic anemometers (60 Hz) the instruments are not fully resolving the entire inertial subrange and might bias any assessment of local isotropy. They also concluded that the local isotropy hypothesis was not suitable for surface-layer measurements, and their results revealed that the crosswise to streamwise spectral ratios were closer to the isotropic value than was the vertical to streamwise ratio. Based on the spectral power ratios derived from this study and presented in Figure 14, the Junior site

shows convergence towards 1.3 (4/3) for crosswise to streamwise components in agreement with the results of Chamecki et al. (2004), while the vertical to streamwise components in the inertial subrange (around 1 Hz) converge to 1, confirming the conclusions of Biltoft (2001). In contrast, when considered from a 3D perspective, the results from the Junior site clearly exhibit an anisotropic behaviour and do not adhere to the local three-dimensional isotropic assumption. In the power ratios from the Senior site for the nighttime case there was some scatter around 1 but the results are not conclusive, while the daytime spectral ratios for both the crosswise and vertical dimensions coincide and converge to a value oscillating around 0.75. These results clearly show that for ridge top velocity spectra the local isotropy hypothesis does not hold, at least for the given experimental conditions and given the sampling rate the measurements were taken at. Evidence of convergence of the spectral ratios for both the crosswise and vertical dimensions was more evident at the more complex upwind topography site (Senior), suggesting that the terrain induced turbulence enhanced the energy cascading process and created near isotropic behaviour.

Measured spectra and the neutral spectral model

Since the measurement periods presented in this research correspond to periods of neutral atmospheric stability (as predicted by the model simulation presented earlier), then the measured spectra were compared with the current existing neutral spectral models. The models used here are the flat terrain Kaimal neutral spectral model and the wind-tunnel von Karman model (Burton et al. 2001). Figure 15 represents the streamwise and vertical spectra for the measured data from the Junior and Senior sites and the corresponding neutral spectral model reproduced from Equations 3, 4 and 5 for the measured wind velocities. The results show that the Junior site revealed a better similarity for both day and nighttime periods with the Kaimal neutral spectra, especially at the higher frequency ranges. The measured vertical spectra fit the power peaks of the model predicted ones, while the measured streamwise power peaks occurred at a slightly lower frequency than the ones predicted by the models. An interesting feature for the Junior site spectra is the power enhancement at the lower end of

the frequency axis, which causes a deviation from the Kaimal spectra for both the streamwise and vertical components. This behaviour suggests that the larger eddy sizes are more dominant over the ridge top than over flat terrain. Another feature of this comparison is seen when examining the vertical day and nighttime spectra for the Junior site, where the data follows the Kaimal model for the high frequencies and then follows the von Karman model for the lower frequencies. As far as the Junior site is concerned, it seems that the current neutral velocity spectra models can represent the high frequency information of the spectra, but not the low frequency end of the spectra. Looking at the Senior site comparison results in Figure 15 the situation was quite different, with the streamwise spectra revealing different results from the flat terrain model and only the vertical spectra at the high frequency range following the Kaimal model results. In general, these results show that existing neutral spectral models can represent the general shape of the turbulence spectrum in locations along the ridge top with simple upwind complexity, although the power peaks were dominantly occurring at lower frequencies than the flat terrain sites, thus suggesting large eddy sizes, while the vertical wind spectra is quite well represented by the flat terrain spectral models. Sites with more orographic complexity (such as the Senior site) and strong vertical wind speeds are often poorly represented using these models.

CONCLUSION

Spectral data analysis at two ridge top locations with rather distinct upwind terrain complexity (measured by terrain steepness) during neutral and weakly stable stratification was undertaken to obtain turbulent statistics, length scales associated with eddy sizes, and an isotropic turbulence assessment in the atmospheric surface-layer in a mountainous setting. Instrument sampling rates were sufficient to capture turbulent velocity spectra extending across the cascade from eddy production to dissipation, with the inertial subrange following the 2/3 slope suggested by Kolmogorov theory. Measured variances were consistent with previous complex terrain research results, but not with flat terrain results that demonstrated anisotropic behaviour. It was also found that the site with higher wind speeds and more complex upwind terrain features (Senior) revealed evidence of isotropy when analysing the crosswise to streamwise, and vertical to streamwise spectral ratios, but the convergence limit was closer to a value of 0.75 and not 1 or 1.3 as suggested previously. Isotropy was not attained for the site with less upwind complex terrain (Junior). Both variance and spectral ratio measurements clearly suggest the significance of locally produced turbulence due to the upwind terrain features that enhance isotropy, as in the case of the Senior site. Measured spectra for the two sites exhibited no significant diurnal variation and very similar large-scale and small-scale turbulent length scales for each site, but the turbulence energy measured by the variances revealed a strong diurnal difference.

The average large-scale lateral turbulent length scales for both sites all fall within and scale to the predicted daytime and nighttime boundary-layer thicknesses (1055 m and 630 m, respectively). This scaling of the measured eddy length scales to the upwind boundary-layer thickness suggests that there is a minor or possibly no effect of the ridge or near upwind topography on the modification of large-scale features such as the boundary-layer depth, while variations still remain in the small-scale features. The prominent production of the double peaked spectra for the site with the more complex upwind terrain complexity indicates the role of steep upwind terrain in producing localised turbulent scales, which also enhances isotropy. The double peaked spectra were observed under neutral stability conditions and suggest a multiscale turbulent

interaction initiated by small surface-layer eddies that are mechanically sheared rather than thermally produced.

Existing neutral spectral models can represent locations along the ridge top with simple upwind complexity, but fail to do that when steepness increases. The vertical wind spectrum, on the other hand, due to its higher frequency range than the streamwise spectrum, adjust quite well to the modelled neutral spectra. These results clearly show the level of complexity when dealing with ridge top measurements due to the variability of small-scale terrain features. Flat terrain spectral models and assumptions should not be used confidently for situations such as described here, but rather a detailed examination of upwind terrain features should be taken into consideration. Isotropic turbulence in the surface-layer above complex topography can be very localised and will vary from site to site, but in general, higher wind speeds and increased terrain relief will aid in attaining isotropy.

ACKNOWLEDGEMENTS

We would like to thank the technical staff at the University of Canterbury for assistance with the field work, and Mainpower for permission and assistance to conduct the research on their site. Also, the comments provided by Dr. D. Fitzjarrald and other anonymous referees helped to improve the manuscript substantially, and we greatly appreciate their efforts.

REFERENCES

Batchelor GK (1986) The theory of homogeneous turbulence. Cambridge University Press, Cambridge, 197 pp.

Biltoft CA (2001) Some thoughts on local isotropy and the 4/3 lateral to longitudinal velocity spectrum ratio. Boundary-Layer Meteorol 100:393-404

Bougeault P, Binder P, Buzzi A, Dirks R, Houze R, Kuettner J, Smith RB, Steinacker R, Volkert H (2001) The MAP special observing period. Bull. Am. Meteorol. Soc 82: 433–462

Bradley EF (1980) An experimental study of the profiles of wind speed, shearing stress and turbulence at the crest of a large hill. Q J Roy Meteorol Soc 106:101-123

Britter RE, Hunt JCR, Richards JK (1981) Air flow over a two-dimensional hill. Studies of velocity speed-up, roughness effects and turbulence. Q J Roy Meteorol Soc 107:91-110

Burton T, Sharpe D, Jenkins N, Bossanyi E (2001) Wind energy handbook. John Wiley and Sons Ltd, West Sussex, 617 pp.

Cao S, Tamura Y, Kikuchi N, Saito M, Nakayama I, Matsuzaki Y (2009) Wind characteristics of a strong typhoon. Journal of Wind Engineering and Industrial Aerodynamics 97:11-21

Chamecki M, Dias NL (2004) The local isotropy hypothesis and the turbulent kinetic energy dissipation rate in the atmospheric surface layer. Q J Roy Meteorol Soc 130:2733-2752

Counihan J (1975). Adiabatic atmospheric boundary layers, a review and analysis of data from the period 1880–1972. Atmospheric Environment 9:871-905

De Franceschi M (2004) Investigation of atmospheric boundary layer dynamics in alpine valleys. Dissertation, University of Trento

Frisch U (1995) Turbulence, the legacy of A.N. Kolmogorov. Cambridge University Press, Cambridge, 296 pp.

Hogstrom U, Hunt JCR, Smedman AS (2002) Theory and measurements for turbulence spectra and variances in the atmospheric neutral surface layer. Boundary-Layer Meteorol 103:101-124

Huaxing LU (2008) Modelling Terrain Complexity. In Advances in Digital Terrain Analysis, Springer, pp. 159-176).

Hunt JCR, Morrison JF (2000) Eddy structure in turbulent boundary layers. Euro J Mech B Fluids 19:673-694

Jackson PS, Hunt JCR (1975) Turbulent wind flow over a low hill. Q J Roy Meteorol Soc 101:929-955

Janjic ZI (1990) The step-mountain coordinate: physical package. Mon Weather Rev 118: 1429-1443

Jiboori MH, Yumao X, Yongfu Q (2001) Turbulence characteristics over complex terrain in west China. Boundary-Layer Meteorol 101:109-126

Kaimal JC, Finnigan JJ (1994) Atmospheric boundary layer flows. Their structure and measurement. Oxford University press, Oxford, 289 pp.

Kaimal JC, Wyngaard JC, Izumi Y, Cote OR (1972) Spectral characteristics of surface layer turbulence. Q J Roy Meteorol Soc 98:563-589

Kaimal JC, Wyngaard JC, Haugen DA, Cote OR, Izumi Y, Caughey SJ et al (1976) Turbulence structure in the convective boundary layer. J A Sci 33:2152-2169

Kolmogorov AN (1941a) The local structure of turbulence in incompressible viscous fluid for very large Reynolds number. Dokl Akad Nauk SSSR 30:299-303

Kolmogorov AN (1941b) Energy dissipation in locally isotropic turbulence. Q J R Meteorol Soc 32:19-21

Li W, Hiyama T, Kobayashi N (2007) Turbulence spectra in the near-neutral surface layer over the Loess plateau in China. Boundary-Layer Meteorol 124:449-463

Lumley J, Yaglom A (2001) A century of turbulence. Flow, turbulence and combustion 66:241-286

McNaughton KG, Brunet Y (2002) Townsend's hypothesis, coherent structures and Monin-Obukhov similarity. Boundary-Layer Meteorol 102:161-175

Martins C, Moraes O, Acevedo O, Degrazia G (2009) Turbulence intensity parameters over a very complex terrain. Boundary-Layer Meteorology 133:35-45

Mellor GL, Yamada T (1982) Development of a turbulence closure model for geophysical fluid problems. Rev Geophys Space Phys 20:851-875

Mickle R, Cook N, Hoff A, Jensen N, Salmon J, Taylor P et al (1988) The Askervein Hill project. Vertical profiles of wind and turbulence. Boundary-Layer Meteorol 43:143-169

Moraes O, Acevedo O, Degrazia G, Anfossi D, da Silva R, Anabor V (2005) Surface layer turbulence parameters over a complex terrain. Atmospheric Environment 39:3103-3112

Obukhov AM (1941) On the energy distribution in the spectrum of a turbulent flow. Ser Geogr Geofiz 5:453-466.

Panofsky HA, Larko D, Lipschutz R, Stone G (1982) Spectra of velocity components over complex terrain. Q J Roy Meteorol Soc 108:215-230

Rotach MW, Zardi D (2007) On the boundary layer structure over highly complex terrain: Key findings from MAP. Q J Roy Meteorol Soc 133:937-948

Skamarock WC, Klemp JB, Dudhia J, Gill DO, Barker DM, Duda MG, Huang X, Wang W, Powers JG (2008) A description of the Advanced Research WRF version 3. NCAR technical note. http://www.mmm.ucar.edu/wrf/users/docs/user_guide_V3.1/contents.html. Accessed 18 December 2009

Sturman A, Tapper N (2006) The weather and climate of Australia and New Zealand. Second edition, Oxford University press, Oxford, 541 pp.

Teunissen HW (1980) Structure of mean wind and turbulence in the planetary boundary layer over rural terrain. Boundary-Layer Meteorol 19:187-221

Townsend AA (1961) Equilibrium layers and wall turbulence. J Fluid Mech 11:97-120

Townsend AA (1972) Flow in a deep turbulent boundary layer over a surface distorted by water waves. J Fluid Mech 55:719-735

Tsvang LR, Koprov BM, Zubkovskii SL, Dyer AJ, Hicks B, Miyake M, Stewart RW, McDonald JW (1973) A comparison of turbulence measurements by different instruments. Tsimlyansk field experiment 1970. Boundary-Layer Meteorol 3:499-521

Tsvang LR (1985) Atmospheric turbulence research at the Tsimlyansk Scientific Station of the Institute of the Physics of the Atmosphere of the USSR Academy of Sciences Izv. Atmos Oceanic Phys 21:261-267

Tsvang LR, Kukharets VP, Perepelkin VG (1998) Atmospheric turbulence characteristics over a temperature-inhomogeneous land surface. Part II: The effect of small-scale inhomogeneities of surface temperature on some characteristics of the atmospheric surface layersurface layer. Boundary-Layer Meteorol 86:103-124

Volkert H, Gutermann T (2007) Inter-domain cooperation for mesoscale atmospheric laboratories : The mesoscale alpine programme as a rich study case Q J Roy Meteorol Soc 133: 949-967

Weigel AP, Rotach MW (2004) Flow structure and turbulence characteristics of the daytime atmosphere in a steep and narrow alpine valley. Q J Roy Meteorol Soc 130:2605-2627

Weigel AP (2005) On the atmospheric boundary layer over highly complex topography. Dissertation, ETH Zurich

Weigel AP, Chow FK, Rotach MW (2007) On the nature of turbulent kinetic energy in a steep and narrow alpine valley. Boundary-Layer Meteorol 123:177-199

Welch P (1967) The use of fast Fourier transform for the estimation of power spectra: A method based on time averaging over short, modified periodograms. IEEE Transactions on Audio Electroacoustics 15:70-73

Whiteman CD (2000) Mountain meteorology, fundamentals and applications. Oxford University Press, Oxford, 355 pp.

Yaglom AM (1994) Fluctuation spectra and variances in convective turbulent boundary layers: A re-evaluation of old models. Physics of Fluids 6:962-972

Zeman O, Jensen NO (1987) Modification of turbulence characteristics in flow over hills. Q J Roy Meteorol Soc 113:55–80

6. Research manuscript M3

Katurji, M., Zhong, S., and Zawar-Reza, P. (2011). Long-range transport of terrain-induced turbulence from high-resolution numerical simulations. ***Atmospheric Chemistry and Physics Discussions***, 11(3), 9797-9829. doi: 10.5194/acpd-11-9797-2011.

LONG-RANGE TRANSPORT OF TERRAIN-INDUCED TURBULENCE FROM HIGH RESOLUTION LES EXPERIMENTS

M. Katurji[1], S. Zhong[2] and P. Zawar-Reza[1]

[1] {Center for Atmospheric Research, University of Canterbury, Christchurch, New Zealand}

[2] {Department of Geography, Michigan State University, Michigan, USA}

Correspondence to: M. Katurji (marwan.katurji@gmail.com)

Abstract Over complex terrain, an important question is how various topographic features may generate or alter wind turbulence and how far the influence can be extended downstream. Current measurement technology limits the capability in providing a long-range snapshot of turbulence as atmospheric eddies travel over terrain, interact with each other, change their productive and dissipative properties, and are then observed tens of kilometers downstream of their source. In this study, we investigate through large eddy simulation (LES) the atmospheric transport of terrain-generated turbulence in an atmosphere that is neutrally stratified. The simulations are two-dimensional with an isotropic spatial resolution of 15 m and run to a quasi-steady state. They are designed in such a way to allow an examination of the effects of a bell-shaped experimental hill with varying height and aspect ratio on turbulence properties generated by another hill 20 km upstream. The averaged fields of the turbulent kinetic energy (TKE) implies that terrain could have a large influence on velocity perturbations at least 30H (H is the terrain height) upstream and downstream of the terrain, with the largest effect happening in the area of the largest pressure perturbations. The results also show that downstream of the terrain the TKE fields are sensitive to its aspect ratio with larger enhancement in turbulence by higher aspect ratio, while upstream there is a suppression of turbulence that does not appear to be sensitive to the terrain aspect ratio. Instantaneous

vorticity fields shows very detailed flow structures that resemble a multitude of eddy scales dynamically interacting while shearing oppositely paired vortices. The knowledge of the turbulence production and modifications by topography from these high-resolution LES can be helpful in understanding long-range terrain-induced turbulence and improving turbulence parameterizations used in lower resolution weather prediction models.

INTRODUCTION

Through Large Eddy Simulation (LES), we examine the transport of turbulence generated by topographic features in the atmospheric boundary layer. Atmospheric flows have high Reynolds number (*Re*) on the order of 10^9 and the turbulent eddies generated typically range from a few metres (surface eddies) to boundary layer height (a couple of kilometres).

Atmospheric turbulence is very complex in nature and is often a combination of many spatial and time scale phenomena, (Lin, 2007; Pielke, 2002; Stull, 1988; Orlanski, 1975), ranging from daily cycles of tens of kilometers to fraction of second events at the sub-millimeter scale. The interest in atmospheric turbulence comes from its importance in the mixing phenomena and high frequency energy transport. Turbulence applications can include air pollution, aviation safety, wind energy, which has been greatly correlated to the development of the super computing capabilities (Anderson et al., 2009). In the boundary layer, turbulent kinetic energy (TKE) per unit mass (m^2s^{-2}) as shown below statistically characterizes turbulence, which is the average sum of the squared perturbation velocities (Equation 6, Stull, 1988).

$$\frac{TKE}{m} = \bar{k} = 0.5(\overline{u'^2} + \overline{v'^2} + \overline{w'^2}) \quad (6)$$

Topography produces TKE by mechanical shear, which represents the transformation of the mean kinetic energy of the flow to the turbulent kinetic energy through turbulent momentum flux interaction with the mean wind shear.

Resolving the smallest-scale atmospheric boundary layer flow poses a huge computational challenge, and to overcome this scientists develop simplifications of the physical system and try to reduce the solution so as not to cover the full

turbulence scale. An example of this is the ongoing development of large eddy simulations (LES). LES was first pioneered by Smagorinsky (1963), in which large-scale turbulence is fully resolved and the sub-grid scale effect is parameterized, based on the energy cascading principle. Details of the numerical process can be found in Mason (1994) and Sagaut (2001). Current application trends in applied LES can be found in cross-disciplinary studies with various success rates like in geophysics, oceanography, medical science, combustion, etc (Bouffanais, 2010). Bouffanais (2010) points out the importance of the mechanisms and difficulties of the cross-disciplinary application of LES, one of which is the choice of the sub-grid parameterization aimed at better representing flow features at smaller scales, in particular near the surface. Theoretically, running LES code with very fine resolution makes the solution invariant to the sub-grid scale parameterization, but improvements can be made by using a hybrid model of more than one sub-grid parameterization scheme or running an ensemble of LES codes (Iizuka and Kondo, 2004; Fedorovich et al., 2004; Beare et al., 2006).

A more practical use of LES is its application in the wind energy industry. Turbulence information is crucial for characterizing the cyclic structural loads that ultimately lead to fatigue and failure of the turbine structure. LES provides more accurate dynamic turbulence information as opposed to the traditional methods used in the European Wind Atlas system (Troen and Petersen, 1989) that were ultimately designed for flat terrain, attached flows, and relied on linear models from Jackson and Hunt (1975) and Mason and Sykes (1979). Many studies reported an underestimation of flow separation, turbulence intensities and gust measurements in the linear model solver, and thus stressing the importance of using non-linear models in the wind resource prediction (Palma et al., 2008; Castro et al., 2003). The importance of LES was highlighted 10 years ago in the review of Wood (2000). In more recent times, the application of LES in the wind energy industry has taken a big stride forward, and its economic application in a full-scale resource assessment has been examined by Tamura (2008), in which the author pointed out that computational costs is not the hindrance but it is the parallelization algorithm that will make a good practical

use of LES. Another application of using LES output in the wind energy industry was reported by Kelly et al., (2004) in which the authors used LES output for atmospheric waves as input for the wind turbine structural design. The above are all examples of the practical use of LES in wind energy applications.

The improvements of LES capabilities as a result of rapid advancements in hardware technology and parallel computing algorithms permits a detailed examination of atmospheric turbulence phenomena that are difficult to observe, but are very important to understand for practical applications. Acquiring real measurements of turbulent eddies, or coherent turbulent structures in the atmospheric boundary layer can be a very difficult task, especially if the dynamic information is required. The limitation is the absence of an instrument that can take a long range snapshot of turbulence as the eddies travel over terrain, interact with each other, change in their productive and dissipative properties, and are then observed tens of kilometres downstream of their source.

To our knowledge, little is known about long-range transports of turbulence, as indicated by turbulent kinetic energy (TKE), from high-resolution model simulations, as is presented in this paper. Previous work has considered the details of rotor dynamics in relation with stability and upstream wind profiles on the immediate lee side of mountains, but did not focus on the long-range transport of TKE. Hertenstein and Kuettner (2005) investigated rotor types produced on the lee side of an idealized mountain using two-dimensional (2D) LES simulations with horizontal grid spacing of 150 m. Doyle and Duran (2007) extended rotor dynamic analysis to include 2D and 3D simulations; their horizontal resolution was 60m and also in a stable atmosphere. Moreover, Harman and Finnigan (2010) in their numerical investigation of turbulence within canopies concluded that to properly assess local turbulence it is important to have knowledge of the terrain in a larger area, which can have influence on the local turbulence measurements. This work focuses on the evolution of TKE field downstream of the turbulent rotor formed by a hill. The turbulent intensity of the rotors as they travel downstream over terrain with varying steepness or aspect ratio (AR) is also examined. The diagnosis of the TKE at this high resolution is crucial in quantifying the velocity intermittency for

practical applications such as wind energy. The TKE derived from the high resolution LES can also provide a good framework for the development of high-order turbulence closure schemes, which are required for lower resolution numerical weather prediction models.

METHODOLOGY

The research approach in this work is purely numerical, and this is due to the technical and economic difficulty in measuring TKE at such a large scale. The model used was the LES version of the Atmospheric Regional Prediction System (ARPS) (Xue et al., 2000, 2001) that was specifically designed to simulate small-scale atmospheric phenomena like thunderstorms and tornados. ARPS was validated successfully in numerous studies (e.g., Chow et al., 2006; Weigel et al., 2006), and also cross-compared with other LES codes for different atmospheric stability conditions (Fedorovich et al., 2004; Beare et al., 2006). ARPS was also used in some idealized high-resolution experiments to investigate turbulent structures over forested hills (Dupont et al., 2008; Fesquet et al., 2009).

The basic idea behind the current design of numerical simulations is to be able to simulate high wind speed scenario that is capable to generate consistent turbulent eddies or rotors in the wake of a terrain feature. The perturbations produced by the terrain feature travel downstream over a relatively long distance of approximately 20 km before they encounter an experimental series of terrain configurations with varying aspect ratios. The turbulent perturbations, assessed by analyzing the resolved TKE, is compared for zones 15 km upstream and downstream of the experimental terrain to study the long-range transport and modification of the TKE field.

Model simulation setup

The simulations are 2D with an isotropic spatial resolution of 15m and run to a quasi-steady state in a neutral atmospheric background, and with horizontal and vertical number of grid points of 4099 and 353, respectively. The simulations are designed in such a way to allow an examination of the effects of a bell-shaped hill with varying steepness or aspect ratio on turbulence properties generated by another hill 20 km upstream. The inflow (westerly) velocity is assumed to be

uniform at 15 ms^{-1} and constant in time. The model domain is 61.5 km in horizontal dimension and 5.3 km in vertical dimension. Bottom boundary condition is non-slip rigid wall, while the top is a zero gradient condition with a Rayleigh damping sponge layer in the upper third of the vertical domain. The lateral inflow (west) and outflow (east) boundary conditions are set to zero gradient while periodic boundary conditions are used at the north and south boundaries, The surface heat exchange processes were turned off so as to consider a pure mechanical turbulent production at this stage of the current research. For the sub-grid turbulence parameterizations the 1.5-order TKE turbulence closure scheme is selected. The computational time step is 0.1 s and all simulations are run to a steady state that was usually reached after 5 hours of simulation time. The analyses results correspond to half hour averages after steady state is reached, which typically takes about 5 days real time on a 32-processor computer cluster.

Terrain setup

The model domain contains two bell-shaped hills separated (peak to peak) by 20 km. The topography of both hills can be described by the following equation:

$$H(x) = \frac{H_{\max}}{1 + (\frac{X - X_c}{X_{hw}})^2} \tag{7}$$

where H_{max} is the maximum height of the hill, X_c is the center position or the coordinate corresponding to H_{max}, and, X_{hw} is the hill half width. The first hill (referred to as turbulence generator) is responsible for producing the background turbulence that is then modified by the downstream or the second hill (referred to as experimental hill).

Two sets of experiments are carried out and constitute in total 7 simulations. Set (I) consists of 5 simulations with an eddy generator of fixed height (H=500 m) and aspect ratio (AR=0.25) and 4 experimental hills of the same height (500 m) but with different aspect ratios. The aspect ratio is calculated based on the ratio of the height of the bell-shaped hill to the hill half width (H_{max}/X_{hw}). So technically the slope of the experimental hill is changing and is based on the

steepest face facing the incoming flow. One of the experiments in set (I) is the base simulation, and this only contains the eddy generator without any downwind experimental terrain. The base simulation is necessary to provide the background flow for estimating the modifications by the experimental hill of the turbulence produced by the eddy generator and advected downstream to the experimental hill. A summary of the terrain setup for set (I) is shown in Figure 17a; the steepness increases gradually for experiments t02E01, t02E02, t02E03 and t02E04 from 14, 18, 26, to 45 degrees. The second set (II) of experiments, shown in Figure 17b, consists of two simulations in which the sensitivity of turbulence fields to the height of the terrain generator and to the height of the experimental hills is examined.

Shown in Figure 18 are selected zones from which the half-hour averaged fields are extracted. Zone (A), located in between the eddy generator and the experimental hill, highlights the upstream effects of the experimental hill on the flow field, while zone (B) is downstream of the experimental hill. Figure 18 also shows the locations of several vertical profiles from which vertical profiles are extracted.

RESULTS AND ANALYSIS

In this section we first present results for the average fields produced by the LES experiment to show agreement with previous published work, and subsequently present the TKE fields. The results are presented in separate sections for set (I) and set (II) of the experimental runs, and all correspond to 30-minute averages. The resolved TKE is calculated from horizontal and vertical velocity perturbations sampled at a frequency of 1 Hz. The velocity perturbations are derived from subtracting the 1-minute mean velocity from the total resolved velocity, which are then used in deriving the 1-minute TKE. The reason behind choosing a 1-minute averaging period for the TKE calculation is based on the turnover cycle of the largest eddies presented in the domain. This is deduced from time series spectral analysis of the vertical velocity that indicated a turnover eddy cycle of around 7 to 11 minutes. So the 1-minute averaging interval is chosen accordingly so as to lie within this large cycle period. An inspection of the parameterized sub-grid scale TKE, deduced from the

turbulence closure scheme, reveals that the model is resolving 97% of the TKE and only 3% is parameterized at the current spatial resolution. For this reason the TKE used in the analysis will be considered to be the resolved TKE.

Vorticity and rotor dynamics

Figure 19 presents three instantaneous fields at three consecutive times (2 minutes apart) of the vorticity extracted from one of the experiments of set (I). The extraction location is between distances 40H to 90H (H is the maximum height of experimental hill (Figure 18) covering a distance of 60 km downstream of the experimental hill. Immediately downstream of the hills, flow separation introduces mechanical shear leading to the formation of eddies that rotate clockwise (negative vorticity). These eddies typically scale to the height of the experimental hill. Between 35 and 38 km small rotor begin to form as the incoming flow over the hill shears and separates from the lee side zone characterizing the circulation zone in the wake of the hill. Smaller rotors of similar vorticity signs join together as shown in the time evolution of rotors (r1), (r2) and (r3) of Figure 19a.

As eddies propagate downstream, they become larger because they gain energy from the background flow. The height of the centre of the large rotors is around the the height above the surface of the experimental hill and the rotor sizes extend to around 1000 m in the vertical and about 1500 m in the horizontal. The large eddies leave behind a trail of smaller eddies that rotate in the same direction. The energetic large scale rotors rotate in a clockwise direction with a clear shear perimeter on the outside of the eddy characterized by the red color; this is evident in the trailing edge of rotor (R3) in Figure 19a. These large rotors, as in (R3) and (R4), join together where rotor (R3) bottom half section tilts forward as shown in Figure 19b to join with the slower moving rotor (R4) as shown in Figure 19c.

Of interest is the shedding of smaller counter-rotating eddies from larger eddies. These interesting features appear to be produced by the shear instability at the outer edge of the larger eddies; smaller rotors detach on the upper edge to produce rotors (v2) and (v1) in Figure 19a, which rotate in the opposite

direction and scale around 300 m in the vertical and 500 m in the horizontal. They tend to shear off and get embedded in the background flow, moving faster downstream than the larger eddies that are attached to the ground leaving a trail of negative vorticity in their wake that appears to interact with the new coming rotors from upstream.

Another interesting feature in the vorticity diagrams is the evidence of very weak background waves (refer to the area enclosed by the square in Figure 19) dispersed throughout the domain trailing behind eddies. These numerical imprints resemble wind generated sand cusps on the beach.

The rotors forming on the upper edge of the circulation zone in the lee side of the experimental hill, rotors (r1), (r2) and (r3), are similar to those previously documented in numerical simulations of lee waves and rotors for stable atmospheres (Doyle et al., 2009). The rotors in the previous studies had similar dynamical properties as the ones in our simulations, except that they were forming further downstream of the hill as an interaction of strong down slope winds with the lifted flow due to the mountain wave in the stable atmosphere, this interaction causes mechanical shearing of sub-rotors that travel along the crest of the wave. In our case the atmosphere is neutral and hence the absence of the lee side mountain wave causes an earlier formation of the rotors that shed off the relatively slower winds in the lee side of the hill. Also, lidar observations during the T-REX field campaign (De Wekker et al., 2009) showed evidence of sub-rotor activity on the leading edge of the main rotor that is embedded in the large-scale wave and rotate counter clockwise with the flow. In our simulations the sub-rotors forming downstream of the experimental hill, are rotating counter clockwise, but additional smaller rotors are formed on the upper edge of the main rotor and then drawn downwards to the surface by the pressure field created by the large rotor advection.

Mean wind speeds

The introduction of topography produces areas of positive and negative pressure perturbation, Figure 20. The perturbations are responsible for accelerating or decelerating the flow field depending on direction of the pressure gradient. The

highest negative pressure perturbation is found in the lee side of both the eddy generator and the experimental hill where mass convergence is observed.

Downstream of the eddy generator, Figure 20(a, b), the pressure perturbation field is quite complex. Below 200 m, there are surface-based patches of positive and negative pressure perturbations. These roughly correspond to the flow feature of the boundary layer eddies as they roll over the surface (i.e. causing a surface return flow). As will be discussed later, these effects manifest as reduced surface winds and increase in wind shear. In Figure 20c, the introduced experimental hill causes an increase in the positive pressure perturbation downstream of the eddy generator with the strongest effect in the 5.5 km mark in zone (A), Figure 20c. Increase in the upstream penetration of positive pressure perturbations at higher altitudes in zone (A) was also occurs.

The mean horizontal U-velocity for the base simulation (t02) and the ensemble average of the 4 experiments (t02E01, t02E02, t02E03 and t02E04) are shown in Figure 21(a, b) and Figure 21(c, d), respectively, and the difference between the base simulation and ensemble average results can be found in Figure 21(e, f). Vertical wind shear of U-velocity extends to a height of 565 m for the base simulation in both zones (A) and (B) in Figure 21(a, b). The introduction of the experimental hills thickens the layer affected by horizontal wind shear to 752 m in zone (A) and (B) in Figure 21(c, d). This thickening increases the gradient of the horizontal wind shear immediately above the return flow (blue colored areas in Figure 21a). Horizontal wind shear of U-velocity is depicted in the wind speed acceleration zone above the return flow (blue color) in Figure 21a.

Another important feature is the separation zone in the lee side of the terrain hills. As expected from the high wind speed flow regime over a sloped terrain, the flow detaches from its streamlined regime and creates a circulation zone in the lee side characterized by negative pressure perturbations and negative pressure gradient force as explained earlier. This zone extends, for the base simulation in Figure 21a, to 6.5 km or 13H downstream of the eddy generator. The presence of the hill downstream of the eddy generator causes the separation zone to shrink towards the hill to 4.4 km or 8.8H as shown in Figure 21e. Breuer

et al. (2009) showed in a series of direct numerical simulations (DNS) and LES of flows over periodic hills that the recirculation zone was around 5*H* downstream of the hill and pushed back as Reynolds number increased. Their simulations were carried out for hill separation distance of 9*H* with a maximum *Re* of 1.0595×10^4, but in our simulations the hill separation distance was 40*H* with *Re* on the order of 10^8. The return flow intensifies in this case by 4 ms^{-1} (Figure 21e) at the 2.5 km mark, which equates to a relative increase of 57%. This reveals a direct relation between the intensity of the surface return flow and the pressure gradient flow in the lee side of the hill, as was previously pointed out in the 2D simulations by Doyle and Durran (2002). A general decrease in mean velocity was induced throughout zone (A), Figure 21e, from 8.5 to 17.5 km between the surface to 1000 m height level. In zone (B), Figure 21f, the experimental hill caused an overall decrease in wind speed, but the interesting features were the surface patches of increased wind speed that were about 3 km apart and correlate to the surface pressure perturbations discussed earlier in this section.

The influence of the hill height on the mean flow is revealed in Figure 22 that show the results from set (II) experiments. In the case of the 1000 m experimental hill, zone (A) exhibits a larger decrease in the mean wind speed upstream of the experimental hill (Figure 22a), as compared to the simulation in set (I) shown in Figure 21c. The major modification that a 1000 m high terrain had on the flow field is depicted in the lee side of the hill in Figure 22(b, c). Between 5.5 and 8.5 km (Figure 22c), and between 6.5 and 10.5 km for the steeper hill (Figure 22b), there is an area of high wind speeds that extended from the surface up to about 1000 m. This region was also characterized by very low vertical shear of U-velocity. This phenomenon is produced for the case of the 1000m hill and indicates a feature that is missing in set (I). The pressure perturbations in Figure 23 indicate a high negative pressure perturbation zone between 2.5 and 4 km. This causes subsidence of high momentum flow from aloft suggested by the mean vertical velocity in Figure 24, thus enhancing the wind speed in the area between 5.5 and 8.5 km. These simulations highlight the importance of the pressure gradient produced between terrain features and

suggest that this forcing can create large horizontal wind speed shear that should be taken into consideration for many practical reasons.

TKE and velocity perturbations

Turbulence generated by the eddy generator extended horizontally a distance of 8.5 km or 17*H* and vertically a distance of 1000 m or 20*H*. For zone (A) (Figure 25a) and zone (B) (Figure 25b) of the baseline simulation, there is a clear interference pattern that is depicted by the periodic high and low values of TKE, which suggests that as the eddies move from left to right, they leave behind some of their trailing influences that either suppresses or enhances the TKE of the approaching eddy. An examination of the interference patterns reveals that the period of the oscillation patterns is similar to the height of the hill, between 500 m and 600 m. There also appears to be a generation of TKE at the surface every 3 km, which correlates with the surface pressure perturbation wave discussed earlier.

The addition of the experimental terrain, 20 km downstream of the eddy generator, induces considerable modifications to the TKE field in both zones (A) and (B), as shown in Figure 25(c, d) that correspond to the ensemble average of the 4 experiments of set (II). The most interesting, and counter intuitive, feature is the reduction of the TKE intensity and horizontal spatial coverage downstream of the eddy generator in zone A, as shown in Figure 25c. The relative difference TKE diagram of Figure 25(e, f) show that there is a decreasing trend in TKE for 8.5 km downstream of the eddy generator, with a maximum decrease reaching 61% at the 4 km mark in zone (A). From 8.5 to 15.5 km there is an increasing trend in TKE reaching 200% relative increase. Zone (B), as shown in Figure 25f, has an overall increase in the background TKE, which has its maximum values center around the 500 m hill height.

To quantify any cumulative change in the TKE field within the entire zones of (A) and (B), a turbulence intensification factor (TIF) is calculated for each of the two zones. The TIF is the zonal or spatial sum of the TKE difference between the ensemble average of the 4 simulations in experimental set (I) and the base simulation (t02) normalized with the spatial mean of the wind speed. So it

represents a non-dimensional parameter that indicates the changes in turbulence intensity averaged spatially and temporally. TIF is plotted separately for zones (A) and (B) versus the experimental hill aspect ratio as shown in Figure 26. The TIF for zone (A) has a negative sign, indicating a reduction in the turbulence level upstream of the experimental hills, while TIF is positive for zone (B) and values are higher in zone (B) than zone (A), indicating a large increase in turbulence downstream of the experimental hills. The results also reveal that the influence on turbulence in zone (A) is not sensitive to the aspect ratios, but downstream in zone (B), the results vary with aspect ratios and the influence appears to be non-linear.

Vertical and horizontal velocity perturbations are extracted from 6 profiles in zone (A) and (B). The extraction locations are given in Figure 18, and the vertical profiles of the velocity perturbations are given in Figure 27. Over flat terrain with neutral atmosphere, the vertical velocity perturbation usually decreases as function of increasing distances from the terrain, since there is no thermal stratification to create vertical motion other than the topographic lifting force. The vertical velocity perturbations of the base simulation (t02), as shown in the gray dotted lines in Figure 27, reduces in intensity with distance downstream of the eddy generator. This is not similar for vertical velocity perturbation of the ensemble average of the four subsequent experiments with the presence of experimental hill (black dotted lines in Figure 27), where there is a consistent peak in intensity near the height of the hill (500 m) throughout zones (A) and (B). Below half of the hill height (200 m), TKE is primarily generated by the horizontal velocity perturbations, while above that vertical velocity perturbations dominate TKE production with a peak between 400 and 500m. These results show the importance of vertical velocity perturbations induced by terrain even in a neutral atmosphere.

The 1000 m hill produces more intense turbulence (almost twice of the 500 m eddy generator), and the strong turbulence is seen in the entire zone (A) of experiment t03E01 in Figure 28c. The TKE field is also characterized by periodic zones of high and low intensities, but this time they scale to the new hill height and are spatially separated by around 1000 m. In zone (A) (Figure 28c) of

experiment t03E01, a gap in turbulence intensity is created in the area of high wind speeds and low wind shear as indicated in the corresponding U-velocity (Figure 22c). This feature produced a low frequency wave (wave length of ~15 km that is equal to the separation distance between the eddy generator and experimental hill) in the TKE field in which a high frequency signal (wave length of 1000 m) is embedded. In zone (B) (Figure 28d), the influence of the 500 m high experimental hill is to damp out the turbulence generated by the eddy generator, and break the long wavelength into smaller periods that now scale to the 500 m high terrain.

As for the experimental run t02E07, shown in Figure 28(a, b), the influence of the 1000 m high experimental hill appears to significantly reduce the upstream TKE, while in zone (B), as shown in Figure 28b, the TKE appears to be the superposition of the low frequency (high wave length, 15 km) TKE coming from the 1000 m high terrain with the high frequency (low wave length, 500 m) TKE produced by the 500 m high eddy generator. The embodiment of high frequency TKE structures within a larger scale (low frequency) wave implies a long-range transport mechanism of turbulence via low frequency waves.

CONCLUSION

In this paper we have presented 2D high-resolution LES for atmospheric boundary layer flow in an attempt to highlight the importance of long-range transport and modification of the average and perturbation velocity fields by topography. The domain consists of two hills: an eddy generator and an experimental hill 15 km downstream and the atmosphere is assumed to be neutral with a constant wind speed of 15 ms^{-1}.

Only slight modification to the mean wind speed was recorded as a result of different hill aspect ratios of the experimental hill with the 500 m fixed height, while the largest influence was recorded for the intensification of the return flow 15km upstream of the experimental hill. More prominent modifications in the mean wind speed were produced when the height of the experimental hill was doubled from 500 to 1000 m, in which the average wind speed in the region upstream of the experimental hill was significantly reduced and relatively strong

horizontal wind shear was recorded downstream. The induced changes in the mean flow were directly correlated to the pressure gradient force introduced by the experimental hills, which had a long-range (15 km) effect on the velocities. There was also evidence of a shallow surface pressure perturbation wave that created distinct and consistent zones of accelerated wind speeds; this wave had a wavelength of around 3 km or 6*H* and was depicted for the set of simulations with 500 m high hills. Instantaneous vorticity fields, in the neutral atmospheric setting considered in the simulations, revealed the formation of small rotors mechanically sheding from the upper edges of the large boundary layer rotors with rotating direction opoosite to that of the main rotor, thus showing a different formation concept to that of the rotors in stable atmospheres.

The averaged fields of the turbulent kinetic energy (TKE) implied that terrain can have a large influence on velocity perturbations at least 15 km upstream and downstream of the terrain, with the largest effect happening in the area of the largest pressure perturbations. Spatially and temporally integrated TKE showed that the results downstream of the terrain are sensitive to its aspect ratio with an enhancement in turbulence by higher aspect ratio, while upstream there was a suppression of turbulence with little sensitivity to the terrain aspect ratio. Further experiments are required to develop the relationship between the terrain shape and the long-range turbulence field. The stronger pressure perturbations induced by the 1000 m high hill produced a TKE wave on the lee side of the hill with a wave length of ~ 15 km. As a result, there was a large suppression of turbulence below its crest and high surface turbulence as its trough reaches the surface. Eddies appeared to follow the path of the strongest wind speed avoiding the stagnation region, thus creating an arch resemblance in their trajectory (Figure 29). Within the 15 km TKE wave there were higher frequency turbulence structures that scaled with the terrain. In one of the presented simulations, a 500 m hill acted as a turbulence suppressor for the TKE background field produced by a 1000 m hill upstream. The TKE field produced by a 1000 m hill and interacting with the TKE field from a 500 m hill shows a solution that proposes a superposition of two wave solutions, but this idea will

require more simulations and analysis before can be used to develop a model for long-range TKE transport.

The knowledge of the turbulence production and modifications by topography from these high resolution LES can be helpful in improving turbulence parameterizations used in lower resolution weather prediction models. Moreover, the understanding of the TKE long-range transport can prove to be very helpful in practical problems like in the initial phases of wind farm prospecting in complex terrain or atmospheric pollution dispersion problems. But more importantly, the work can have implications towards analysis of wave modeling or multiple-scale perturbations to mathematically represent the transport of the high-frequency vortical structures within the low-frequency waves, which can be the key to understanding long-range terrain-induced turbulence.

ACKNOWLEDGEMENTS

This research was supported by a grant from the Centre for Atmospheric Research at the University of Canterbury and by the U.S. National Science Foundation through grant CDI-0941373 and ATM-0646299. The authors would like to thank Tony Dale from the High-Performance Computing Centre at the University of Canterbury (BlueFern). The authors wish to thank Mike Kiefer, Xindi Bian and Joseph Charney at the U.S. Forest Service Northern Research Station for many useful discussions.

REFERENCES

Anderson, J., Degrez, G., Degtoote, J., Dick, E., Grundmann R., Vierendeels J.: Computational fluid dynamics an introduction (third ed.), Springer, Berlin, 332 pp., 2009.

Beare, R., Macvean, M., Holtslag, A., Cuxart, J., Esau, I., Golaz, J.-C., Jimenez, M., Khairoutdinov, M., Kosovic, B., Lewellen, D., Lund, T., Lundquist, J., McCabe, A., Moene, A., Noh, Y., Raasch, S., and Sullivan, P.: An intercomparison of large-eddy simulations of the stable boundary layer, Boundary-Layer Meteorology, 118, 247-272, 2006.

Bouffanais, R.: Advances and challenges of applied large-eddy simulation, Computers and Fluids, 39, 735-738, 2010.

Breuer, M., Peller, N., Rapp, C., and Manhart, M.: Flow over periodic hills - Numerical and experimental study in a wide range of Reynolds numbers, Computers and Fluids, 38, 433-457, 2009.

Castro, F. A., Palma, J. M. L. M., Silva Lopes, A.: Simulation of the Askervein flow. Part 1: Reynolds averaged Navier–Stokes equations (k–ε turbulence model), Boundary Layer Meteorology, 107, 501-530, 2003.

Chow, F. K., Andreas, P. W., Robert, L. S., Mathias, W. R., and Ming, X.: High-resolution large-eddy Simulations of flow in a steep alpine valley. Part I: Methodology, verification, and sensitivity experiments, Journal of Applied Meteorology and Climatology, 45, 63, 2006.

DeWekker, S. F. J., Mayor, s.D.: Observations of atmospheric structure and dynamics in the Owens Valley of California with a ground-based, eye-safe, scanning aerosol lidar, Journal of Applied Meteorology and Climatology, in press, 2009

Doyle, J. D., Durran, D. R.: The dynamics of mountain-wave-induced rotors, Journal of the Atmospheric Sciences, 59, 186–201, 2002.

Doyle, J. D., and Durran, D. R.: Rotor and subrotor dynamics in the lee of three-dimensional terrain, Journal of the Atmospheric Sciences, 64, 4202-4221, 2007.

Doyle, J. D., Grubisic, V., Brown, W. O. J., De Wekker, S. F. J., Dornbrack, A., Jiang, Q. F., Mayor, S. D., and Weissmann, M.: Observations and numerical simulations of subrotor vortices during T-REX, Journal of the Atmospheric Sciences, 66, 1229-1249, 2009.

Dupont, S., Brunet, Y., and Finnigan, J. J.: Large-eddy simulation of turbulent flow over a forested hill: Validation and coherent structure identification, Quarterly Journal of the Royal Meteorological Society, 134, 1911-1929, 2008.

Fedorovich, E., Conzemius, R., Esau, I., Katopodes Chow, F., Lewellen, D., Moeng, C. H., Sullivan, P., Pino, D., and Vil√†-Guerau de Arellano, J.: Entrainment into

sheared convective boundary layers as predicted by different large eddy simulation codes, 16th Symp. On Boundary Layers and Turbulence, 2004.

Fesquet, C., Dupont, S., Drobinski, P., Dubos, T., and Barthlott, C.: Impact of terrain heterogeneity on coherent structure properties: Numerical approach, Boundary-Layer Meteorology, 133, 71-92, 2009.

Harman, I., and Finnigan, J.: Flow over hills covered by a plant canopy: Extension to generalised two-dimensional topography, Boundary-Layer Meteorology, 135, 51-65, 2010.

Hertenstein, R. F., and Kuettner, J. P.: Rotor types associated with steep lee topography: influence of the wind profile, Tellus A, 57, 117-135, 2005.

Iizuka, S., and Kondo, H.: Performance of various sub-grid scale models in large-eddy simulations of turbulent flow over complex terrain, Atmospheric Environment, 38, 7083-7091, 2004.

Jackson, P. S., and Hunt, J. C.: Turbulent wind flow over a low hill, Quarterly Journal of the Royal Meteorological Society, 101, 929-955, 1975.

Kelly, N., Shirazi, M., Jager, D., Wilde, S, Adams, J., BuhL, M., Sullivan, P., Patton, E.: Low-level jet project interim report, Technical Report NREL/TP-500-34593, National Renewable Energy Laboratories, 2004.

Lin, Y. L.: Mesoscale dynamics, Cambridge Univeristy Press, Cambridge, 630 pp, 2007.

Mason, P. J., and Sykes, R. I.: Flow over an isolated hill of moderate slope, Quarterly Journal of the Royal Meteorological Society, 105, 383-395, 1979.

Mason, P. J.: Large-eddy simulation: A critical review of the technique, Quarterly Journal of the Royal Meteorological Society, 120, 1-26, 1994.

Orlanski, I.: A rational subdivision of scales for atmospheric processes, Bulletin of the American Meteorological Society, 56, 527-530, 1975

Palma, J. M. L. M., Castro, F. A., Ribeiro, L. F., Rodrigues, A. H., and Pinto, A. P.: Linear and nonlinear models in wind resource assessment and wind turbine

micro-siting in complex terrain, Journal of Wind Engineering and Industrial Aerodynamics, 96, 2308-2326, 2008.

Pielke. R. A: Mesoscale meteorological modeling (second ed.), Academic Press, San Diego, 673 pp., 2002.

Sagaut, P.: Large eddy simulations for incompressible flows: An introduction, Springer, Berlin, 2001.

Smagorinsky, J.: General circulation experiments with the primitive equations, Monthly Weather Review, 91, 99-164, 1963.

Stull, R. B.: An Introduction to boundary layer meteorology, First ed., Kluwer Academic Publishers Group, 666 pp., 1988.

Tamura, T.: Towards practical use of LES in wind engineering, Journal of Wind Engineering and Industrial Aerodynamics, 96, 1451-1471, 2008.

Troen, I., Petersen, E. L.: The European wind atlas, Risø National Laboratories, Denmark, 656pp., 1989.

Weigel, A., Chow, F. K., Mathias, W. R., Robert, L. S., and Ming, X.: High-resolution large-eddy simulations of flow in a steep alpine valley. Part II: Flow structure and heat budgets, Journal of Applied Meteorology and Climatology, 45, 87, 2006.

Wood, N.: Wind Flow Over Complex Terrain: A historical perspective and the prospect for large-eddy modelling, Boundary-Layer Meteorology, 96, 11-32, 2000.

Xue, M., Droegemeier, K., and Wong, V.: The Advanced Regional Prediction System (ARPS) - A multi-scale nonhydrostatic atmospheric simulation and prediction model. Part I: Model dynamics and verification, Meteorology and Atmospheric Physics, 75, 161-193, 2000.

Xue, M., Droegemeier, K., Wong, V., Shapiro, A., Brewster, K., Carr, F., Weber, D., Liu, Y., and Wang, D.: The Advanced Regional Prediction System (ARPS) - A multi-scale nonhydrostatic atmospheric simulation and prediction tool. Part II: Model

physics and applications, Meteorology and Atmospheric Physics, 76, 143-165, 2001.

FIGURES

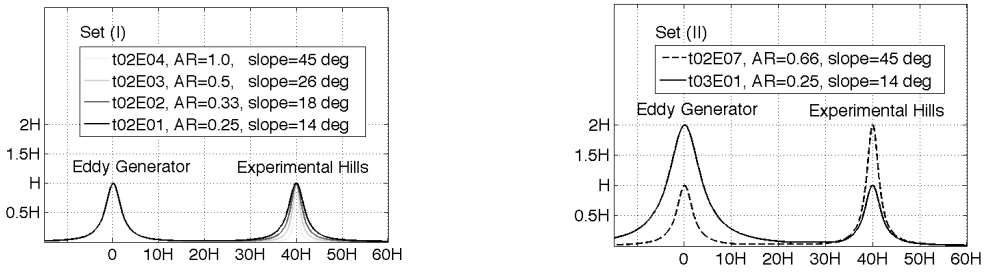

(a) **(b)**

Figure 17. Experimental terrain setup for set (I) and set (II) of simulations, H= 500 m.

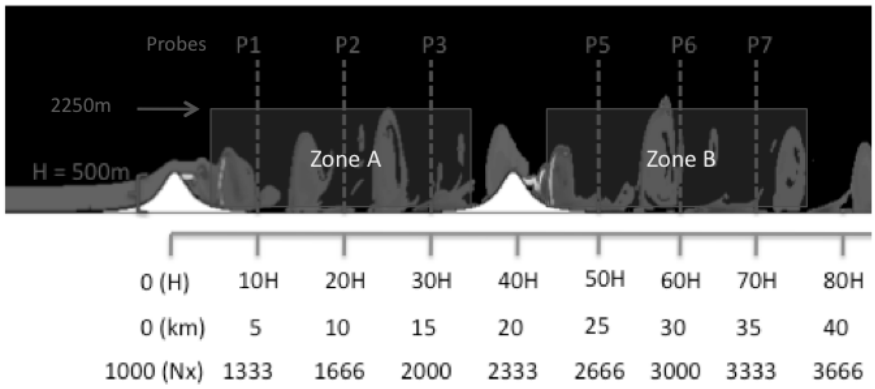

Figure 18. Dimensions and locations of the analysis zones A and B, and the profile locations for vertical profiles.

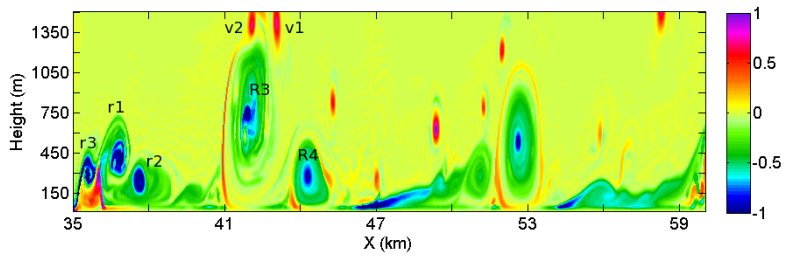

(a)

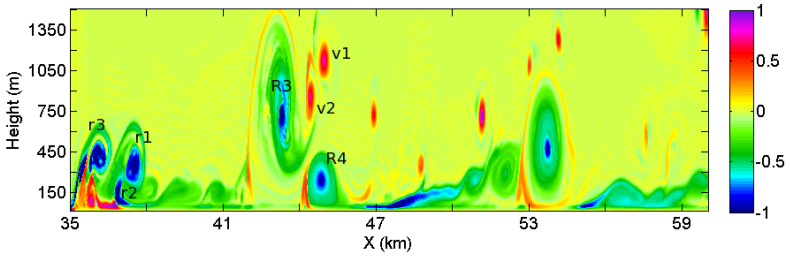

(b)

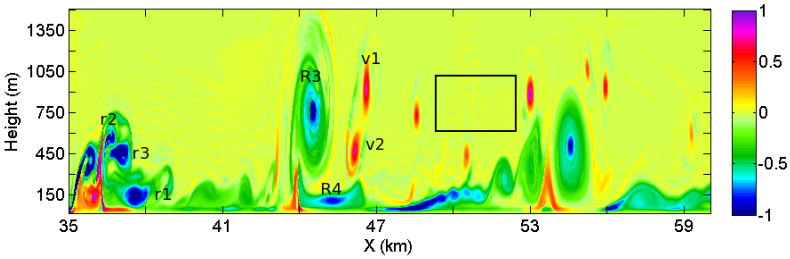

(c)

Figure 19. Y-component vorticity (s^{-1}) extracted from locations 40H to 90H (see Figure 17) extending 25 km downstream from the center of the experimental hill. Red color indicates counter clockwise eddy rotation, while blue color indicates clockwise eddy rotation. Note that the vertical and horizontal axes scales are different.

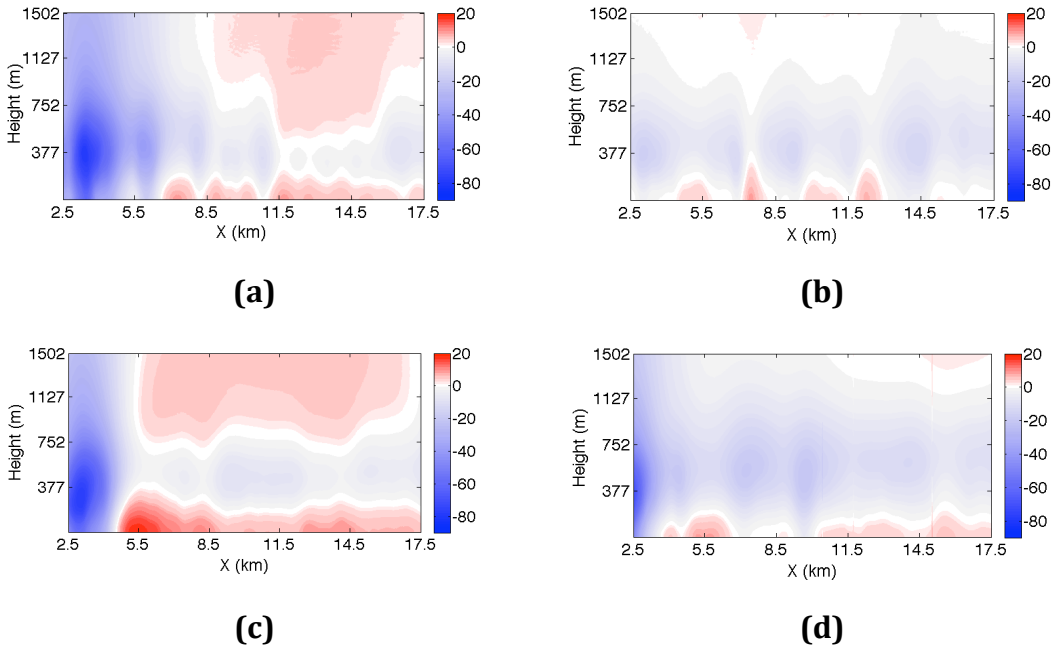

Figure 20. 30-minute average pressure perturbations (Pa) for the base simulation (t02) in (a) and (b), and for the ensemble average of the 4 set (I) experiments in (c) and (d). Zone (A) (refer to Figure 17) correspond to the left column while zone (B) correspond to the right column.

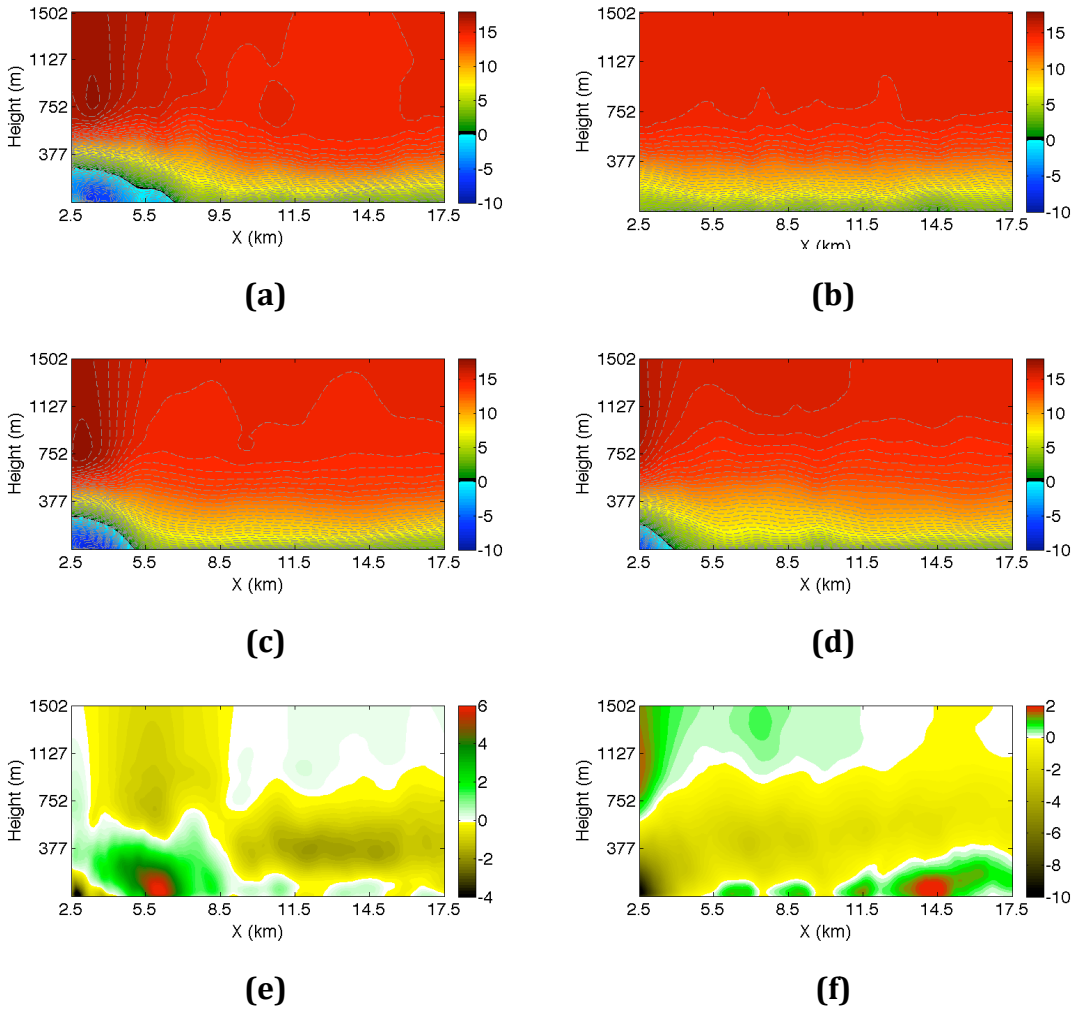

Figure 21. 30-minute average u-velocity (ms^{-1}) for the base simulation (t02) in (a) and (b), and for the ensemble average of the 4 set (I) experiments in (c) and (d). The relative change of the ensemble average and the base simulation is presented in (e) and (f). Zone (A) (refer to Figure 17) correspond to the left column while zone (B) correspond to the right column.

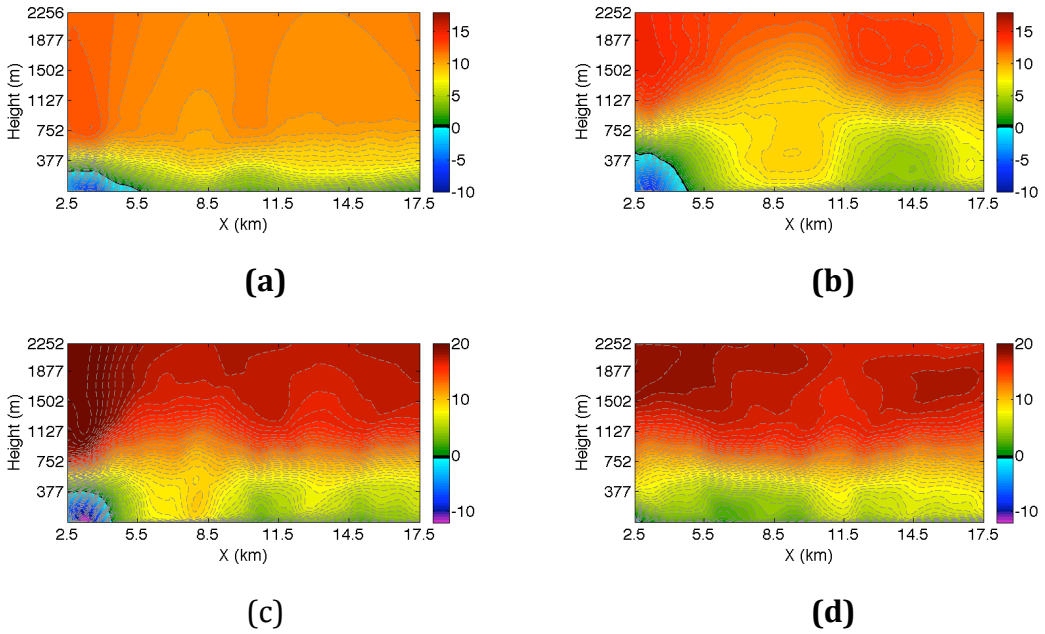

Figure 22. 30-minute average u-velocity (ms^{-1}) for set (II) of experimental runs t02E07 (a, b), and t03E01 (c, d). Zone (A) (refer to Figure 17) correspond to the left column while zone (B) correspond to the right column.

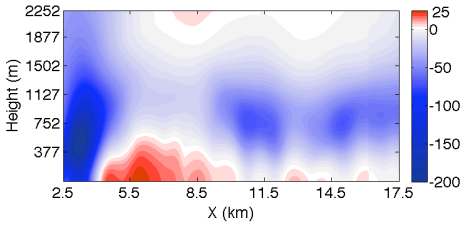

Figure 23. 30-minute average pressure perturbation (Pa) for set (II) experimental run t03E01 zone (A).

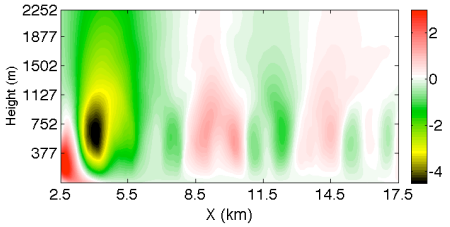

Figure 24. 30-minute average w-velocity (ms^{-1}) for set (II) experimental run t03E01 zone (A).

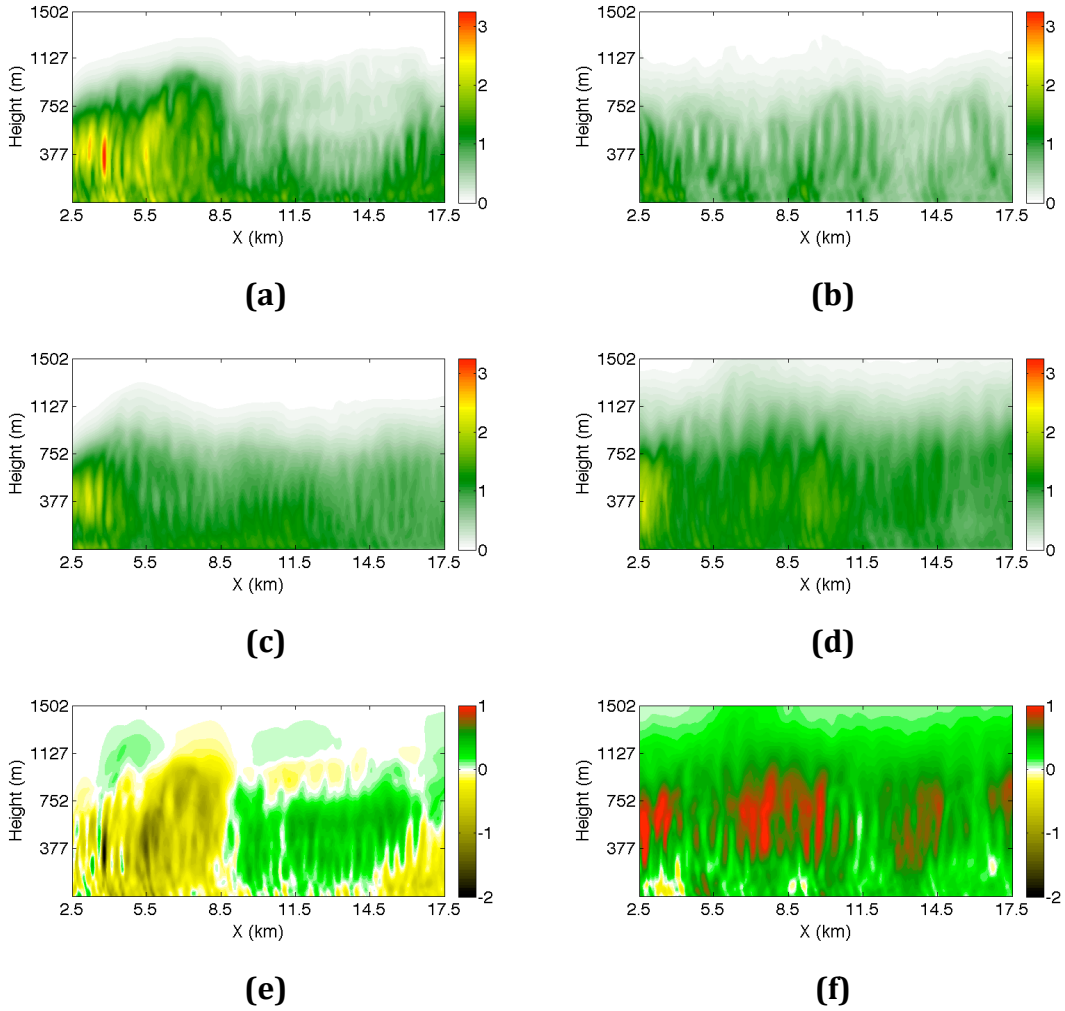

Figure 25. 30-minute average TKE (m^2s^{-2}) for the base simulation (t02) in (a) and (b), and for the ensemble average of the 4 set (I) experiments in (c) and (d). The relative change of the ensemble average and the base simulation is presented in (e) and (f). Zone (A) (refer to Figure 17) correspond to the left column while zone (B) correspond to the right column.

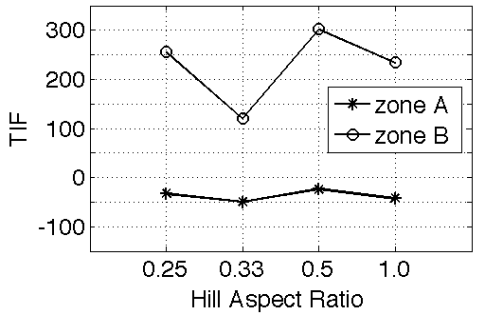

Figure 26. Turbulence intensification factor (TIF) plotted against experimental aspect ratio for the 4 runs of set (I) for zones (A) and (B).

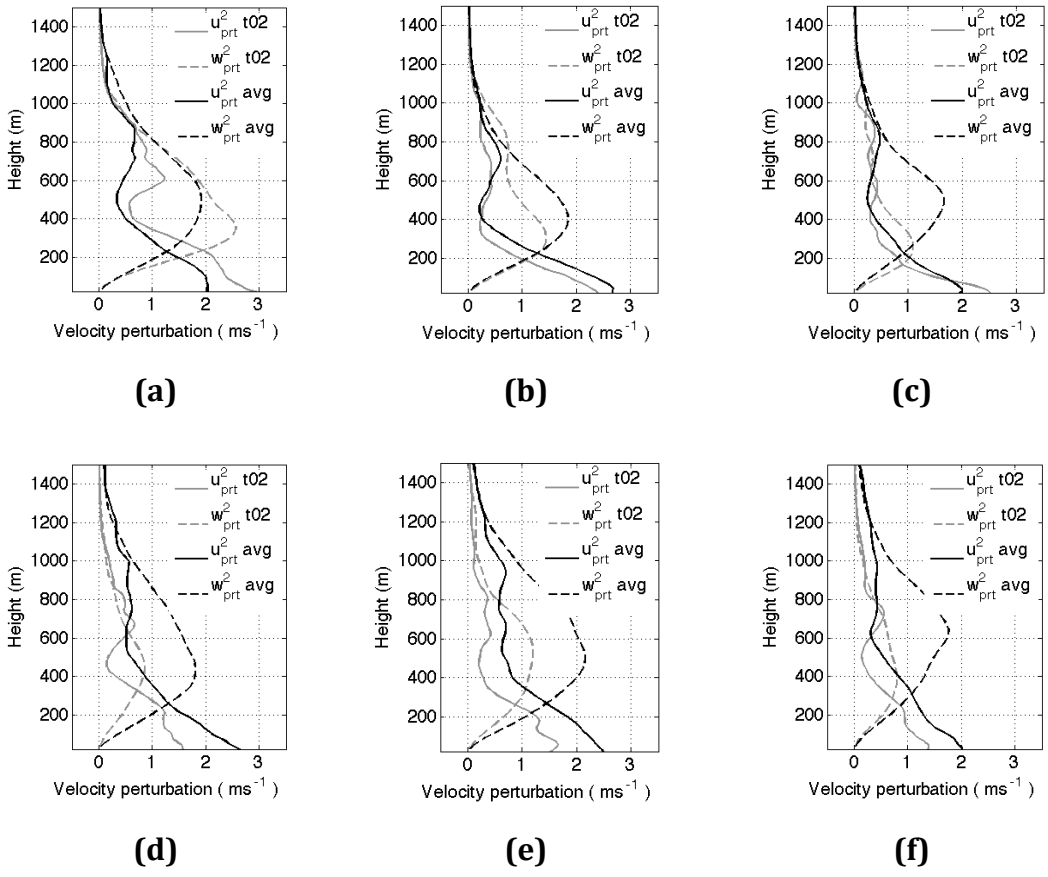

Figure 27. Horizontal (u) and vertical (w) velocity perturbations for the base simulation (black) and the ensemble average of the 4 experiments (grey). (a, b, c) correspond to profile locations 1, 2 and 3, and (d, e, f) for profile locations 5, 6 and 7. See Figure 17 for profile locations.

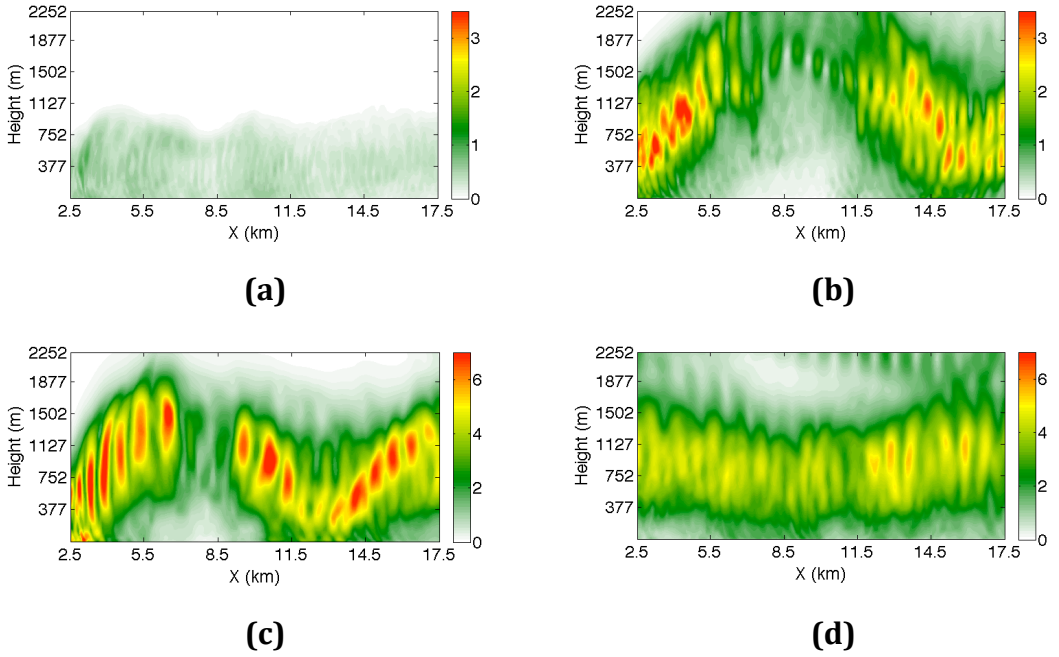

Figure 28. 30-minute average TKE (m^2s^{-2}) for set (II) of experimental runs t02E07 (a, b), and t03E01 (c, d). Zone (A) (refer to Figure 2) correspond to the left column while zone (B) correspond to the right column.

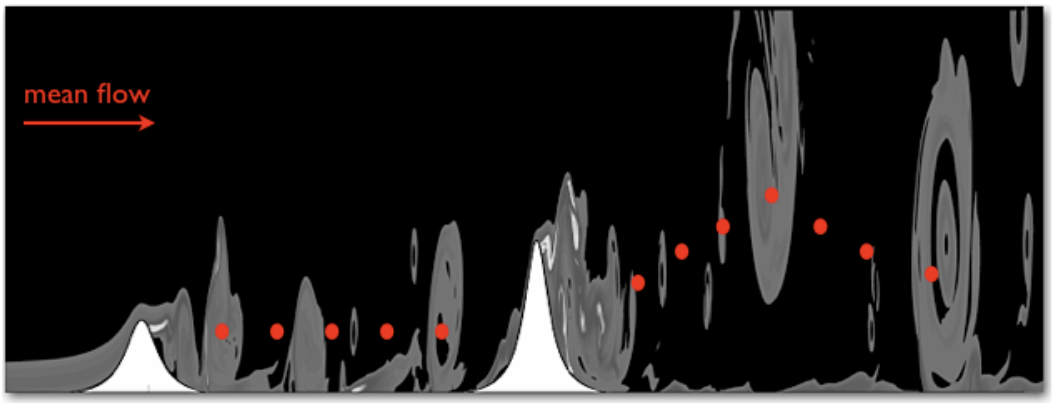

Figure 29. A schematic of eddy (grey shade) trajectory for experimental run t02E07 showing the difference between a 500 and 1000 m high hill. Red dots indicate the mean eddy path.

7. Summary and future perspectives

This research included observational and numerical analysis of the sources of wind turbulence and its evolution in the context of suitability for wind farming. This work also attempted to identify patterns, behaviours, and methods in turbulence analysis and research. Turbulence was measured from point sensors and numerically modeled (2D and 3D) and simulated to capture its spatial characteristics. Combinations of statistical and deterministic techniques were employed to investigate the variability of turbulence over complex terrain.

Turbulence statistics, although very robust in describing physical phenomena, will always have drawbacks, mainly that they are not based on representing the variation of the absolute measured variable, but introduce higher order models for its variability (like averages, variances, covariance's, spectra, etc...). Turbulence is unpredictable in the instantaneous space-time dimension, but possesses some degree of predictability in the statistical domain; for example, the mean of a turbulence quantity for a fixed space is predictable. The same applies for higher order statistics of the turbulent variable. On the other hand, deterministic approaches are represented by classical fluid mechanics and the partial analytical solution of the Navier-Stokes equation. The direct numerical simulation (DNS) method is an example of these approaches. The time averaged Reynolds model or the spatial averaged large eddy simulation model of turbulent fields include in their formulation some sort of statistical representation of higher order moments with lower ordered ones, which introduces the turbulent closure dilemma and turbulence modelling.

It is not suggested that the author is campaigning for DNS of atmospheric flow problems, this will be extremely unachievable by today's computational capabilities, but rather highlight to the reader the linkage between the statistical and deterministic approaches. The following summary includes, to some extent, the philosophies from both approaches.

A 4-month measurement campaign and computer simulations were carried out on an isolated coastal ridge proposed for wind farming. The analysis was focused on identifying key features of wind dynamics, effects of topography on wind

turbulence from both the short and long range perspective, and casting light on the difficulty of wind turbine placement in complex terrain.

Thermal wind circulations and upstream steep topography will dictate the wind shear profile, and consequently have a large impact on wind turbine selection and placement.

The vertical profile of average wind speed, derived from sodar measurements, revealed a prominent diurnal oscillation of winds along the coastal ridge top. Even at 500 m elevation, the summer time easterly sea breeze was strong enough to reduce the wind speed intensity of the prevailing westerly winds, and if not accounted for, can equate to a relative power density loss of 37 %. The measured wind speed profile failed to fit the neutral surface layer wind speed profile model, which is normally extrapolated vertically from surface measurements. Both the logarithmic and power law profiles, with the standard semi-empirical coefficients, were not sufficient to produce a good fit with the observed data. The analysis showed that the bias was mainly due to the upstream steep terrain and the interaction of the sea breeze with the prevailing winds. This highlights the extreme difficulty and uncertainty in using these models and methods to derive the vertical profile of wind speed for wind power density calculations for complex terrain. The sodar, on the other hand, proved to be useful in this situation, and an excellent tool for deriving averaged wind speed vertical profiles. The sodar used in this research covered a vertical range up to 300 m, revealing three different vertical zones, as identified in their relevant sections. This vertical zone classification is very crucial for the placement of the wind turbines along the ridge, in which the effect of the wind shear affects the selection process of a turbine, based on hub height and blade length. In situations were sodar measurements above 100 m are very expensive and sometimes not feasible to verify, the use of computer simulations may be the only option for analysing the wind speed.

Atmospheric flow modelling via a semi-idealized 3D simulation confirmed the observed profiles, and showed interaction of the easterly winds undercutting the westerly winds and causing the reduction in the observed wind speed. This

shear interaction along the boundary interface, of the westerly winds aloft and easterly undercutting ones, caused vertical momentum mixing to around 300 m in height, resulting in the observed reduction in the daytime wind speed between 60 and 125 m height levels. These results highlight the complexities of wind resource assessment over such a heterogeneous terrain configuration. It is highly recommended, based on this research, to incorporate some sort of vertical wind speed profiling (sodar or lidar, etc…) measurements and not rely on wind shear models from surface measurement extrapolations in complex terrain.

A physical experiment over the ridge top, and analysis in the real and Fourier space revealed the following:

1) ***In general, local isotropy can be attained in cases of higher wind speeds and increased terrain relief.***

2) ***The neutral flat terrain spectral model can, sometimes, represent the turbulent frequency response of the flow for sites with simple upwind terrain complexity, but fails to do so for more complex upwind topography.***

3) ***Large upwind turbulent length scales, or "eddies", scaled to the upwind boundary layer depth, but small scale features were terrain dependent.***

An investigation into high Reynolds number turbulent flow over the ridge top site was described based on high-resolution in-situ measurements, using ultrasonic anemometers for two separate locations on the same ridge. The analysis was carried out in both the real and Fourier (frequency) space during neutral and weakly stable stratification. This experiment was unique in the sense that it reflected turbulent wind features from two sites having different upwind terrain complexity, but with the same overall wind flow regime in terms of atmospheric stability and boundary layer depths. The results can be very helpful for wind farming, where often the biggest challenge is turbine placement within the wind farm itself, especially in complex terrain. In attempts to identify universality or site-specific properties of the measured flow, the variances,

spectral power, isotropy assessment and turbulent length scale derivations were carried out for the two sites on the ridge top.

One of the interesting features was the isotropic nature of the flow revealed by both the variance of the velocity field and the spectral power ratios. The "physical" significance of velocity variances can only be interpreted by the degree of randomness exhibited by the turbulent velocity perturbation in any spatial direction. Through spectral power ratios, the power or energy at a given frequency is attained, and can be interpreted as the energy contribution from that frequency, eddy cycle or turbulent length scale. Ratios of lateral to vertical velocity variances of both sites showed convergence towards unity. When isotropy is attained from variance, this means that the turbulent measurement has high degree of randomness in the 3 spatial dimensions, and this is true for the two sites. One can only infer the magnitude of randomness at this stage. This conclusion compared really well with other measured variances in complex terrain from previous literature, but fails to compare to flat terrain studies in which the flow expressed an anisotropic behaviour. This finding seems to reflect the true nature of turbulence and its interaction with boundaries such as the underlying topography to enhance isotropy. The turbulent intermittency seems to increase in the streamwise direction for flat terrain situations, this is in the direction of the main flow, but in complex terrain the added multi-directional perturbations from the underlying roughness redistribute the statistical variations (measured by variances) in the three spatial dimensions. Isotropy also held true for the energy spectrum via Fourier analysis of the high temporal resolution data, but not for both sites. The site with higher upwind terrain complexity (Senior site) showed evidence of converging spectral power ratios (crosswise and vertical to streamwise), but the results also showed different convergence limits from those suggested by the local isotropy hypothesis explained in Section 6.1.3. The site with less upwind terrain complexity (Junior) showed inclination toward an anisotropic condition contradicting what was revealed by the velocity variance.

The above stated results clearly identify contradictions in assessing the turbulence isotropy in both the real space (statistically through variances) and

the Fourier space (through power spectrum analysis). Given the fact that both the power spectral ratio method and variances are purely statistical, and have weak physical interpretations, the local isotropy hypothesis (discussed in Section 6.1.3) failed to be proven under the given experimental conditions, and the results exhibited variability in attaining isotropic turbulence. Nevertheless, the trend in the results from both methods can indicate the direct correlation between attaining turbulence isotropy and degree of terrain complexity. This finding suggests a cautionary approach in deriving or interpreting turbulence spectrum information for wind turbine design and selection.

Numerical 2D experiments for turbulent flow over isolated hills, in neutral atmospheric stability, revealed evidence of turbulence memory in the atmosphere with clear footprints from underlying terrain.

It is often the case that when nearby topography such as slopes and ridges are the defining factors for wind turbine placement within a wind farm site. What is non-intuitive is the advected or transported turbulence from long range (>15 km) terrain features upwind of the site. At this scale, this knowledge becomes useful for the wind farm site prospecting, and this research has indicated such information.

What follows is a summary of how turbulent kinetic energy (TKE) can attain long range memory of underlying terrain and then react accordingly with upcoming terrain. For this purpose, 2D-LES experiments were carried out to investigate effects of different terrain aspect ratios using a large enough numerical domain size to include 15 km upstream and downstream zones.

Before introducing the summary of the TKE field, the mean wind speed modifications due to the terrain, and consequently the mean energy of the flow would be as important to wind farming, as is the TKE field. The results of the mean wind speed from the steady state solution of the simulation, and for the series of different hill aspect ratios, all showed only slight modification of the wind speeds upstream of the experimental hill. Mainly, the modifications showed increased return flow intensity (from the detached circulation downstream of the experimental hill) and horizontal wind shear on the lee side of the eddy

generator hill. The detached circulation zone extended 8.8H downstream of the hill with height H. The major modification of the mean wind speeds did not come from the different aspect ratios, but was more sensitive to doubling the height of the experimental hill. In this case, the return flow downstream of the new higher hill intensified, and a considerable zone of high wind speeds and reduced wind shear was created to around 10H downstream of the hill. This downstream area, representing a mean turbulent energy gap of the flow field, should be taken into consideration when locating a wind farm in such locations.

The simulations from which the velocity perturbations producing the TKE fields were derived from, provided a virtual measurement tool that was capable of reproducing the spatial and temporal variability of turbulence on such a large scale, which was otherwise impossible to observe in the real world. Under the high wind speed scenarios, that are suitable for wind farming, and over relatively complex terrain, the flow retained some aspects of terrain information to at least 30H (H is the terrain height) upstream and downstream of the experimental hill. In general, as the turbulent field travels over new terrain it tends to increase in intensity downstream of that feature, and the newly modified TKE field acquires geometric features from the underlying terrain. These features mainly register as amplifications in the wave structure of the field at wavelengths comparable to the height of the underlying terrain. As the height of the underlying terrain increases, this introduces a large-scale wave structure with a wavelength comparable to the height of the terrain, while within this large-scale turbulent wave there seems to be a superposition of a smaller wavelength oscillation that scales to the hill height producing the turbulent field in the first place. There is also more sensitivity of turbulence to the aspect ratio of the terrain in the region downstream of the features, while the results showed no considerable sensitivity to the levels of advected turbulence upstream of the terrain.

The answers to the questions posed by this research brought to light new ideas for future investigation and new questions to be answered. The challenge yet remains to include results from a variety of stability regimes, and carefully examine the wave-like superposition of turbulent signals. With a complete enough set of simulations, a simplified mathematical representation of how TKE

is advected and modified by terrain can be derived. Another very important future perspective that can emerge from this work is to investigate the effects of surface roughness elements, and look into their contribution to the turbulent advection. The analysis of the turbulence spectrum and TKE advection were carried out during neutral or near neutral conditions. The most difficult aspect of turbulence research really lies in its representation in very stable atmospheres, and this is an ongoing research area. Nevertheless, this work has shown that there is still a lot to understand even in the neutral case. The extension of the 2D simulation into 3D is necessary, but the author highly advises developing repeatability in the results in 2D first, and eventually including the complexity arising from vortex stretching and lateral perturbation effects. One of the most interesting features presented in this work, and not mentioned in the above summary, is the vorticity production and its travel downstream of the hill. As mentioned in its relevant section, the vortex shedding of smaller structures pealing of the main rotor is something that intrigues any turbulence researcher, and also has very relevant practical applications, especially for wind gusts. The questions that the author wants to examine in the future are; what governs the mechanism of production of these small energetic structures? What is the number and energy distribution as a function of wind speeds, terrain shape and atmospheric stability? What changes might occur if thermal buoyancy due to surface heating was included in the simulations?

No doubt that there are limitations to this work, and the results are by no means to be generalized. The observations of statistical turbulence, as presented here, are always limited by the Taylor's hypothesis and maximum hardware sampling resolution. Idealized simulations have their own strengths and weaknesses. The obvious weakness is the inability to verify the results, but is countered by the opportunity to visualize complex turbulent dynamics using contemporary analytical methods. On the other hand, what should be encouraged is approaching turbulence research by stripping it from all its complexities, and consequently to understand its nature through a bottom up approach using more complex real scenarios. There is a lot to learn from this approach to studying the nature of turbulence, and this was to some extent demonstrated by the idealized

simulations. The author, based again on his humble and limited experience, would like to encourage this approach to turbulence research. This approach imposes a turbulent structure (eddies from a source), and then examines its natural evolution based on fluid dynamic simulations.

"The essence of knowledge is its application."

Confucius [Chou Dynasty], (ca. 525 B.C)

8. References

Anderson, J., Degrez, G., Degtoote, J., Dick, E., Grundmann R., and Vierendeels J. (2009). *Computational fluid dynamics an introduction (third ed.)*, Springer, Berlin, 332 pp.

Batchelor, G. K. (1986). *The theory of homogeneous turbulence*: Cambridge University Press, Cambridge, 197 pp.

Beal, D. N., Hover, F. S., Triantafyllou, M. S., Liao, J. C., and Lauder, G. V. (2006). Passive propulsion in vortex wakes. *Journal of Fluid Mechanics, 549*, 385-402.

Beare, R., Macvean, M., Holtslag, A., Cuxart, J., Esau, I., Golaz, J. C., et al. (2006). An Intercomparison of Large-Eddy Simulations of the Stable Boundary Layer. *Boundary Layer Meteorology, 118*(2), 247-272.

Berge, E., Gravdahl, A., Schelling, J., Tallhaug, L., and Undheim, O. (2006). Wind in complex terrain. A comparison of WAsP and two CFD-models. Paper presented at the European wind energy conference (EWEC), Athens.

Biltoft, C. A. (2001). Some thoughts on local isotropy and the 4/3 lateral to longitudinal velocity spectrum ratio. *Boundary Layer Meteorology 100*:393-404.

Bouffanais, R. (2010). Advances and challenges of applied large-eddy simulation. *Computers and Fluids, 39*(5), 735-738.

Bougeault, P., Binder, P., Buzzi, A., Dirks, R., Houze, R., Kuettner, J., Smith, R. B., Steinacker, R., and Volkert, H. (2001) The MAP special observing period. *Bulletin of the American Meteorological Society, 82*: 433–462.

Bradley, E. F. (1980). An experimental study of the profiles of wind speed, shearing stress and turbulence at the crest of a large hill. *Quarterly Journal of the Royal Meteorological Society, 106*(447), 101-123.

Bradshaw, P. (1976). Complex turbulent flows. In: Koiter, W.T. (ed.), Proceedings of the Fourteenth IUTAM Congress. Theoretical and Applied Mechanics, North Holland, Delft. 103–113.

Breuer, M., Peller, N., Rapp, C., and Manhart, M. (2009). Flow over periodic hills - Numerical and experimental study in a wide range of Reynolds numbers. *Computers and Fluids, 38*, 433-457.

Britter R. E., Hunt J. C. R., and J., R. K. (1981). Air flow over a two-dimensional hill: Studies of velocity speed-up, roughness effects and turbulence. *Quarterly Journal of the Royal Meteorological Society, 107*(451), 91-110.

Burton, T., Sharpe, D., Jenkins, N., and Bossayni, E. (2001). *Wind Energy Handbook*: John Wiley and Sons Ltd.

Carlotti, P. (2002). Two-point properties of atmospheric turbulence very close to the ground: Comparison of a high resolution LES with theoretical models. *Boundary Layer Meteorology, 104*(3), 381-410.

Cao, S,. Tamura, Y., Kikuchi, N., Saito, M., Nakayama, I., and Matsuzaki, Y. (2009). Wind characteristics of a strong typhoon. *Journal of Wind Engineering and Industrial Aerodynamics 97*:11-21.

Castro, F. A., Palma, J. M. L. M., and Silva Lopes, A. (2003). Simulation of the Askervein flow. Part 1: Reynolds averaged Navier–Stokes equations (k–ε turbulence model). *Boundary Layer Meteorology, 107*, 501-530.

Challa, V.S., Indracanti, J., Rabarison, M.K., Patrick, C., Baham, J.M., Young, J., Hughes, R., Hardy, M.G., Swanier, S.J. and Yerramilli, A. (2008). A simulation study of mesoscale coastal circulations in Mississippi Gulf coast. *Atmospheric Research, 91*, 9-25.

Chamecki, M., and Dias, N. L. (2004). The local isotropy hypothesis and the turbulent kinetic energy dissipation rate in the atmospheric surface layer. *Quarterly Journal of the Royal Meteorological Society, 130*:2733-2752.

Chow, F. K., Andreas, P. W., Robert, L. S., Mathias, W. R., and Ming, X. (2006). High-resolution large-eddy simulations of flow in a steep alpine valley.

Part I: Methodology, verification, and sensitivity experiments. *Journal of Applied Meteorology and Climatology, 45*, 63.

Costantino, B., and Sandro, P. (1956). *Leonardo da Vinci*: Istituto di Leonardo da Vinci. Reynal. New York.

Counihan, J. (1975). Adiabatic atmospheric boundary layers, a review and analysis of data from the period 1880–1972. *Atmospheric Environment 9*:871-905.

Crescenti, G. H., (1997). A look back on two decades of doppler sodar comparison studies. *Bulletin of the American Meteorological Society. 78*, 651-673.

Davidson, P. A. (2006). *Turbulence. An introduction for scientists and engineers*: Oxford university press.

DeWekker, S. F. J., and Mayor, S. D. (2009). Observations of atmospheric structure and dynamics in the Owens Valley of California with a ground-based, eye-safe, scanning aerosol lidar. *Journal of Applied Meteorology and Climatology*, in press.

Deardorff, J. W. (1970a). A three-dimensional numerical investigation of the idealized numerical boundary layer. *Geophysical Fluid Dynamics, 1*, 377-410.

Deardorff, J. W. (1970b). Convective velocity and temperature scales for the unstable planetary boundary layer and for Raleigh convection. *Journal of the Atmospheric Sciences, 27*, 1211-1213.

Deardorff, J. W. (1972a). Numerical investigation of the neutral and unstable planetary boundary layers. *Journal of the Atmospheric Sciences, 29*, 91-115.

Deardorff, J. W. (1972b). Parameterization of the planetary boundary layer for use in general circulation models. *Journal of the Atmospheric Sciences, 100*, 93-106.

Deardorff, J. W. (1973). Three dimensional numerical modeling of the planetary boundary layer. Paper presented at the Workshop on Micrometeorology, Boston, MA.

de Franceschi, M., (2004). *Investigation of atmospheric boundary layer dynamics in alpine valleys*. Dissertation, University of Trento.

de Noord, M., Curvers, A., Eecen, P., Antoniou, I., Jorgensen, H.E., Pedersen, T.F., Bradley, S., Von Hünerbein, S., Kindler, D., Mellinghoff, H., and Emeis, S., (2001). Report WISE (Wind Energy Sodar Evaluation), EC Contract n°NNES.

Doyle, J. D., and Durran, D. R. (2002). The dynamics of mountain-wave-induced rotors. *Journal of the Atmospheric Sciences, 59*, 186–201.

Doyle, J. D., and Durran, D. R. (2007). Rotor and subrotor dynamics in the lee of three-dimensional terrain. *Journal of the Atmospheric Sciences, 64*, 4202-4221.

Doyle, J. D., Grubisic, V., Brown, W. O. J., De Wekker, S. F. J., Dornbrack, A., Jiang, Q. F., Mayor, S. D., and Weissmann, M. (2009). Observations and numerical simulations of subrotor vortices during T-REX. *Journal of the Atmospheric Sciences, 66*, 1229-1249.

Drobinski, P. and Foster, R. C. (2003). On the origin of near-surface streaks in the neutrally stratified planetary boundary layer. *Boundary Layer Meteorology, 108*(2), 247-256.

Drobinski P., Carlotti, P., Redelsperger P., Banta J. L., Masson R. M., Newsom V., and Rob K. (2007). Numerical and experimental investigation of the neutral atmospheric surface layer. *Journal of the Atmospheric Sciences, 64*(1), 137.

Dupont, E., and Flori, J. P., (2007). Comparison of sodar measurements with ultra sonic and cup anemometers for wind energy applications. Report EDF-RandD/ENPC .

Dupont, S., Brunet, Y., and Finnigan, J. J. (2008). Large-eddy simulation of turbulent flow over a forested hill: Validation and coherent structure identification. *Quarterly Journal of the Royal Meteorological Society, 134*, 1911-1929.

Farrugia, R.N., (2003). The wind shear exponent in a Mediterranean island climate. *Renewable Energy. 28*, 647–53.

Fedorovich, E., Conzemius, R., Esau, I., Katopodes Chow, F., Lewellen, D., Moeng, C. H., et al. (2004). Entrainment into sheared convective boundary layers as predicted by different large eddy simulation codes. In 16th Symp. On Boundary Layers and Turbulence, American Meteorological Society.

Fesquet, C., Dupont, S., Drobinski, P., Dubos, T., and Barthlott, C. (2009). Impact of terrain heterogeneity on coherent structure properties: Numerical approach. *Boundary Layer Meteorology, 133*, 71-92.

Frisch, U. (1995). *Turbulence, the legacy of A.N. Kolmogorov*: Cambridge University Press, Cambridge, 296 pp.

Harman, I., and Finnigan, J. (2010). Flow over hills covered by a plant canopy: Extension to generalised two-dimensional topography. *Boundary Layer Meteorology, 135*, 51-65.

Hertenstein, R. F., and Kuettner, J. P. (2005). Rotor types associated with steep lee topography: influence of the wind profile. *Tellus A, 57*(2), 117-135.

Hogstrom, U., Hunt, J. C. R., and Smedman, A. S. (2002). Theory and measurements for turbulence spectra and variances in the atmospheric neutral surface layer. *Boundary Layer Meteorology, 103*(1), 101-124.

Hrebtov, M. Y., Ilyushin, B. B., and Krasinsky, D. V. (2010). Inverse energy cascade in a turbulent round jet. *Physical Review E, 81*(1), 2-7.

Huaxing, L. U. (2008). *Modelling terrain complexity*. In Advances in Digital Terrain Analysis, Springer, pp. 159-176.

Hunt, J. C. R, and Morrison, J. F. (2000). Eddy structure in turbulent boundary layers. *Euro J. Mech. B. Fluids*, *19*, 673-694.

Hunt, J. C. R., and Carlotti, P. (2001). Statistical structure at the wall of the high Reynolds number turbulent boundary layer. *Flow, Turbulence and Combustion, 66*, 453-475.

Hussain, M., (2001). Dependence of power law index on surface wind speed. *Energy Conversion and Management. 43*, 467-472.

Iizuka, S., and Kondo, H. (2004). Performance of various sub-grid scale models in large-eddy simulations of turbulent flow over complex terrain. *Atmospheric Environment, 38*(40), 7083-7091.

Jackson, P. S., and Hunt, J. C. (1975). Turbulent wind flow over a low hill. *Quarterly Journal of the Royal Meteorological Society, 101*(430), 929-955.

Jiboori M. H., Yumao X., and Yongfu, Q. (2001). Turbulence characteristics over complex terrain in west China. *Boundary Layer Meteorology, 101*, 109-126.

Kaimal, J. C., Wyngaard, J. C., Izumi, Y., and Cote, O. R. (1972). Spectral characteristics of surface-layer turbulence. *Quarterly Journal of the Royal Meteorological Society, 98*(417), 563-589.

Kaimal, J. C., Wyngaard, J. C., Haugen, D. A., Cote, O. R., Izumi, Y., Caughey, S. J., et al. (1976). Turbulence Structure in the Convective Boundary Layer. Journal of the *Atmospheric Sciences, 33*(11), 2152-2169.

Kelly, N., Shirazi, M., Jager, D., Wilde, S, Adams, J., BuhL, M., Sullivan, P., and Patton, E. (2004). Low-level jet project interim report, Technical Report NREL/TP-500-34593, National Renewable Energy Laboratories.

Kolmogorov, A. N. (1941a). Energy dissipation in locally isotropic turbulence. Quarterly *Journal of the Royal Meteorological Society, 32*(1), 19-21.

Kolmogorov, A. N. (1941b). Local structure of turbulence in an incompressible fluid at very high reynolds numbers. *Dokl. Akad. Nauk SSSR, 30*, 299-303.

Li, W., Hiyama, T., and Kobayashi, N. (2007). Turbulence spectra in the near-neutral surface layer over the Loess Plateau in China. *Boundary Layer Meteorology, 124*(3), 449-463.

Lin, Y. L. (2007). *Mesoscale dynamics*: Cambridge Univeristy Press, Cambridge, 630 pp.

Lumley, J., and Yaglom, A. (2001). A century of turbulence. *Flow, Turbulence and Combustion, 66*(3), 241-286.

Mainpower (2009). Http://www.localgeneration.co.nz. Accessed on September 10, 2009.

Martins, C., Moraes, O., Acevedo, O., and Degrazia, G. (2009). Turbulence intensity parameters over a very complex terrain. *Boundary Layer Meteorology 133*:35-45.

Mason, P. J. (1994). Large-eddy simulation: A critical review of the technique. *Quarterly Journal of the Royal Meteorological Society, 120*, 1-26.

Mason, P. J., and Sykes, R. I. (1979). Flow over an isolated hill of moderate slope. *Quarterly Journal of the Royal Meteorological Society, 105*(444), 383-395.

Maurizi, A., Palma, J. M, and Castro, F. A., (1998). Numerical simulation of the atmospheric flow in a mountainous region of the North of Portugal. *Journal of Wind Engineering and Industrial Aerodynamics, 74–76,* 219–228.

McNaughton, K. G., and Brunet, Y. (2002). Townsend's hypothesis, coherent structures and Monin-Obukhov similarity. *Boundary Layer Meteorology, 102*(2), 161-175.

Mellinghoff, H., and Albers, A., (2000). Sodar measurements of the wind conditions in Oberzeiring, Austria. Report DEWI 4015O9903-35-01/2000-01.

Michalakes, J., Dudhia, J., Klemp, J.B. and Skamarock, W.C. (2006). Design of next-generation regional Weather Research and Forecast Model, WRF Users

Workshop, 19-Jun. 2006, Mesoscale and Microscale Meteorological Division / NCAR, BOULDER, Colorado, p. 12.

Mickle, R., Cook, N., Hoff, A., Jensen, N., Salmon, J., Taylor, P., et al. (1988). The Askervein Hill project: Vertical profiles of wind and turbulence. *Boundary Layer Meteorology, 43*(1), 143-169.

Migoyaa, E., Crespoa, A., Garcıa, J., Morenob, F., Manuela, F., Jimeneza, A., et al. (2007). Comparative study of the behavior of wind-turbines in a wind farm. *Energy, 32*(10), 1871-1885.

Moeng, C. H., and Sullivan, P. (1994). A comparison of shear and buoyancy driven planetary boundary layer flows. *Journal of the Atmospheric Sciences, 51*, 999-1022.

Moraes, O., Acevedo, O., Degrazia, G., Anfossi, D., da Silva, R., and Anabor, V. (2005). Surface layer turbulence parameters over a complex terrain. *Atmospheric Environment 39*:3103-3112

NZWEA (2009). New Zealand Wind Energy Association. Http://windenergy.org.nz. Accessed on September 19, 2009.

Obukhov, A.M. (1941). Energy distribution in the spectrum of a turbulent flow. *Ser. Geogr. Geofiz., 4-5*, 453-466.

Obukhov, A. M. (1971). Turbulence in an atmosphere with a non-uniform temperature. *Boundary Layer Meteorology, 2*(1), 7-29.

Orlanski, I. (1975). A rational subdivision of scales for atmospheric processes. *Bulletin of the American Meteorological Society, 56*, 527-530.

Palma, J. M. L. M., Castro, F. A., Ribeiro, L. F., Rodrigues, A. H., and Pinto, A. P. (2008). Linear and nonlinear models in wind resource assessment and wind turbine micro-siting in complex terrain. *Journal of Wind Engineering and Industrial Aerodynamics, 96*(12), 2308-2326.

Panofsky, H. A., Larko, D., Lipschutz, R., and Stone, G. (1982). Spectra of velocity components over complex terrain. *Quarterly Journal of the Royal Meteorological Society, 108*, 215-230.

Perez, I. A., Garcia M. A., Sanchez, M. L., and de Torre, B., (2004). Analysis of height variations of sodar-derived wind speeds in Northern Spain. *Journal of Wind Engineering and Industrial Aerodynamics. 92*, 875–894.

Pielke. R. A. (2002). *Mesoscale meteorological modeling* (second ed.), Academic Press, San Diego, 673 pp.

Prandtl, L. (1925). Über die ausgebildete turbulenz. Z. angew. *Math. Mech., 5*, 136-139.

Prandtl, L. (1932). Meteorologische anwendungen der strömungslehre. *Beitr. Phys. Fr. Atmosph., 19*, 188-202.

Prandtl, L. (1945). Über ein neues formelsystem für die ausgebildete turbulenz. *Nachr. Akad. Wiss. Göttingen, Math.-Phys.Kl.*, 6–19.

Rampanelli, G., Zardi, D., and Rotunno, R. (2004). Mechanisms of up-valley winds. *Journal of the Atmospheric Sciences, 61*(24), 3097-3111.

Rehman, S., Al-Abbadi, N. M., (2007). Wind shear coefficients and energy yield for Dhahran, Saudi Arabia. *Renewable Energy. 5*, 738-749.

Rotach, M. W., and Zardi, D. (2007). On the boundary-layer structure over highly complex terrain: Key findings from MAP. *The Royal Meteorological Society, 133*, 937-948.

Sagaut, P. (2001). *Large eddy simulations for incompressible flows: An introduction*. Springer, Berlin.

Sathyajith, M. (2006). *Wind energy: Fundamentals, resource analysis and economics.* Springer.

Scott, R. B., and Wang, F. (2005). Direct Evidence of an Oceanic Inverse Kinetic Energy Cascade from Satellite Altimetry. *Journal of Physical Oceanography, 35*(9), 1650-1666.

Smagorinsky, J. (1963). General circulation experiments with the primitive equations. *Monthly Weather Review, 91*, 99-164.

Sinclair Knight Merz, (2006). Renewable energy assessment, Canterbury region. Report EECA (Energy Efficiency and Conservation Authority), Wellington, New Zealand.

Skamarock, W. C., Klemp, J. B., Dudhia, J., Gill, D. O., Barker, D. M., Duda, M. G., Huang, X., Wang, W., and Powers, J. G. (2008). A description of the Advanced Research WRF version 3. NCAR technical note. http://www.mmm.ucar.edu/wrf/users/docs/user_guide_V3.1/contents.html. Accessed 18 December 2009.

Stull, R.B., (1988). *An introduction to boundary layer meteorology:* Kluwer Academic Publishers Group, Dordrecht.

Tamura, T. (2008). Towards practical use of LES in wind engineering. *Journal of Wind Engineering and Industrial Aerodynamics, 96*(10-11), 1451-1471.

Taylor, G. I. (1915). Eddy motion in the atmosphere. *Philosophical Transactions of the Royal Society of London. Series A, Containing Papers of a Mathematical or Physical Character, 215*, 1-26.

Teunissen, H. W. (1980). Structure of mean wind and turbulence in the planetary boundary layer over rural terrain. *Boundary Layer Meteorology 19*:187-221.

Townsend, A. A. (1956). *The structure of turbulent shear flow*: Cambridge University Press, Cambridge, UK.

Townsend, A. A. (1961). Equilibrium layers and wall turbulence. *Journal of Fluid Mechanics Digital Archive, 11*(01), 97-120.

Townsend, A. A. (1972). Flow in a deep turbulent boundary layer over a surface distorted by water waves. *Journal of Fluid Mechanics Digital Archive, 55*(04), 719-735.

Troen, I., Petersen, E. L. (1989). European wind atlas. Risø national laboratory, Roskilde. ISBN 87-550-1482-8

Tsvang, L. R., Koprov, B. M., Zubkovskii, S. L., Dyer, A. J., Hicks, B., Miyake, M., et al. (1973). A comparison of turbulence measurements by different instruments; Tsimlyansk field experiment 1970. *Boundary Layer Meteorology, 3*(4), 499-521.

Tsvang, L. R. (1985). Atmospheric turbulence research at the Tsimlyansk Scientific Station of the Institute of the Physics of the Atmosphere of the USSR Academy of Sciences. *Izv.. Atmos. Oceanic Phys. 21*(4), 261–267.

Tsvang, L. R., Kukharets, V. P., and Perepelkin, V. G. (1998). Atmospheric turbulence characteristics over a temperature-inhomogeneous land surface. Part II: The effect of small-scale inhomogeneities of surface temperature on some characteristics of the atmospheric surface layer. *Boundary Layer Meteorology, 86*(1), 103-124.

Uriel, F. (1995). *Turbulence: the legacy of A.N. Kolmogorov*: Cambridge University Press, Cambridge, UK.

van den Berg, G. P. (2007). Wind turbine power and sound in relation to atmospheric stability. *Wind Energy. 11,* 151-169.

Volkert, H., and Gutermann, T. (2007). Inter-domain cooperation for mesoscale atmospheric laboratories : The mesoscale alpine programme as a rich study case. *Quarterly Journal of the Royal Meteorological Society, 133*: 949-967.

von Kármán, T. (1930). Mechanische anlichkeit und turbulenz. In: Proceedings 3rd International Congress of Applied Mechanics, Part I, Stockholm. 85–105.

von Kármán, T. (1935). Some aspects of the turbulence problem. In: Proceedings of the 4th International Congress of Applied Mechanics, Cambridge, England, July 3–9, 1934. Cambridge University Press, Cambridge, UK. 54–91.

Weigel, A. P., and Rotach, M. W. (2004). Flow structure and turbulence characteristics of the daytime atmosphere in a steep and narrow Alpine valley. *Quarterly Journal of the Royal Meteorological Society, 130*(602), 2605-2627.

Weigel, A. P. (2005). *On the atmospheric boundary layer over highly complex topography.* Thesis.

Weigel, A., Chow, F. K., Mathias, W. R., Robert, L. S., and Ming, X. (2006). High-resolution large-eddy simulations of flow in a steep alpine valley. Part II: Flow structure and heat budgets. *Journal of Applied Meteorology and Climatology, 45*, 87.

Weigel, A. P., Chow, F. K., and Rotach, M. W. (2007). On the nature of turbulent kinetic energy in a steep and narrow alpine valley. *Boundary Layer Meteorology, 123*:177-199

Whiteman C. D. (2000). *Mountain meteorology: Fundamentals and applications*. Oxford University Press: Oxford and New York.

Wieringa, J. (1992). Updating the Davenport roughness classification. *Journal of Wind Engineering and Industrial Aerodynamics, 41*, 357-368.

Wieringa, J. (1993). Representative roughness parameters for homogeneous terrain. *Boundary Layer Meteorology, 63*, 323-363.

Wood, N. (2000). Wind Flow Over Complex Terrain: A Historical Perspective and the Prospect for Large-Eddy Modelling. *Boundary Layer Meteorology, 96*(1), 11-32.

Xue, M., Droegemeier, K., and Wong, V. (2000). The Advanced Regional Prediction System (ARPS) - A multi-scale nonhydrostatic atmospheric simulation and prediction model. Part I: Model dynamics and verification. *Meteorology and Atmospheric Physics, 75*, 161-193.

Yaglom, A. M. (1994). Fluctuation spectra and variances in convective turbulent boundary layers: A reevaluation of old models. *Physics of Fluids, 6*(2), 962-972.

Zeman, O. and Jensen, N. O. (1987). Modification of turbulence characteristics in flow over hills. *Quarterly Journal of the Royal Meteorological Society, 113*, 55–80.